

Advanced Energy Materials

Interfaces in perovskite solar cells

--Manuscript Draft--

Manuscript Number:	
Full Title:	Interfaces in perovskite solar cells
Article Type:	Invited Review
Section/Category:	
Keywords:	perovskite solar cells; interfaces; stability; electron selective contact; hole selective contact
Corresponding Author:	Ivan Mora-Sero University Jaume I SPAIN
Additional Information:	
Question	Response
<p>Please submit a plain text version of your cover letter here.</p> <p>If you are submitting a revision of your manuscript, please do not overwrite your original cover letter. There is an opportunity for you to provide your responses to the reviewers later; please do not add them here.</p>	<p>Dear Editor Carolina Novo da Silva:</p> <p>Following your kind invitation to prepare a review for your journal, and after our discussion about the topic, it is a pleasure to submit our manuscript entitled "Interfaces in Perovskite Solar Cells " to be considered for publication in Advanced Energy Materials as a Review. The manuscript has been prepared by Azhar Fakharuddin, Lukas Schmidt-Mende, Germà Garcia-Belmonte, Rajan Jose, and Ivan Mora-Sero, with Dr. Fakharuddin, Prof. Jose and Ass. Prof. Mora-Sero as corresponding authors.</p> <p>Halide perovskite is without any doubt one of the families of materials that are currently attracting more interest due especially to the high efficiencies that have been reported for solar cells. This fact has boosted the interest on these materials and systems. The goodness of halide perovskite in order to produce high efficiency perovskite devices is based on the properties of these materials. However, to take full advantage of this potentiality proper charge selective extracting contacts have to be used. Consequently, contacts and their corresponding interfaces with perovskite play a major role in perovskite solar cell (PSC) efficiency and stability. Despite numerous reviews on perovskite field are already available, there is no one focusing specifically on interfaces and on the interfaces in the rich variety of PSC configurations, and we consider that our manuscript can cover this lack.</p> <p>The review is divided in different sections and basically into two parts. The first one (sections 2-5), after the introduction, focuses on the physical effect of interfaces on PSCs, while the second part (sections 6-8) reviews extensively the different configurations utilized in perovskite solar cells focusing on the implications of interfaces in the final performance, and also very importantly highlighting the effect of these interfaces in the final device stability.</p> <p>The most exciting physics happens at the interfaces, so a better understanding of the details of the interfacial process will also give us more information on current limitations and ideas how to overcome these.</p> <p>We hope the present work can be considered suitable for publication in Advanced Energy Materials, given the deep overview of the important role of interfaces in Perovskite Solar Cells. We also consider it would be of interest to a wide community due to the generality of the approach.</p> <p>Sincerely yours, Ass. Prof. Iván Mora-Seró Research ID: E-4781-2014</p>
Do you or any of your co-authors have a conflict of interest to declare?	No. The authors declare no conflict of interest.
Corresponding Author Secondary Information:	

Corresponding Author's Institution:	University Jaume I
Corresponding Author's Secondary Institution:	
First Author:	Azhar Fakharuddin
First Author Secondary Information:	
Order of Authors:	Azhar Fakharuddin
	Lukas Schmidt-Mende
	Germa Garcia-Belmonte
	Rajan Jose
	Ivan Mora-Sero
Order of Authors Secondary Information:	
Abstract:	<p>Emergence of photoconversion efficiency (PCE) of perovskite solar cells (PSCs) similar to that of crystalline silicon solar cells have taken the photovoltaic (PV) community with a surprise. Together with efforts to push the PCE of PSCs to record values >22%, origin of their PV action and underlying physical processes are also deeply investigated worldwide in diverse device configurations. A typical PSC consists of a perovskite film (300 - 500 nm) sandwiched between an electron selective contact (ESC) and a hole selective contact (HSC); thereby creating two interfaces - i.e., ESC/perovskite and perovskite/HSC interfaces. These interfaces play a dramatic role in determining the performance, device stability, and hysteresis of PSCs. The crucial role of interfaces in the perovskite crystallization that determine the PCE, stability, and hysteresis is explained. Generally, semiconductors, either organic or inorganic, are popular choice as charge selective contacts in solar cells, interestingly, with insulating materials as a scaffold - these provide wealth of information in determining the PV action in PSCs. We define ideal charge selective contacts, which would not only determine the PCE of PSCs but also, equally importantly, influence their processing cost and operational stability to pitch PV market.</p>

Interfaces in perovskite solar cells

Azhar Fakharuddin^{*1,2,4}, Lukas Schmidt-Mende¹, Germà Garcia-Belmonte³, Rajan Jose², Ivan Mora-Sero^{*3}

¹Department of Physics, University of Konstanz, D-78457, Konstanz, Germany

²Nanostructured Renewable Energy Materials Laboratory, Universiti Malaysia Pahang, Kuantan, Malaysia

³Institute of Advanced Materials (INAM), Universitat Jaume I, 12006 Castelló, Spain

⁴Nanosciences and Technology Department, National Center for Physics, Quaid-i-Azam University, Islamabad, Pakistan

Emergence of photoconversion efficiency (PCE) of solution processable organometallic hybrid perovskite solar cells (PSCs) similar to that of crystalline silicon solar cells have taken the photovoltaic (PV) community with a surprise. Together with efforts to push the PCE of PSCs to record values >22%, origin of their PV action and underlying physical processes are also deeply investigated worldwide in diverse device configurations. A typical PSC consists of a perovskite film (300 – 500 nm) sandwiched between an electron selective contact (ESC) and a hole selective contact (HSC); thereby creating two interfaces – i.e., ESC/perovskite and perovskite/HSC interfaces. These interfaces play a dramatic role in determining the performance, device stability, and hysteresis of PSCs. Herein, we review PSCs built on rigid and flexible substrates with diverse device designs both in materials and in engineering perspectives and analyze origin of PV action and open circuit voltage in them from an interface perspective. The crucial role of interfaces in the perovskite crystallization that determine the PCE, stability, and hysteresis is explained. Generally, semiconductors, either organic or inorganic, are popular choice as charge selective contacts in solar cells, however, PSCs showed photovoltaic action without them and also, interestingly, with insulating materials as a scaffold – these provide wealth of information in determining the PV action in PSCs as well as expected to initiate extensive investigation on the electronic properties of thin films. We define ideal charge selective contacts, which would not only determine the PCE of PSCs but also, equally importantly, influence their processing cost and operational stability to pitch PV market.

1 Introduction

Progress in organic-inorganic hybrid perovskite solar cells (PSCs) has been remarkably impressive since its inception in 2009. The organic-inorganic hybrid perovskites have been known for applications in optical devices^[1] and field-effect transistors^[2] since early 1990's; however, their usefulness in a photo-energy conversion device is realized only in 2009 by Miyasaka et al.^[3] They crystallized $\text{CH}_3\text{NH}_3\text{PbI}_3$ or $\text{CH}_3\text{NH}_3\text{PbBr}_3$ hybrid perovskites as light absorbers onto a 8 – 12 μm thick TiO_2 layer, an architecture similar to the dye-sensitized solar cells (DSCs),^[4] and by making a junction with iodide/triiodide redox electrolyte as a hole transporting medium (HTM) demonstrated a photoconversion efficiency (PCE) ~3.8%. Subsequently, Park et al.^[5] demonstrated PCE up to 6.5% in similar device but with a TiO_2 film of lower thickness (~4 μm). However, these devices exhibited poor operational stability, typically less than an hour, due to the liquid electrolyte used. The first solid-state device based on $\text{CH}_3\text{NH}_3\text{PbI}_3$ as an absorber was reported by Kim et al.^[6] that employed a mesoporous TiO_2 scaffold (~1 μm) in conjunction with 2,2',7,7'-tetrakis-(N,N-p-dimethoxy-phenylamino)-9,9'-spirobifluorene (Spiro-OMeTAD) as a hole conductor and reported a remarkable PCE ~9.7%. Subsequent developments in PSCs such as enabling better charge extraction at electron and hole selective contacts (ESC and HSC), optimizing the perovskite composition, for example, incorporation of formamidinium (FA) or Caesium (Cs) or both into methylammoniumcation (MA), and optimizing the morphology of perovskite layer brought PSCs to deliver PCE 20 - 22%.^[7-12] Besides their high PCE which is comparable to silicon and thin film solar cells, they have also shown fair stability up to few thousand hours,^[8, 13-16] added functionalities such as possibility to be printed on flexible substrates,^[17, 18, 19] transparency^[20] and their workability in low light condition,^[21] thereby marking them as a potential candidate for future solar cell technology that can offer the 'golden four' of a solar cell technology,^[22] i.e. low-cost, stability, efficiency and added functionality. These achievements are partly because PSCs offer a wider variety of device designs as well as

1 varied choice materials combinations for electron and hole selective contacts as shown in
2 **Fig.1**, where the charge separation mechanism varies from that of sensitized cell to band
3 type. This makes it hard to generalize the working principle for all these designs, and
4 consequently, various underlying physical processes such as charge transport mechanism,
5 hysteresis and device instability are still not fully understood.
6
7
8
9
10

11
12 The first all-solid PSC employs a perovskite absorber is interfaced between an ESC on
13 a conducting glass substrate (FTO) and a HSC (**Fig. 1 a**) with a metal back contact on top.
14 The working principle of this device was initially conceived to be similar to that of DSSCs,
15 i.e., perovskite is a light absorber and ESC (typically TiO₂) takes part in charge separation and
16 electron transport whereas the holes are transferred to HSC although subsequent research
17 showed the working principle to be not excitonic. This design holds the state-of-the-art PCE
18 ~20-22% with (i) a compact (pin-hole free) hole blocking layer between FTO and TiO₂
19 scaffold, (ii) a dense perovskite capping layer over TiO₂ scaffold with perovskite infiltrated
20 within the pores, and (iii) optimized interfaces.^[12, 23-25] In the next design (**Fig.2b**), the
21 semiconducting TiO₂ scaffold is replaced with insulating Al₂O₃ or ZrO₂ and has reported a
22 maximum PCE ~15.9%.^[26] Herein, the charges are carried by the perovskite itself, thereby
23 evidencing that PSCs work without an electrically conducting ESC.^[27] Alternatively, devices
24 without any mesoporous TiO₂ scaffold (planar, **Fig. 2c**) have also shown impressive
25 photovoltaic performance (PCE ~19.3%, but with hysteresis)^[11] where a compact layer
26 (usually compact TiO₂) is employed to prevent a direct contact of perovskite or HSC with
27 FTO. The PSCs even without an ESC^[28] and also an HSC^[29] (**Fig. 2d & e**) have also been
28 tested and shown significantly high PCE 14-16%. In addition, inverted solar cell
29 configuration in which holes, instead of electrons, are collected at the FTO/ITO are also
30 reported (**Fig. 2f**) with PCE >18%.^[30, 31-33] In such devices, NiO and PEDOT:PSS are
31
32
33
34
35
36
37
38
39
40
41
42
43
44
45
46
47
48
49
50
51
52
53
54
55
56
57
58
59
60
61
62
63
64
65

commonly utilized HSCs whereas a thin layer (<50 nm) of phenyl-C61-butyric acid methylester (PCBM) or other fullerene derivatives are employed as ESC.

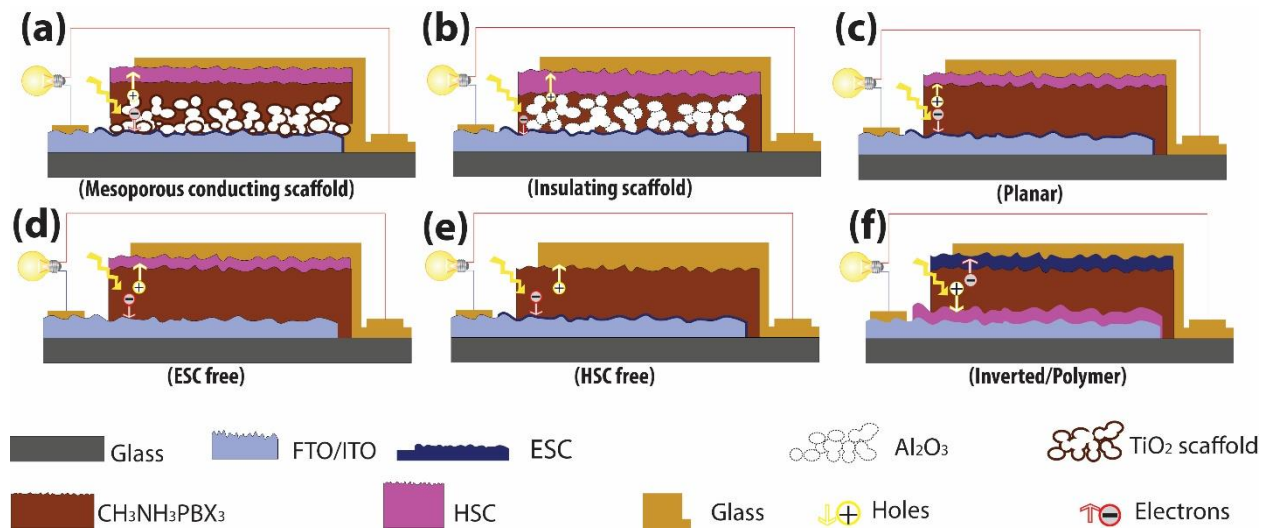


Fig. 1: A schematic on various common perovskite device architectures reported with or without charge (electron/hole) transport layers (a) a conducting metal oxide semiconductor (MOS), typically mesoporous TiO₂, is employed as a electron transport media, an architecture similar to solid-state DSCs, (b) MOS is replaced with insulating scaffold (Al₂O₃ or ZrO₂), (c) no scaffold is employed and instead a thin compact hole blocking layer (<100 nm) is employed on FTO, (d) no ETL and no hole blocking layer is employed and perovskite is deposited directly on surface modified FTO/ITO, (e) the architecture without a HTM and holes are transported via perovskite itself. The design however employs a thin n-type hole blocking layer on FTO (but often it also employs a mesoporous layer), and (f) and inverted device architecture where holes are collected on the FTO using a p-type carrier layer, typically NiO, whereas electrons are collected through metal back contact. In the architectures b –d, electrons are transported to FTO via perovskite.

As the PSCs are fabricated in a range of architectures, their photovoltaic performance over time and hysteresis in current – voltage characteristics largely depend on the electrical and morphological properties of the selective contacts. For example, perovskite crystals' size and morphology have shown to largely depend on the nature of ESC–CH₃NH₃PbX₃ interface and plays a key role in the final PCE.^[34, 35, 36] Furthermore, when it comes to the practical deployment of PSCs, it is not only their PCE but operational stability also determines the success of the technology for real-life application. In PSCs, ESC and HSC have shown significant impact on thermal, electrical, structural, UV-light and long-term operation stability thereby establishing its quintessence.^[16, 36-40]

The wide variety of PSCs' design architectures make the role of the interfaces ambiguous and raises questions such as does a mesoporous TiO₂ scaffold or compact layer

(c-TiO₂) takes part in charge separation? What is the contribution of ESC/HSC towards charge dynamics (transfer/recombination) and open circuit voltage (V_{OC}) in the various device designs? This is particularly intriguing after the reports where SnO₂, an MOS with a conduction band edge ~300 mV lower than TiO₂,^[41, 42] resulted in a similar V_{OC} (~1.1 V) as of the latter^[43] suggesting that, contrary to initial reports on the origin of the V_{OC} to be $E_F - E_{RED}$, it is rather due to splitting of the quasi-Fermi energy level of electrons and holes in perovskite itself. Questions also arise that if efficient PSCs can be made ESC- or HSC-free, as they have shown PCEs of ~16 and 14%, respectively, why is that most of the device architectures still require a mesoporous layer, or at least a flat n-type layer underneath perovskite along with an HSC? Furthermore, even if high efficiency PSCs can be made without a mesoporous scaffold, such as in the case of n-i-p (PCE ~20.7%) or p-i-n (PCE ~18.3%) planar PSCs, how stable are such devices and can they pave road to the commercial deployment of PSCs? Similarly, if selective contacts are crucial for long term stable operation of PSCs, which particular materials and morphology must be employed? In addition, how do the interfaces help eliminating the anomalous hysteresis in PSCs? The answers to such questions remain elusive despite the rapid increase in publication trends in PSCs. Comparisons of results from different labs do not always allow conclusions for two reasons: 1) Small changes in preparation conditions can influence largely the performance, so that results are not always easily reproduced and it is not clear, whether the cells have already fully been optimized or can be further improved, and 2) efficiency measurements largely vary as the measurement protocol for PSCs is quite different in different labs and reported values are often not stabilized efficiencies. Herein, compare the two selective contacts, i.e., ESC and HSC in PSCs to address these important questions, conclude its essentiality for a practically deployable device, and provide guidelines for future research. We visualize that selection of the selective contacts will determine, to a great extent, elimination of the anomalous

1 hysteresis, improving the charge dynamics at ESC-HSC/perovskite interfaces, and most
2 importantly upscaling of PSCs from a current laboratory scale to a commercially applicable
3 level.
4
5
6
7
8

9 **2 Chemistry of metal halide perovskites and origin of their properties**

10 The crystal chemistry of inorganic perovskites, such as BaTiO₃, is one of the widely
11 studied topics because of a range of diverse electrical properties they offer – they are
12 insulators and superconductors, antiferroelectrics and ferroelectrics, piezoelectric and
13 pyroelectric and so on. An ideal organic-inorganic hybrid perovskite crystal structure is
14 cubic^[44, 45] with space group $Pm\bar{3}m$ and can be represented by a general formula ABX₃ (**Fig.**
15 **2**), where A and B are 12-fold and 6-fold coordinated cations, respectively, and X is generally
16 a halogen or oxygen; the structure can be visualized as corner shared BX₆ octahedra running
17 along the three crystallographic axes and the dodecahedral interstice thereby produced is
18 filled by the A cation. In the case of the perovskites that have shown high PCE
19 (organometallic hybrid perovskite, such as CH₃NH₃PbI₃), A is typically aliphatic or aromatic
20 ammonium cation but also the use of inorganic Cs is extended, B is a divalent metal cation
21 (typically Pb²⁺ or Sn²⁺) and X is a halogen atom (anion) binding A and B.^[44, 46] In the case of,
22 the A site is occupied by an organic group ion rather than an atomic ion in inorganic
23 perovskite. In both cases, stability and crystal structure of the perovskite material is
24 determined from a tolerance factor (t) defined as $t = \frac{R_A + R_X}{\sqrt{2}(R_B + R_X)}$, where R 's are the
25 Goldsmith ionic radius of the respective ions and $0.75 < t < 1$. i.e., the perovskite phase is
26 favoured only if $R_A > R_B > R_X$. Ideal cubic perovskite structure is formed for $t = 1$, for which the
27 octahedra is vertical. Deviation of t from unity make the octahedra to tilt and the perovskite
28 crystal transform into structures of lower symmetry. The octahedral tilting gives spontaneous
29 polarizability to perovskite crystals and the associated phase transition with this tilting are the
30
31
32
33
34
35
36
37
38
39
40
41
42
43
44
45
46
47
48
49
50
51
52
53
54
55
56
57
58
59
60
61
62
63
64
65

1 source of diverse range of electrical properties of perovskites. The tolerance factor of most of
2 the hybrid halid perovskites lies in the range 0.8 – 0.85. i.e., they form distorted BX_6
3 octahedra and consequently offer spontaneous electrical polarity. Of particular interest in
4 such a scenario is the occupancy of an organic ion in it's A site, which is polar, thereby
5 offering a situation of interaction of two polarities of different origin (one from the octahedral
6 tilting and the other from the geometry of the organic molecule) in the same unit cell. This
7 geometry could be the unique source of optoelectronic and non-linear optical properties of
8 organometallic halide perovskites. For a detailed overview of the crystal structure of
9 perovskite including the three-dimensional lead halide perovskite, origin of its exceptional di-
10 electric, optical and electronic properties we refer to a comprehensive review by Saparov and
11 Mitzi.^[47]

12
13
14
15
16
17
18
19
20
21
22
23
24
25
26
27 As optoelectronic materials, molecular dynamics, absorbing and emitting states of the
28 hybrid perovskites are important information to understand the origin of the device
29 performance parameters. As the energy for molecular rotation is of the order of few meV,
30 which thermal quanta at the normal temperatures would provide; the A-site ion, i.e.,
31 methylammonium, is mobile even under low bias conditions. Many experimental
32 measurements and quantum chemical calculations have shown that $MAPbX_3$ is a direct band
33 gap semiconductor with two transitions at 760 and 480 nm and its absorbing and emitting
34 states are constituted by PbX_6 octahedra. In the case of $MAPbI_3$, top of the valence band for
35 both transitions are composed of p-orbitals of I mixed with 6p and 6s orbitals of Pb; the
36 bottom of the conduction band is formed of σ -antibonding orbitals of 6p of Pb and 5s of I and
37 π -antibonding orbitals of 6p of Pb and 5p of I. The MA ion do not play any significant role in
38 the absorbing and emitting states $MAPbI_3$ perovskites, their energy levels falls within the
39 bands.

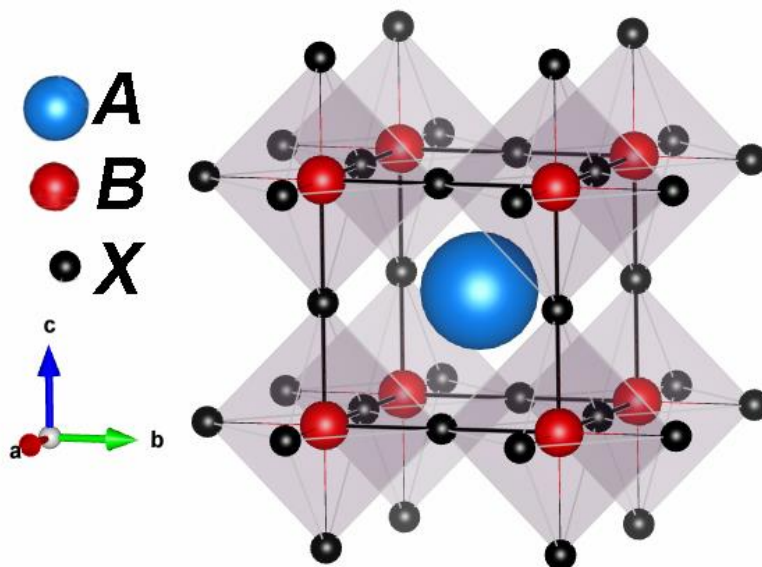


Figure 2: Scheme of a typical perovskite cubic crystal structure where A is CH_3NH_3^+ , B is Pb^{2+} and X is I $^-$ for one of the typical $\text{CH}_3\text{NH}_3\text{PbI}_3$ perovskite semiconductors used in solar cells. Figure reproduced with permission from ^[48]. Copyright of The Royal Society of Chemistry.

The archetypical organometallic hybrid perovskite, i.e., MAPbI_3 , crystallizes in 4 phases, three of which are perovskites called α , β and γ , while the fourth δ -phase does not exhibit a perovskite structure. The MAPbI_3 shows a pseudo-cubical α -phase above 327 K, see **Fig. 2**, below which it is tetragonal β -phase. In both α and β the orientation of MA is not defined; as pointed out earlier, a reorientation under electrical field or incident light explains its ferroelectric response. However, arguments against and towards ferroelectric behaviour in MAPbI_3 and MAPbBr_3 exist^[49] and ferroelectric effect is arguably induced by the applied electric field as the measurements require applying high electric field of hundreds of Vcm^{-1} .^[50] Nonetheless, above 162 K, the MAPbI_3 perovskite displays an orthorhombic γ -phase. The transition to the δ -phase is observed in the presence of a solvent. If iodine is partially substituted with a smaller cation such as Br, the phase transition temperature from β to α -phase gradually increases, and a Br content of $\sim 13\%$ stabilizes $\text{MAPbI}_{3-x}\text{Br}_x$ (which shows the best PV characteristics) into cubic phase at room temperature. A detailed solid state and physical chemistry of MAPbX_3 perovskites are beyond the scope of this paper; the readers may refer reviews on this topic elsewhere.

3 Selective contacts and charge transport, accumulation and transfer/recombination in perovskite films

The photovoltaic process requires two successive steps: photo-induced charge generation via light absorption, and charge separation as a second step in order to extract efficient electrical work from the photovoltaic device.^[51] From a semiconductor point of view, the first step; i.e., light absorption excites electrons at the VB to the CB producing the splitting of Fermi level of these two bands, i.e., $(E_{Fn} - E_{Fp})$ where E_{Fn} and E_{Fp} are the electron and hole quasi-Fermi levels in the perovskite film. This splitting represents the free energy that potentially can be used as work, and also the maximum V_{OC} (obtained by dividing the Fermi level splitting by the elementary charge). However, this energy is not yet available to be employed as electrical work until the second step takes place; i.e., the charge separation, and it is where selective contacts and their corresponding interfaces with light absorbing material (perovskite) plays a fundamental role in determining the performance of a solar cell.

An ideal selective contact does not deteriorate the light absorbing layer and also does not induce degradation within the device. In addition, there are also no energy losses when photogenerated carriers are injected from the light absorbing material into the selective contact, no recombination at the interface, and the Fermi level of its corresponding carrier is maintained at the interface without any drop. As an ideal selective contact allows injection of only one kind of carriers and there are no recombination losses in the bulk of the selecting contact as just one type of carrier is present in the contact. Finally, an ideal selective contact has an infinite charge mobility, producing no transport losses. It must also be balanced with respect to perovskite layer as otherwise it would lead to charge accumulation at selective contact and interfacial charge recombination thereby. Any modification of this ideal scenario will have a deleterious effect in the cell performance so that the achievable power is less than

1 the Fermi level splitting ($E_{Fn} - E_{Fp}$). If factors related to the reactivity and chemical stability
2 are not taken into account, the non-ideality of a selective contact can arise from: i) interface
3 recombination, ii) charge injection losses and iii) charge transport losses.
4
5

6
7 The density of photogenerated free-charge carriers in a PSC is expressed as:^[52]
8

$$\frac{\partial n(t)}{\partial t} = -k_3 n^3 - k_2 n^2 - k_1 n \quad (1)$$

9
10
11
12
13
14

15 Herein, k_1 , k_2 , k_3 are the monomolecular (trap-assisted), bimolecular (interfacial),
16 and Auger recombination rate constants. For a perovskite device, the dominant recombination
17 is first and second order only. Being a wide bandgap material, the Auger recombination
18 process is negligible (the rate constant for Auger recombination at 1 sun is negligible). It is
19 also reported that, typically, for efficient devices with highly crystalline perovskite films, the
20 electron-hole recombination within the perovskite film is negligible.^[53] The dominant
21 bimolecular recombination in perovskite films arises from (i) morphological and structural
22 defects within the perovskite film due to lattice mismatch and thermal vibrations,^[54, 55] (ii) the
23 arguably imbalanced charge transport in the perovskite film arising from shorter electron
24 diffusion length than the holes^[56] (iii) the energy offset between perovskite and selective
25 contacts,^[11, 57] (iv) the sub-bandgap states and surface defects of the selective contacts such as
26 TiO₂ or ZnO (ESC) or NiO (HSC),^[58, 59, 60] and (v) the poor physical contact between
27 perovskite and metal back contact^[61] (in the case of HSC-free architectures).
28
29
30
31
32
33
34
35
36
37
38
39
40
41
42
43
44
45
46

47 So far, these various recombination processes are not fully understood in the case of
48 PSCs despite their intensive research reports since 2012 and impressive PCE >22% till date.
49 Understanding and characterization of these interfacial processes are therefore mandatory not
50 only to further develop this photovoltaic technology but also for the development of other
51 optoelectronic devices based on the halide perovskites. Towards this end, impedance and
52 transient absorption spectroscopies can provide insights on the role of contacts and their
53
54
55
56
57
58
59
60
61
62
63
64
65

1
2
3
4
5
6
7
8
9
10
11
12
13
14
15
16
17
18
19
20
21
22
23
24
25
26
27
28
29
30
31
32
33
34
35
36
37
38
39
40
41
42
43
44
45
46
47
48
49
50
51
52
53
54
55
56
57
58
59
60
61
62
63
64
65

respective interfaces in the performance of PSCs, and in this section, we use it to emphasize the contribution of contacts and interfaces in PSCs. Impedance spectroscopy (IS) is a characterization method in the frequency domain that allows decoupling processes associated with different characteristic time domains and has been used to characterize PSCs since very early stages of their research.^[62] Despite the fact that till date there is no general model to describe the impedance spectra of PSCs in the complete frequency range and for all the different device configurations, IS can still provide useful implications about interfacial charge kinetics.

Fig. 3a shows the J-V curves of PSC prepared with and without one or both selective contacts.^[63] Complete PSC with an extended and standard configuration have been prepared by the successive deposition of thin film layer on top of glass/FTO transparent contact in order to form a complete device: glass/FTO/compact TiO₂/CH₃NH₃PbI₃ perovskite/spiro-OMeTAD/Au, denoted as EPH as it contains compact TiO₂ ESC (E), perovskite light absorbing layer (P) and spiro-OMeTAD HSC (H). In addition, devices without HSC (EP sample), without ESC (PH sample) or without both (P sample) have been also analyzed. From **Fig. 3a** it can be clearly observed that removing of a selective contact has deleterious effect on cell performance. PSCs with high efficiency have been reported for devices without ESC or HSC, as it is reviewed in **Section 6**, nevertheless, the maximum reported efficiency for those configurations has always been well below compared to the devices employing both selective contacts. IS was employed to analyze the effect of selective contact.^[63] Fig. 6 b & c show the impedance pattern of the analyzed samples under 1 sun illumination at 0.1 V applied voltage. A rich pattern can be appreciated, basically formed by two arcs at high and low frequencies. IS pattern has been fitted using equivalent circuits discussed in Ref.^[63] (solid curves in **Fig. 3b and c**). Three characteristic resistances can be extracted upon fitting. The diameter of the high frequency feature defines a resistance, R_{sc}, corresponding to

the selective contacts, while the diameter of the low frequency feature is related to the recombination resistance, R_{rec} . In addition the real part of the impedance where high frequency feature starts indicate the series resistance, R_s , of the device due to the extracting contacts and wiring.

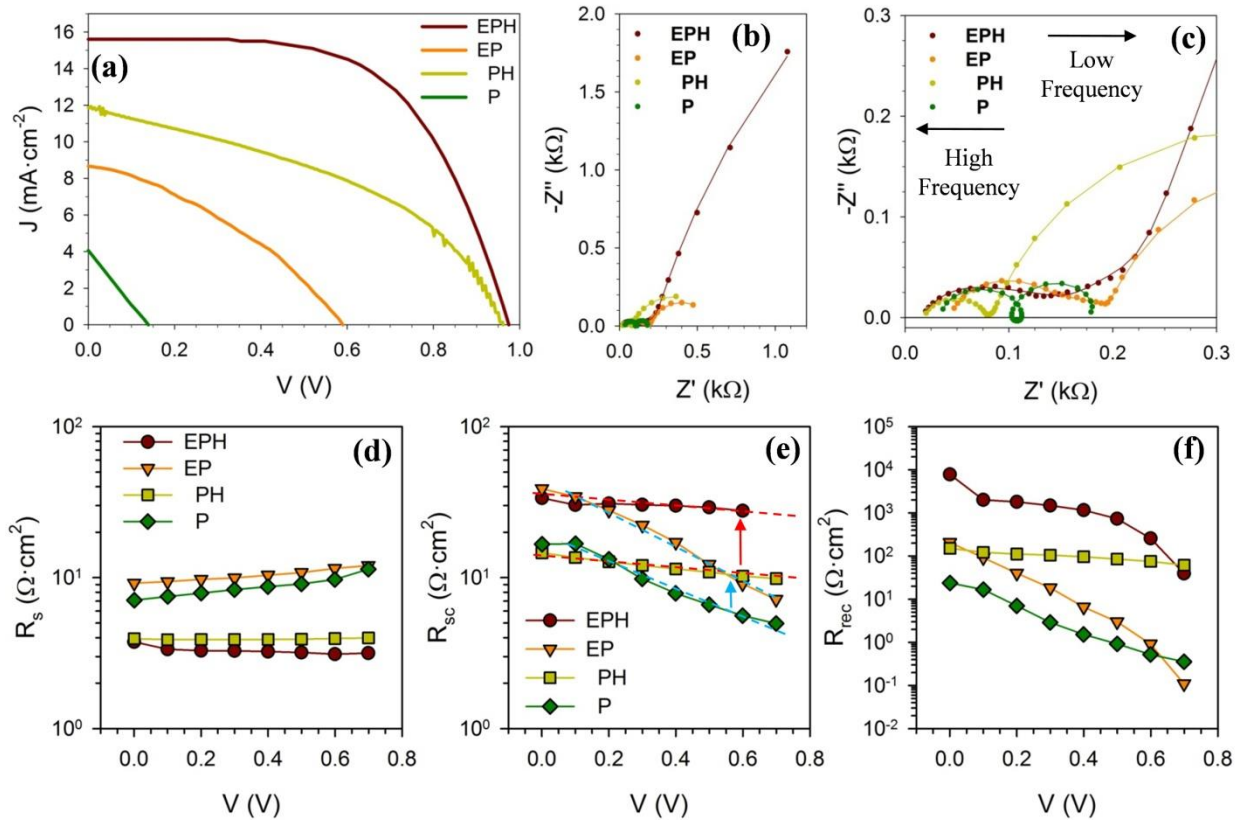


Fig. 3: J-V curves and impedance spectroscopy analysis of different PSCs with a without selective contacts. Complete cell (EPH) presents: (E) compact TiO_2 electron selecting contact; (P) MAPbI_3 Perovskite layer and (H) spiro-OMeTAD as hole selecting contact. Following this notation EP samples has no hole selecting contact while P sample does not have any of the two selective contacts and perovskite layer is directly contacted by the extracting contacts FTO and Au. (a) J-V curve, reverse scan. (b) Impedance spectra of the different devices under 1 sun illumination at 0.1 V applied bias. (c) Zoom of high frequency region in (b), high and low frequency regions are indicated, solid lines are fitting curves obtained by the use of equivalent circuits detailed in Ref. ^[63, 64]. (d) Series resistance; (e) high frequency feature resistance, dashed lines are eye guides. Red and dashed lines indicate the devices with and without a hole selective contact, respectively. Red and blue arrows indicate the increase in resistance observed when electron selective contact is added to PH and P samples respectively. (f) Recombination resistance.^[63] Reproduced with permission references. Copyright of American Chemical Society

Fig. 3d depicts R_s for the four devices analyzed in this study. High series resistance (R_s) can be noted for devices without HSC suggesting a contact resistance (R_{CON}) between perovskite and Au that disappears when spiro-OMeTAD is added and points out a first beneficial effect of including selective layer in order to couple efficiently the perovskite

1 absorbing layer with the extracting contacts. R_{sc} is also affected significantly by the presence
2 of extracting contacts as shown in the **Fig. 3e**. The slope of R_{sc} vs. V depends on the presence
3 of HSC, lower in the presence of selective contact, as displayed in the blue and the red
4 dashed lines for devices with and without HSC in **Fig. 3e**. This fact indicates that hole
5 transport resistance along the HSC is contributing to R_{sc} . Moreover, electron transport
6 resistance along ESC is also contributing to R_{sc} , as it is observed from the upwards shift of
7 the devices containing ESC with respect to their counterparts without it (see red and blue
8 arrows in **Fig. 6e**). Finally, the presence of selective contacts also affects the recombination
9 rate as can be noted from the effect on R_{rec} (**Fig. 3f**) because recombination resistance is
10 inversely proportional to the recombination rate.^[65] Note that the highest R_{rec} , i.e., the lowest
11 recombination rate, is observed for the complete device EPH, while removing any of the
12 selective contacts imply an increase of recombination. The variation is significant if the
13 interfacing material being removed is the HSC.

14
15
16
17
18
19
20
21
22
23
24
25
26
27
28
29
30
31 It is evident that the main role of a selective contact is to reduce the interfacial
32 recombination between perovskite light absorbing layer and the FTO and Au extracting
33 contacts. However, their use adds a deleterious effect due to the carrier transport resistance
34 and affects cell parameters particularly, the FF. Consequently, a good selective contact has to
35 be as thin as possible in order to reduce the transport resistance but thick enough to avoid
36 pinholes, hindering effectively charge recombination.
37
38
39
40
41
42
43
44
45
46
47
48
49
50
51
52
53
54
55
56
57
58
59
60
61
62
63
64
65

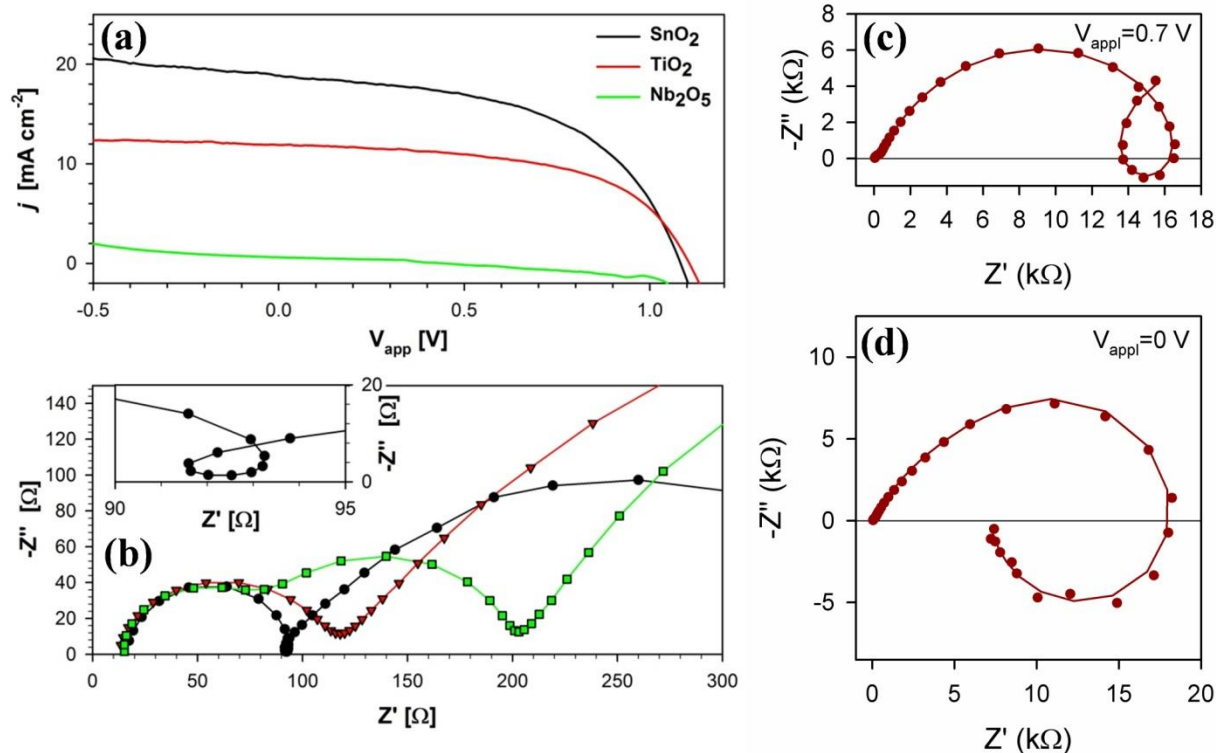


Fig. 4: a) J-V curves of PSCs with different electron selective contacts, (b) impedance spectra of the high frequency region for the same devices measured under 1 sun conditions and without an applied bias, inset shows an enlarged view of an inductive loop element observed in the spectra of the sample using SnO₂ as ESC.^[64] (c) and (d) Nyquist plots under 1 sun illumination with an applied DC bias (V_{app}) of 0.7 and 0V respectively. The PSC measured has an unconventional scaffold deposited on top of TiO₂ electron selecting contact formed by the sequential deposition of SiO₂ and TiO₂ mesoporous layers.^[66] Concretely for the samples characterized in (c) and (d), the scaffold on top of conducting FTO is formed by sequential deposition of TiO₂/SiO₂/ TiO₂/SiO₂/ TiO₂/SiO₂/ TiO₂. Copyright of The Royal Society of Chemistry.

Obviously the goodness of an interfacing material for an efficient electron transport in PSC will depend on the nature and interactions of the chosen selecting contact with the light absorbing perovskite layer. We therefore analyze, in the next sections, the effect of a wide variety of selecting contacts. As an example, **Fig. 4a** shows J-V curves of PSCs prepared following a similar procedure but using different ESCs.^[64] The different ESCs have been prepared by ALD while the materials and deposition conditions for the rest of the layers were kept constant. This simple change results in large variation in the PV performance of the devices; from 17% for SnO₂ESC to nearly zero (0.20%) for Nb₂O₅, passing through an intermediate value for the TiO₂. Again IS give important clues on the origin of this difference, see **Fig. 4b**. While for SnO₂, merely two arcs are observed in the impedance

1 spectra, an intermediate arc is observed for Nb₂O₅ based devices, introducing an additional
2 resistance, probably related with an interfacial process between Nb₂O₅ and perovskite. This
3 assumption is reinforced by the observation of an inductive loop at intermediate frequencies
4 when SnO₂ is used as ESC, see inset in **Fig. 4b**. This loop behavior has been previously
5 observed in solar cells and LEDs and it has been attributed to complex multistep injection
6 processes.^[67] Consequently, injection processes at the interfaces are also significantly
7 important. However the presence of an interfacial electrostatic potential with a retarded time
8 response, that we discuss below, has probably an important role on the apparition of this
9 feature.

10
11
12
13
14
15
16
17
18
19
20
21
22 The relationship of this inductive loop with interfacial process has been very recently
23 demonstrated using unconventional scaffold forcing the photogenerated electrons to follow
24 multistep perovskite/TiO₂ injection processes until they are extracted.^[66] The use of a
25 scaffold formed by successive thin layers of low porosity (~5%) TiO₂ and mesoporous SiO₂
26 (~40% porosity) makes that photogenerated electrons in the perovskite have two parallel
27 paths in order to arrive to the electron extracting contact, percolating through the perovskite
28 present in the low porosity TiO₂ and being injected in TiO₂ and reinjected back into the
29 perovskite. Note that injected electrons into TiO₂ cannot recombine, as there are no holes
30 present in TiO₂. The low porosity of TiO₂ increases the weight of the second path in the
31 transport of electrons until the extracting contact and consequently the fingerprint of the
32 interfacial processes at Perovskite/TiO₂ is magnified. Exaggerated inductive loops are clearly
33 observed in these samples, see Fig. 4c, indicating a clear relation of this feature and
34 interfacial processes. This loop is clearly observed even at short circuit conditions, see Fig
35 4d. The future determination of physical processes producing this loop will undoubtedly help
36 in the characterization of interfacial processes in PSCs. At this point it is important to
37 highlight that this feature is not linked to bad performing devices, as loops have been
38
39
40
41
42
43
44
45
46
47
48
49
50
51
52
53
54
55
56
57
58
59
60
61
62
63
64
65

1 observed in 18% efficiency PSCs.^[64] Consequently this feature is related with a general
2 process on PSCs and it cannot be considered just an exotic element.
3

4
5 Nevertheless, inductive loops is not the unique "surprise" that the analysis of
6 impedance spectra of perovskite solar cells has provided. One of the strongest points of the IS
7 analysis is the possibility of characterization of capacitive effects, and an accurate analysis of
8 capacitance could allow to unambiguously link the IS features with well-determined physical
9 processes. Probably the most surprising aspect of the IS of PSCs is the observation of 3-4
10 orders of magnitude increase in capacitance for the measurements in dark conditions and at 1
11 sun illumination(at low frequency), see **Fig. 5a**. This enormous variation has not been
12 observed in any other photovoltaic material, for example, crystalline silicon exhibits an
13 increment of low frequency characterization in just a factor 2-3. Zarazua et al.^[68, 69] have
14 explained this capacitance as an accumulation capacitance due to the accumulation of hole
15 majority carriers at the perovskite/TiO₂ interface. They observed that at open circuit
16 conditions this capacitance is not dependent of the perovskite thickness, pointing to an
17 interfacial effect, while at different light intensities it follows the expected behavior for an
18 accumulation capacitance. More recently Contreras et al.^[70] observed the same behavior by
19 impedance spectroscopy whereas, Bergmann et al. ^[71] detected charge accumulation at the
20 ESC by Kelvin probe force microscopy. Furthermore, in a recent report, Chen et al.^[72]
21 observed a band bending with majority hole accumulation at perovskite interface confirming
22 the accumulation capacitance interpretation.
23
24
25
26
27
28
29
30
31
32
33
34
35
36
37
38
39
40
41
42
43
44
45
46
47
48
49
50
51
52
53
54
55
56
57
58
59
60
61
62
63
64
65

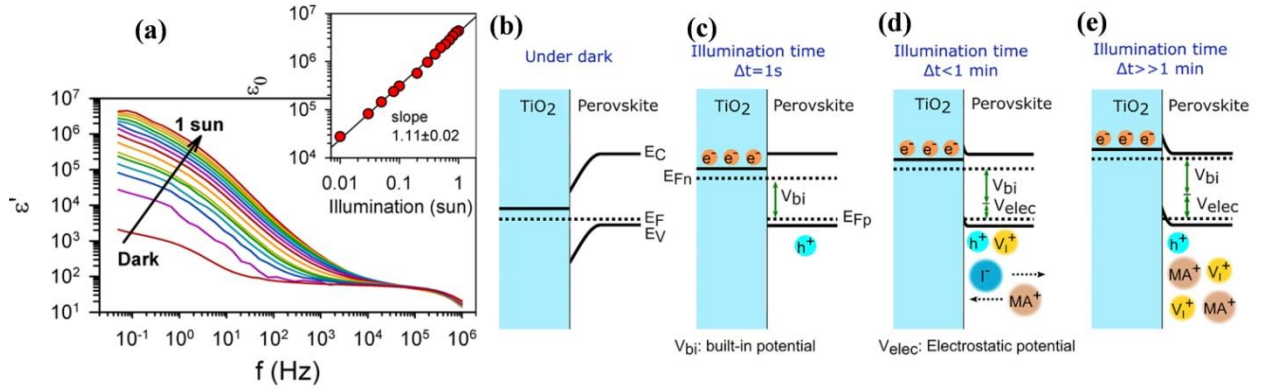
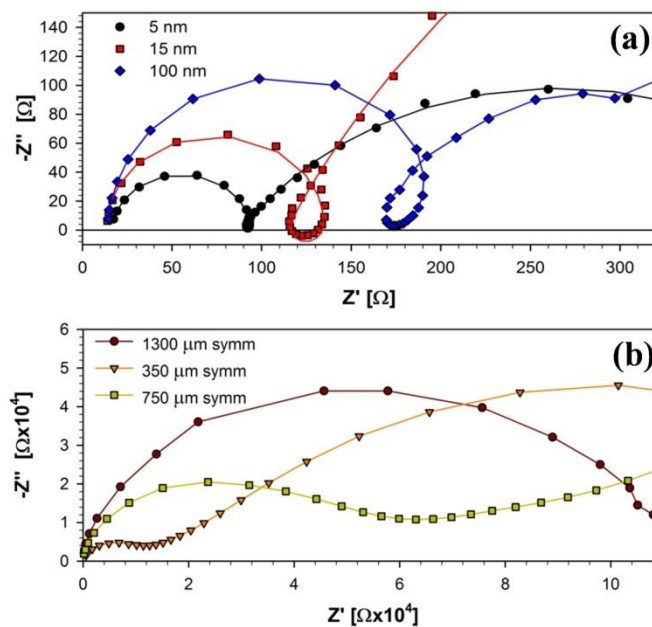


Fig. 5: a) Bode plot of dielectric constant for PSCs with standard TiO₂ and spiro-OMeTAD as ESC and HSC, respectively, at different light illumination. Note that the capacitance is linearly related with the dielectric constant. Inset: Dielectric constant (capacitance) is linearly related with light intensity.^[73] b) Band diagram of perovskite and TiO₂ ESC in equilibrium under dark conditions. E_C, E_V and E_F represent the position of Conduction Band, Valence Band and equilibrium Fermi Level respectively. c) Illumination produces the Fermi level splitting producing a built-in potential, E_{Fn} and E_{Fp} represent the electron and hole quasi Fermi level respectively. d) Slow photoinduced ion migration produces an accumulation region at the interface and the apparition of an electrostatic potential. e) after long illumination time steady state is attained and V_{elec} and accumulation region fully developed.^[74]

This accumulation capacitance is an electronic phenomenon; however, it is strongly influenced by the presence of mobile ions in halide perovskite materials. This effect has been recently highlighted by Gottesman et al.^[74] analyzing the open circuit voltage decay in perovskite solar cells and employing theoretical simulations. In equilibrium under dark condition TiO₂, perovskite and consequently their interface present a common flat Fermi level, see **Fig. 5b**. When light is switch on carrier photogeneration produces rapidly a Fermi level splitting with the formation of a built-in potential, see **Fig. 5c**. However this is not the only effect produced by light illumination. De Quilletes at al.^[75] has reported a photo-induced halide redistribution in perovskite films. This is a slow process that require relatively long times, even seconds time scales, in order to attain the steady state, see **Fig. 5d** and **5e**. As a consequence the hole charge accumulation at the ESC interface is ruled by the slow dynamics of ion migration. The ion redistribution at the interface produces an electrostatic potential, see **Fig. 5d** and **5e**. The formation of the V_{elec} has been confirmed by the analysis of the open circuit voltage decay with different pre- light soaking times. With no light soaking, a fast decay is observed. However when measurements are made after few minutes of light soaking,

1 a slow Voc decay is observed for longer times, as in this conditions ions have had enough
 2 time to migrate and form V_{elec} , and removing this potential requires again the slow migration
 3 of these ions, producing a slower Voc decay.^[74]
 4
 5
 6

7 The presence of this accumulation capacitance mediated by ion migration has
 8 enormous implication on OSC performance. On one hand, V_{elec} , increases the Fermi level
 9 splitting which has important implications for open circuit potential as we discuss in the next
 10 section. On the other hand, majority accumulation at the interface indicates higher majority
 11 density and consequently higher recombination at the interface as recombination is directly
 12 proportional to charge density. In this sense, recombination at the interface is the dominant
 13 carrier recombination process in PSCs.^[69]
 14
 15
 16
 17
 18
 19
 20
 21
 22
 23



24
 25
 26
 27
 28
 29
 30
 31
 32
 33
 34
 35
 36
 37
 38
 39
 40
 41
 42
 43
 44
 45
 46
 47 **Fig. 6:** a) Impedance spectra of the high frequency region for samples using different thickness SnO_2 as ESC, measured under 1 sun conditions and no applied bias, (b) Impedance spectra of the high frequency region for symmetric devices fabricated with perovskite pellets with different thickness and measured under dark conditions and no applied bias.^[64] Copyright of The American Chemical Society.

48
 49
 50
 51
 52
 53 Injection, accumulation and recombination, are not the only ways in which a selective
 54 contact can affect the cell performance. As it has been discussed previously the charge
 55 transport along the selective contact also influences the cell performance. **Fig. 6a** shows the
 56
 57
 58
 59
 60
 61
 62
 63
 64
 65

1 impedance patterns of samples using SnO₂ ESC with different thickness. As the thickness of
2 the ESC increases the diameter of high frequency pattern augment consistently with an
3 increase in the electron transport resistance at the ESC. The highest efficiency (16.9%) has
4 been observed for 15 nm thick ESC, probably for a thinner layer of 5 nm (13.3%) the
5 selective contact is too thin to block completely the interfacial recombination, while in the
6 case of a thicker layer ~100 nm ESC (10.2%), the transport resistance at the selective contact
7 reduces the FF (not shown here) and the final performance.^[64] Unfortunately, single features
8 in PSCs are not due to just a single process but are affected by multiple processes within
9 similar characteristic time scale. For example, **Fig. 6b** shows the impedance spectra of the
10 high frequency region for symmetric devices fabricated with perovskite pellets of different
11 thickness and measured with no applied bias under dark conditions. It can be seen that the
12 high frequency impedance feature is also affected by sample bulk properties as it becomes
13 bigger with increasing the thickness of the perovskite pellets. These findings points out the
14 difficulty in order to obtain a complete PSC IS model.

15
16
17
18
19
20
21
22
23
24
25
26
27
28
29
30
31
32
33
34 Similarly, ultrafast transient optical absorption spectroscopy is employed to directly
35 evidence the role of selective contacts towards interfacial charge dynamics.^[76] The efficiency
36 of charge injection ($A_2/\Delta A_0$ at 25 ps, with $\Delta A_0 = 1$ ps) is calculated from ratio of amplitude
37 (A_2) with respect to the normalized amplitude (ΔA_0). This leads to $A_2/\Delta A_0$ 0.14 and 0.24 for
38 Al₂O₃ and TiO₂ without a HSC and 0.26 and 0.34, when impregnated with HSC, respectively
39 (**Fig.7**). In case of Al₂O₃- perovskite film (Al₂O₃ is an insulating scaffold that does not take
40 part in charge transport) the signal completely diminishes prior to reaching a nanoscale,
41 whereas the carriers in TiO₂-perovskite film are longer lived. Due to the absence of any
42 HSCs, the diminishing of signal in the former is due to decay of carrier population due to
43 recombination within the perovskite film, which upon interfacing with spiro-OMeTAD
44 results in long living charge carriers. It also evidences electron injection from perovskite into

1
2
3
4
5
6
7
8
9
10
11
12
13
14
15
16
17
18
19
20
21
22
23
24
25
26
27
28
29
30
31
32
33
34
35
36
37
38
39
40
41
42
43
44
45
46
47
48
49
50
51
52
53
54
55
56
57
58
59
60
61
62
63
64
65

TiO₂. The most efficient charge extraction takes place when both selective contacts, i.e., TiO₂ and spiro-OMeTAD are present. Alternatively, charge recombination dynamics, probed via nanosecond transient optical absorption spectroscopy revealed ~6–7 times faster recombination for Al₂O₃ than TiO₂ (Al₂O₃ ~15 μs, TiO₂~99 μs).

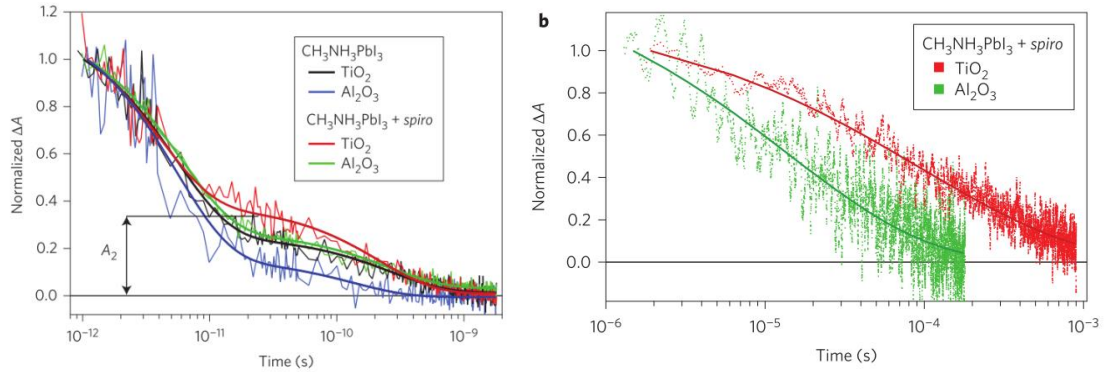


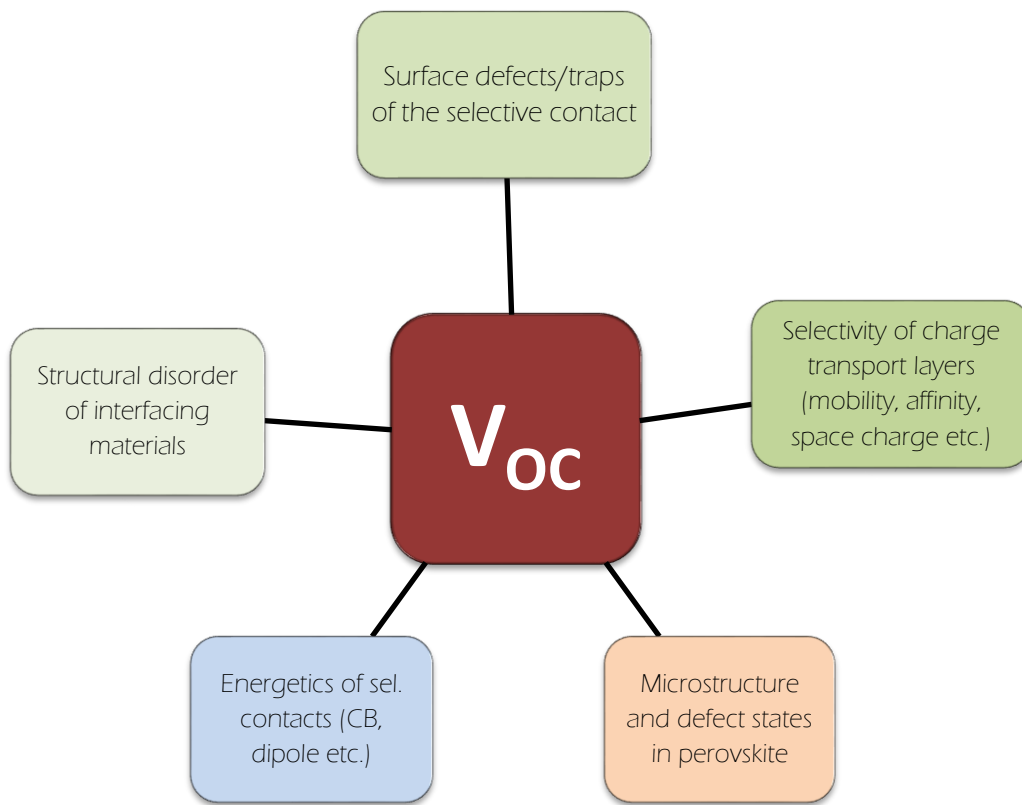
Figure 7: Transient absorption spectra to measure charge carrier dynamics in CH₃NH₃PbI₃ on TiO₂ (black);CH₃NH₃PbI₃ on Al₂O₃ (blue); CH₃NH₃PbI₃ and spiro-OMeTAD on TiO₂ (red); CH₃NH₃PbI₃ and spiro-OMeTAD on Al₂O₃ (green). The solid lines show bi-exponential fits of experimental data, (b) charge recombination dynamics obtained from nanosecond-laser flash photolysis of the various systems. Thick lines are the exponential fits of the experimental data. Figure obtained with permission from reference [76]. Copyright of Macmillan Publishers Limited.

These spectroscopy experiments emphasize that although the superior charge mobility, optical absorption, density of traps, and energetics provides a platform to build high efficiency PV device, screening of rightful selective contacts (such as TiO₂, SnO₂ etc.; Al₂O₃ is only a scaffold) is ineludible. Excellent performing contacts will minimize the interfacial recombination and interfacial charge transfer resistance while not introducing significant carrier transport resistance. An appropriated balance of these characteristics will determine the most efficient contact and interfaces for PSCs.

4 Selective contacts and open circuit voltage in perovskite solar cells

PSCs have surpassed the performance of other solution deposition solar cell technologies mainly due to the outstanding V_{OC} obtained which accounts for a voltage loss ($E_G - qV_{OC}$) of <0.4 V in state-of-the-art devices (See **Table 1**). The interfacial effects are crucial in order to further push up photovoltage values. The maximum attainable photovoltage is determined by the Fermi level splitting at the perovskite layer $V_{OC,max} = (1/q)(E_{Fn} - E_{Fp})$ where E_{Fn} and E_{Fp} are the electron and hole quasi-Fermi levels in the perovskite film. As we have described in the previous section charge accumulation at interfaces produces an interfacial electrostatic potential that contributes to the Fermi level splitting and eventually increases the V_{OC} , see **Fig. 5d** and **5e**.^[74] Herein, the unique accumulation properties of halide perovskite due to the ion migration are reflected in the high V_{OC} of PSCs. Note that $V_{OC,max}$ already takes into account the bulk recombination in the perovskite layer affecting the Fermi level splitting. Considering an almost negligible recombination, i.e. radiative recombination, $V_{OC,max} = 1.33$ V for $MAPbI_3$.^[77] Although in a first analysis it could be considered that interfaces do not influence the bulk recombination, it is not the case in PSCs as the substrate and its interface plays an important role on the growth process of perovskite layer affecting the microstructure and defect states in bulk perovskite, and eventually the V_{OC} .^[78] Climent-Pascual et al.^[79] have shown that the substrate influences not only the grain size or preferential orientation of the perovskite layer but the lattice parameters, emission properties and degradation pathways, probably as different substrates induce different majority defects in the layers. After this first consideration, if an ideal selective contacts were used, $V_{OC,max}$ would be the final PSCs photovoltage. However, in a device under operation, there are multiple ways in which selective contacts produces a reduction of V_{OC} respect is maximum possible value, see **Fig. 8**. **Table 1** compares various state-of-the-art V_{OC} reports for PSCs. Although, $MAPbBr_3$ demonstrated higher V_{OC} 1.3 –1.6

1 V(owing to its bandgap, $E_g \sim 2.3$ eV) than MAPbI₃ based PSCs (V_{OC} up to 1.2 V, $E_g \sim 1.6$ eV),
 2 the goodness of a PV device requires an account of the voltage loss and not just the obtained
 3 V_{OC} . The $E_g - qV_{OC}$ is ~ 0.7 eV for the former and ~ 0.4 eV for the latter (a lower $E_g - qV_{OC}$ is
 4 preferred). This leads to an excellent $V_{OC}/E_g \sim 0.75$ in the case of MAPbI₃ despite the
 5 polycrystalline nature of perovskite films which is comparable to silicon (0.8), and much
 6 higher than organic solar cells (0.55).^[80]
 7
 8
 9
 10
 11
 12
 13
 14
 15
 16
 17
 18
 19
 20
 21
 22
 23
 24
 25
 26
 27
 28
 29
 30
 31
 32
 33
 34
 35
 36
 37
 38
 39
 40
 41
 42
 43
 44



45 **Figure 8:** The various limiting factor of the open-circuit voltage in perovskite solar cells. For a details
 46 description of each, please refer to text.
 47
 48
 49

50 Selective contacts can directly influence the V_{OC} by the presence of surface
 51 defects/traps producing an interfacial recombination. This explains the large deviancy in the
 52 V_{OC} values for TiO₂ (from 0.6 – 1.1 V, see **Table 1 and 3**), a material well-known for mid-
 53 bandgap traps. Furthermore, appropriate ESC and HSC significantly reduces interfacial
 54 recombination.^[63] For example, in a comparative study of MAPbI₃ perovskite films
 55
 56
 57
 58
 59
 60
 61
 62
 63
 64
 65

1 deposited on top of TiO₂ with and without a HSC (spiro-OMeTD), the former showed 0.25 V
2 higher V_{OC} than the latter.^[77]
3

4
5 Energetics of the selective contacts also influence the V_{OC}. For example, regarding the
6 dependency of V_{OC} on HSC HOMO level (or LUMO of the ESC), it showed ~0.45 V
7 increment (from 1.05 to 1.51 V) when P3HT (E_{HOMO}=-5.0 eV) is replaced with PIF8-TAA
8 (E_{HOMO}=-5.51 eV).^[81] However, band alignment is not the most determinant factor limiting
9 the V_{OC}. This is the reason of higher V_{OC} in SnO₂ than TiO₂,^[82] a material with ~300 meV
10 lower CB edge than TiO₂, yet with higher electron mobility and lesser surface defects than
11 TiO₂,^[41, 42] making the V_{OC} of the former overcome the one of the later despite an *a priori*
12 worst level alignment. Similarly, the V_{OC} is also influenced by the selectivity of a contacts^{[83,}
13
14
15
16
17
18
19
20
21
22
23
24
25
26
27
28
29
30
31
32
33
34
35
36
37
38
39
40
41
42
43
44
45
46
47
48
49
50
51
52
53
54
55
56
57
58
59
60
61
62
63
64
65

66
67
68
69
70
71
72
73
74
75
76
77
78
79
80
81
82
83
84
85
86
87
88
89
90
91
92
93
94
95
96
97
98
99
100
101
102
103
104
105
106
107
108
109
110
111
112
113
114
115
116
117
118
119
120
121
122
123
124
125
126
127
128
129
130
131
132
133
134
135
136
137
138
139
140
141
142
143
144
145
146
147
148
149
150
151
152
153
154
155
156
157
158
159
160
161
162
163
164
165
166
167
168
169
170
171
172
173
174
175
176
177
178
179
180
181
182
183
184
185
186
187
188
189
190
191
192
193
194
195
196
197
198
199
200
201
202
203
204
205
206
207
208
209
210
211
212
213
214
215
216
217
218
219
220
221
222
223
224
225
226
227
228
229
230
231
232
233
234
235
236
237
238
239
240
241
242
243
244
245
246
247
248
249
250
251
252
253
254
255
256
257
258
259
260
261
262
263
264
265
266
267
268
269
270
271
272
273
274
275
276
277
278
279
280
281
282
283
284
285
286
287
288
289
290
291
292
293
294
295
296
297
298
299
300
301
302
303
304
305
306
307
308
309
310
311
312
313
314
315
316
317
318
319
320
321
322
323
324
325
326
327
328
329
330
331
332
333
334
335
336
337
338
339
340
341
342
343
344
345
346
347
348
349
350
351
352
353
354
355
356
357
358
359
360
361
362
363
364
365
366
367
368
369
370
371
372
373
374
375
376
377
378
379
380
381
382
383
384
385
386
387
388
389
390
391
392
393
394
395
396
397
398
399
400
401
402
403
404
405
406
407
408
409
410
411
412
413
414
415
416
417
418
419
420
421
422
423
424
425
426
427
428
429
430
431
432
433
434
435
436
437
438
439
440
441
442
443
444
445
446
447
448
449
450
451
452
453
454
455
456
457
458
459
460
461
462
463
464
465
466
467
468
469
470
471
472
473
474
475
476
477
478
479
480
481
482
483
484
485
486
487
488
489
490
491
492
493
494
495
496
497
498
499
500
501
502
503
504
505
506
507
508
509
510
511
512
513
514
515
516
517
518
519
520
521
522
523
524
525
526
527
528
529
530
531
532
533
534
535
536
537
538
539
540
541
542
543
544
545
546
547
548
549
550
551
552
553
554
555
556
557
558
559
560
561
562
563
564
565
566
567
568
569
570
571
572
573
574
575
576
577
578
579
580
581
582
583
584
585
586
587
588
589
590
591
592
593
594
595
596
597
598
599
600
601
602
603
604
605
606
607
608
609
610
611
612
613
614
615
616
617
618
619
620
621
622
623
624
625
626
627
628
629
630
631
632
633
634
635
636
637
638
639
640
641
642
643
644
645
646
647
648
649
650
651
652
653
654
655
656
657
658
659
660
661
662
663
664
665
666
667
668
669
670
671
672
673
674
675
676
677
678
679
680
681
682
683
684
685
686
687
688
689
690
691
692
693
694
695
696
697
698
699
700
701
702
703
704
705
706
707
708
709
710
711
712
713
714
715
716
717
718
719
720
721
722
723
724
725
726
727
728
729
730
731
732
733
734
735
736
737
738
739
740
741
742
743
744
745
746
747
748
749
750
751
752
753
754
755
756
757
758
759
760
761
762
763
764
765
766
767
768
769
770
771
772
773
774
775
776
777
778
779
780
781
782
783
784
785
786
787
788
789
790
791
792
793
794
795
796
797
798
799
800
801
802
803
804
805
806
807
808
809
810
811
812
813
814
815
816
817
818
819
820
821
822
823
824
825
826
827
828
829
830
831
832
833
834
835
836
837
838
839
840
841
842
843
844
845
846
847
848
849
850
851
852
853
854
855
856
857
858
859
860
861
862
863
864
865
866
867
868
869
870
871
872
873
874
875
876
877
878
879
880
881
882
883
884
885
886
887
888
889
890
891
892
893
894
895
896
897
898
899
900
901
902
903
904
905
906
907
908
909
910
911
912
913
914
915
916
917
918
919
920
921
922
923
924
925
926
927
928
929
930
931
932
933
934
935
936
937
938
939
940
941
942
943
944
945
946
947
948
949
950
951
952
953
954
955
956
957
958
959
960
961
962
963
964
965
966
967
968
969
970
971
972
973
974
975
976
977
978
979
980
981
982
983
984
985
986
987
988
989
990
991
992
993
994
995
996
997
998
999
1000

1 despite its lower electron mobility ($0.0069 \text{ cm}^2\text{V}^{-1}\text{s}^{-1}$) than the latter ($0.061 \text{ cm}^2\text{V}^{-1}\text{s}^{-1}$). Here,
2 the higher lying LUMO level of ICBA facilitated better balancing electron quasi-Fermi level
3
4 during device operation under illumination which would have created a higher built in
5
6 potential across the device.^[88]
7
8
9
10
11
12
13
14
15
16
17
18
19
20
21
22
23
24
25
26
27
28
29
30
31
32
33
34
35
36
37
38
39
40
41
42
43
44
45
46
47
48
49
50
51
52
53
54
55
56
57
58
59
60
61
62
63
64
65

Table 1: A comparison of state-of-the-art open circuit voltage obtained using various halide perovskites in conjunction with a diverse range of electron and hole selective contacts. The CB and VB edges for MAPbI₃ and MAPbBr₃ are (-3.9/-5.4) eV and (-3.4/-5.6) eV, respectively.

V _{oc} (V)	J _{sc} (mA/cm ²)	FF	PCE (%)	ESC	Device architecture	HSC	Band edges (CB/HUMO) [†]	Electron/Hole mobility (cm ² V ⁻¹ s ⁻¹)	Device	qV _{oc} /E _G (%)	E _G -qV _{oc} (eV)	Reference
1.21	22.5	0.77	20.7	c-SnO ₂	Triple cation (Cs,MA,FA) and mixed Halide(I, Br) based	Spiro-OMETAD	--	~150 (SnO ₂) ^[89]	Planar	76	0.38	[82]
1.13	22.5	--	19.4	PCBM/C ₆₀ /BCP	MAPbI ₃	PTAA ^{*a}	-3.9 [■]	10 ⁻³ (PCBM)	planar	71	0.47	[83]
1.11	21.00	0.76	17.9	c,m-TiO ₂	Cs _x (MA _{0.17} FA _{0.83}) _(100x) Pb(I _{0.83} Br _{0.17}) ₃	Spiro-OMETAD	-4.4 [■] /-5.11 [▲]	10 ⁻³ - 10 ⁻⁴ (HSC), ^[90]	Mesoporous PSC	72	0.44	[12]
1.13	22.7	0.75	19.3	Y-TiO ₂ ^{*b}	CH ₃ NH ₃ PbI _{3-x} Cl _x	Spiro-OMETAD	-5.11 [▲]	10 ⁻³ - 10 ⁻⁴ (HSC), ^[90]	n-i-p planar	61	0.72	[11]
1.29	6.60	0.70	5.9	TiO ₂	MAPbBr ₃	P-TAA	-5.14 [▲]	>0.1 (HSC), ^[91]		56	1.01	[92]
1.36	6.30	0.70	6.0	TiO ₂	MAPbBr ₃	PF8-TAA ^{*c}	-5.44 [▲]	4×10 ⁻³ (HSC)	Mesoporous PSC	59	0.94	
1.40	6.10	0.79	6.7	TiO ₂	MAPbBr ₃	PIF8-TAA ^{*c}	-5.51 [▲]	4×10 ⁻² (HSC)		61	0.90	
1.04	21.3	0.73	16.2	TiO ₂	MAPbI ₃	P-TAA	-5.14 [▲]	>0.1, ^[91] (HSC)		67	0.51	
0.92	8.90	0.56	4.6	TiO ₂	MAPbI ₃	PF8-TAA	-5.44 [▲]	4×10 ⁻³ (HSC)		59	0.63	
1.04	19.0	0.46	9.1	TiO ₂	MAPbI ₃	PIF8-TAA	-5.51 [▲]	4×10 ⁻² (HSC)		67	0.51	
1.50	4.00	0.47	2.7	Al ₂ O ₃	MAPbBr _{3-x} Cl _x	CBP ^{*d}	6 – 6.2 [▲] [93]		MSSC	70	0.73	[87]
1.38	5.2	0.78	5.6	PCBM ^{*e}	MAPbBr ₃	PEDOT:PSS	-3.9 [■] /-5.3 [▲]		p-i-n	60	0.92	[94]
1.61	6.04	0.77	7.5	ICBA ^{*f}	MAPbBr ₃	PEDOT:PSS	-3.7 [■] /-5.3 [▲]		inverted	70	0.69	[94]

^{*a}**P-TAA**: Poly[bis(4-phenyl)(2,4,6-trimethylphenyl)amine]

^{*c}**PIF8-TAA**: poly-indenofluorene-8-triarylamine

^{*e}**PCBM**: Phenyl-C61-butyric acid methyl ester

^{*b}**Y-TiO₂**: Yttrium doped TiO₂

^{*d}**CPB**: 4,4'-bis(N-carbazolyl)-1,1'-biphenyl

^{*f}**ICBA**: 1',1'',4',4''-tetrahydro-di[1,4]methanonaphthaleno[1,2:2',3',5,6:2'',3''] [5,6] fullerene-C60

■ for CB/conduction band edge of ESC and ▲ for HUMO of HSC

5 Hysteresis in PSCs - Role of interfaces

The hybrid perovskites show exceptional optoelectronic properties so as to be incorporated in new kind of devices with efficient architectures.^[3, 95] However, the observations of particular phenomena as $J-V$ curve hysteresis, and switchable response by voltage pretreatment,^[96] point to the fact that mechanisms underlying PSCs performance are still only partially understood. Particularly intriguing is the scan-rate dependent hysteresis in the $J-V$ curves^[97, 98, 99] that result in an overestimation of the photovoltaic performance when current is registered from forward-to-reverse bias sweep direction. If voltage is swept oppositely one finds lower performances, mainly through reduction in the FF as shown in **Fig. 9**. Hysteresis has been related to a number of different explanations, as ferroelectric properties of the perovskite materials,^[100] delayed electronic trapping processes,^[101] slow ion migration,^[98, 102] or interfacial capacitive effect.^[103] Because the performance of PSCs is heavily affected by voltage scan rate and preconditioning procedures^[101, 104] concerns about device stability and reliability have appeared. As a consequence recommendations were also provided so as to show photovoltaic behavior without masking the detrimental hysteresis effect.^[105]

It is widely observed that hysteresis is more apparent in planar architectures of regular deposition sequence (ITO/c-TiO₂/perovskite/*spiro*-OMeTAD/Au),^[99] in opposition to devices comprising a mesoscopic TiO₂ layer which exhibit reduced hysteretic effect.^[97, 106] The degree of hysteresis is however highly dependent on the perovskite preparation route, type and deposition method of interfaces, and specific testing conditions.^[107] It is widely recognized that operation modes of PSCs greatly depend on the structure and composition of the cathode contact. Several researchers have shown a significant hysteresis reduction in planar PSCs when MOS ETLs at cathode contacts are modified. The incorporation of a self-assembled monolayer (SAM) of C₆₀ on the planar TiO₂ film acting as electron collector was demonstrated to change dramatically the

operation characteristic of $\text{CH}_3\text{NH}_3\text{PbI}_{3-x}\text{Cl}_x$ PSCs, and reduces hysteresis effects.^[108] It is believed that the fullerene derivative-SAM inhibits the formation of trap states at the TiO_2 /perovskite interface, blocking as a consequence recombination paths. Modifying TiO_2 interface by fullerene post treatment has improved solar cell operation.^[109] An alternative way aimed at reducing the hysteresis effect is the treatment of TiO_2 layer with Li. Li-treated TiO_2 matrix is formed by spin Bis(trifluoromethane)sulfonimide lithium salt (Li-TFSI)/acetonitrile solution on the untreated mesoscopic TiO_2 . It is shown that $J-V$ hysteresis is further reduced by suppression of surface traps in comparison to bare mesoporous TiO_2 -based PSCs.^[110] Similarly, incorporation of Zr into TiO_2 also demonstrated reduced hysteresis compared to a bare analogue due to interface modification and passivation of defect sites.^[111]

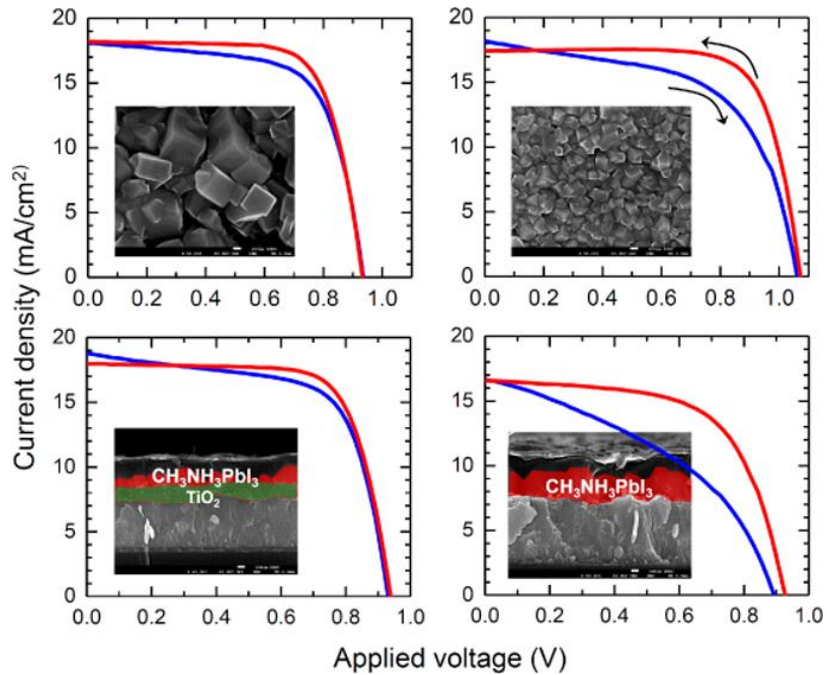


Fig. 9: Some examples of the variation of the hysteretic response as a function of the $\text{CH}_3\text{NH}_3\text{PbI}_3$ crystal size and solar cell structure. Reprinted with permission from ref.^[107]

Inverted planar architectures in which the cathode contact is deposited on top of the layer stack, replicating the OPVs, have exhibited significant or total hysteresis suppression (**Fig. 10**),

1
2
3
4 pointing to the important role of interfaces in this effect. For instance, devices comprising
5
6 poly(3,4-ethylenedioxythiophene) poly(styrenesulfonate) (PEDOT:PSS) as anode contact and
7
8 thin PCBM (20 nm)/C₆₀ (20 nm) films as ETL showed improved operating characteristics.^[101]
9
10 Again, the reduction in hysteresis was connected to the PCBM-induced passivation of
11
12 CH₃NH₃PbI₃ interfacial traps. Incorporation of LiF on PCBM also produced beneficial outcomes
13
14 in terms of hysteresis reduction and photocurrent increment.^[112] Very recently it has been
15
16 observed that a reduction in hysteresis occurs not only by cathode layer engineering but also by
17
18 deposition of hybrid PCBM/perovskite absorbers between planar TiO₂ and *spiro*-OMeTAD
19
20 transporting layers.^[113] This would suggest that hysteresis is largely related to the characteristics
21
22 of selective contacts, as also depicted in **Fig. 10**, which compares hysteresis profile of various
23
24 best performing devices from all six device architectures of PSCs and also those built on flexible
25
26 substrates.
27
28
29
30
31
32
33
34
35
36
37
38
39
40
41
42
43
44
45
46
47
48
49
50
51
52
53
54
55
56
57
58
59
60
61
62
63
64
65

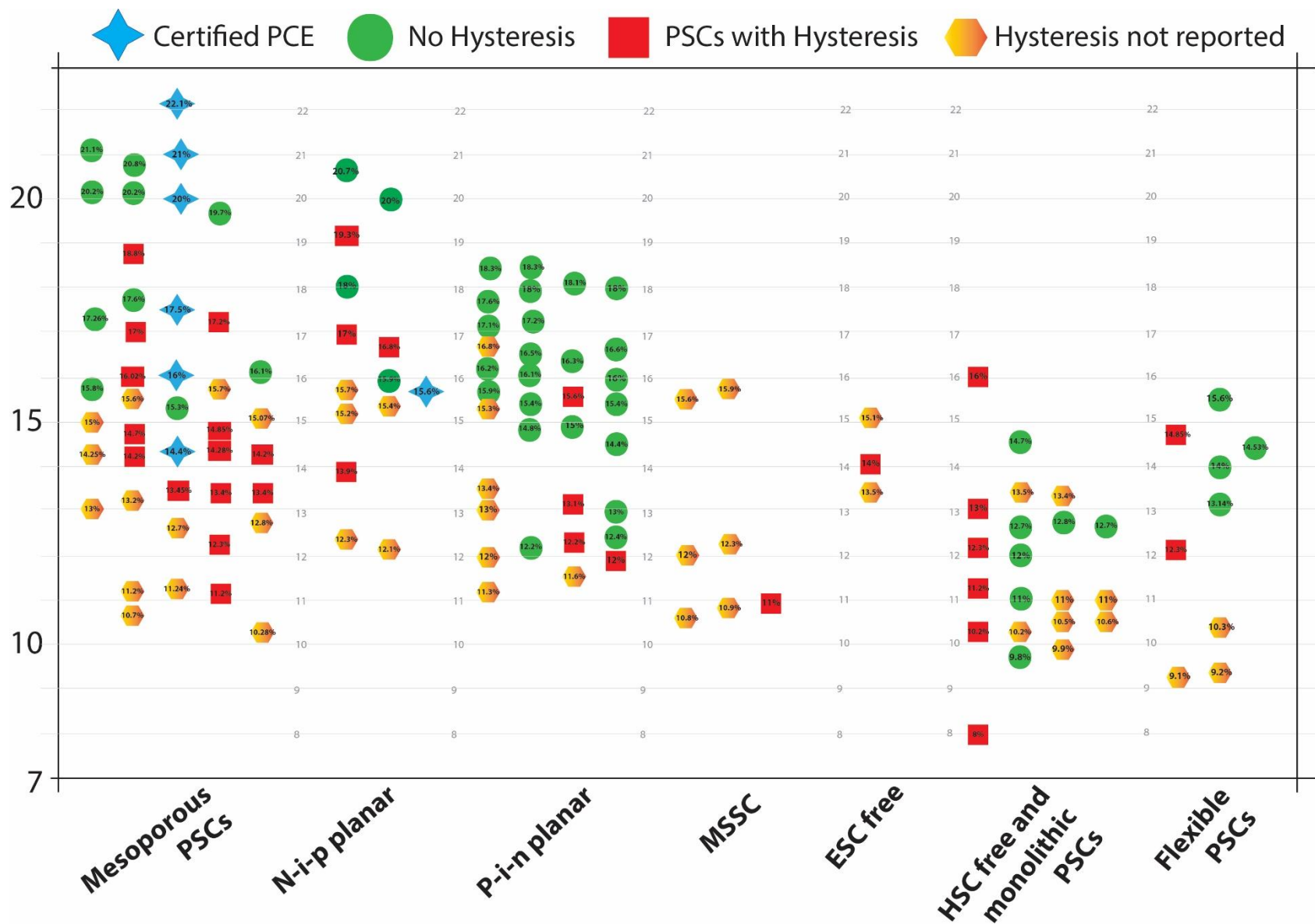


Figure 10: PCE and hysteresis measured for most successful PSCs in all six architectures and also the flexible PSCs (a total of 132). A device with relative variation $\leq 5\%$ in PCE is only considered to be hysteresis-free. Detail PVs parameters (including J_{sc} , V_{oc} , FF), details on material components (ESC, HSC, perovskite), and reference of each corresponding PSC will be explained in **Table 2** of the manuscript.

1
2
3
4 Suppression of the $J-V$ hysteresis observed with inverted structures comprising
5
6 fullerene molecules as cathode interlayers at varying scan rates is usually checked at room
7
8 temperature. This opens the question of the kinetic origin for the hysteresis reduction. If the time
9
10 scale underlying the hysteresis is greater than the time window defined by the scan rate, $J-V$
11
12 distortion is expected to be invisible. By cooling $\text{CH}_3\text{NH}_3\text{PbI}_3$ solar cells with top cathode
13
14 containing fullerenes below room temperature significant hysteresis does appears where the
15
16 thermally activated kinetic processes have been slowed down.^[114] Slower relaxation of hysteretic
17
18 processes seems to be behind $J-V$ curve insensitivity on scan direction at higher
19
20 temperatures/rates.^[115] Recently a distinction between capacitive and non-capacitive hysteretic
21
22 currents has been made.^[116] The former being related to the charge, both ionic and electronic,
23
24 accumulation ability of the TiO_2 /perovskite interface without any influence on the steady-state
25
26 operation.
27
28
29
30
31
32

33 Non-capacitive hysteresis is observable in all kind of architectures being more prominent
34
35 in inverted architectures, including organic compounds as bottom hole selective layers and
36
37 fullerene materials as top contact, with larger distortions caused by the inherent reactivity of
38
39 contact materials and absorber perovskites.^[116] While capacitive hysteresis gives rise to reversible
40
41 variations of the $J-V$ curves that enlarge with the scan rate, non-capacitive hysteresis yields
42
43 pronounced distortions of the operation currents at slow time scale.^[117] Importantly,
44
45 noncapacitive hysteresis behaves in the opposite way (positive current contributions for reverse
46
47 sweep directions) in comparison to capacitive contributions.^[116] Irreversible chemical
48
49 interactions at the perovskite/contact interfaces in relation to aging processes have been proposed
50
51 to account for noncapacitive hysteresis,^[118] along with strong electrical field enhancement by
52
53 dipole layers in the vicinity of the contacts.^[119] Recent reports reinforce the previously discussed
54
55
56
57
58
59
60
61
62
63
64
65

1
2
3
4 explanation of hysteretic phenomena in terms of mechanisms occurring at the outer interfaces of
5
6 the perovskite solar cells.^[120, 121]
7
8
9

10 **6 Interface engineering and device designs in PSCs**

11 Research in interface engineering can be classified into two categories: (i) interface
12 engineering via screening alternative selective contact materials or their various morphologies,
13
14 and (ii) surface modification of selective contact (mostly TiO₂ and ZnO) to alter the charge
15
16 carrier dynamics – both to influence stability, working mechanism, improving charge kinetics
17
18 and hysteresis in PSCs. Owing to the crucial role the interfaces (or the interfacing materials) play
19
20 for PSCs, a rise in dedicated research activities can also be observed for them (see **Fig. 11**) in a
21
22 similar fashion to that of the PSCs. For example, the conventionally employed TiO₂ or ZnO –
23
24 well-known for their inferior electronic transport and surface defects, respectively, are replaced
25
26 with high mobility SnO₂ or their doped counterparts and various binary oxides such as BaSnO₂,
27
28 Zn₂SnO₄, and SrTiO₃. Similar, high performance (PCE 18 –19%) and stability of few hundreds
29
30 of hours in planar architectures of PSCs, which often demonstrates reduced trap-assisted non-
31
32 radiative recombination, is also noticed owing to the judicious selection of interfacing materials.
33
34 For example, inverted PSCs (p-i-n) are known for unstable performance due to the presence of
35
36 organic selective contacts (PEDOT:PSS and PCBM). Replacement of organic HSC
37
38 (PEDOT:PSS) by an inorganic counterpart (NiO) and PCBM by inorganic TiO₂ or ZnO has
39
40 shown that the device could retain >90% of initial PCE after 60 days of testing at ambient.^[122]
41
42 Similarly, surface modification of ESC (TiO₂) has also improved UV-photo stability of the
43
44 devices^[123] and also restricted degradation of perovskite at the ESC-perovskite interface,^[36, 124] as
45
46 will be discussed in the stability section of this article.
47
48
49
50
51
52
53
54
55
56
57
58
59
60
61
62
63
64
65

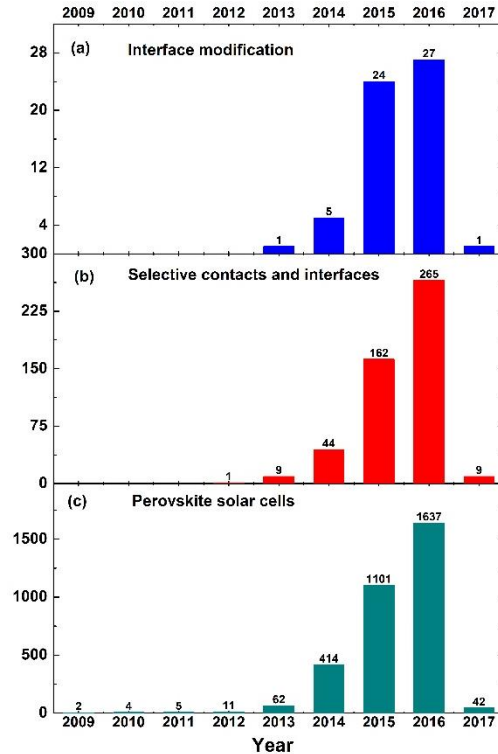


Figure 11: A trend of research publications showing a comparison between total articles on perovskite solar cells, selective contacts and interfaces, and interface engineering/modification in PSCs since their inception in 2009 till date (14December 2016). The data is obtained from Scopus using key words “*perovskite solar cells*”, “*perovskite solar cells and interface*” and “*perovskite solar cells AND interface modification/engineering*”, respectively.

6.1 Nanostructured scaffolds for perovskite solar cells

Typically, the state-of-the-art efficiency (20- 22%) is obtained for devices with TiO₂ scaffold (See Table 3 and Fig.10), although recently a first planar PSC with PCE >20% is also demonstrated.^[125] Despite the fact that the origin of this effect is not fully understood, Anaya et al.^[66] suggested that the mesoporous scaffold could hinder ion migration producing lower majority carrier accumulation at the interface and consequently a lower recombination thereby. A more clear interpretation of the advantageous effects of the scaffold can be understood in the case of lead-free perovskites. Given the diffusion length (L_D) of perovskite is shorter for such perovskites than the light absorption length, scaffold helps in the photocarrier collection. For

1
2
3
4 example, no photocurrent is measured in planar ASnX_3PSCs whereas the mesoporous rivals
5
6 showed high J_{SC} ($15 - 21 \text{ mA cm}^{-2}$).^[126]
7
8

9 Ever since the first report on PSCs,^[3] TiO_2 nanoparticles (NPs) scaffold has been a
10 successful material of choice and the highest PCE $\sim 20 - 22.2\%$ in PSCs is achieved using the
11 them in conjunction with optimized perovskite, i.e., combining formamidinium (FA) and methyl
12 ammonium (MA) as inorganic cations^[23] and I and Br as anions, and using molecularly
13 engineered HSC.^[24] For example, a high PCE $\sim 20.8\%$ is obtained using mixed perovskite
14 containing MA and FA and also I and Br over TiO_2 scaffold whereas the device reporting PCE
15 21.1% utilized a perovskite with triple cation (MA/FA/Cs).^[12, 25] The key reason behind the
16 success of TiO_2 NPs is the intensive research being carried out to develop high quality pastes that
17 provide a porous architecture ultimately providing a desired scaffold for perovskite crystals.
18
19
20
21
22
23
24
25
26
27
28
29
30

31 Despite the fact that the TiO_2 NPs are the champion material, they offer various
32 challenges that ought for a commercial deployment of PSCs that would require efficient, stable
33 and cost-effective material constituents. The key problems associated with TiO_2 NPs are their
34 susceptibility to UV light^[37], its low electron mobility ($\mu_e < 0.1 \text{ cm}^2 \text{ v}^{-1} \text{ s}^{-1}$)^[89, 127] their sub-bandgap
35 trap states that hinders charge collection, their surface defects that are reported to act as a
36 humidity trap and also known to form a reactive interface to perovskite making it vulnerable to
37 degradation.^[36, 124] Also, TiO_2 layer require sintering at high temperature ($\sim 450^\circ\text{C}$)^[19, 128] which
38 is not compatible with roll-to-roll production. This brings into account the UV-stable SnO_2 ^[41, 42]
39 and low-temperature processable ZnO nanostructures^[129-131]; materials that offer higher electron
40 mobility than TiO_2 . However, ZnO nanoparticles have not been a very successful choice in
41 PSCs, particularly when employed as a mesoporous scaffold, resulting in a typical PCE $9 -$
42 10.5% .^[132, 133] Despite the fact that ZnO films can be processed at temperature as low as
43
44
45
46
47
48
49
50
51
52
53
54
55
56
57
58
59
60
61
62
63
64
65

1
2
3
4 ~70°C,^[133] they typically experience interfacial charge recombination, primarily due to presence
5
6 of defect states in ZnO and a lower PCE thereby. The reasons for lower performance in ZnO
7
8 based PSCs is also understood to be the decomposition of perovskite crystals when deposited on
9
10 ZnO-NPs surface. An investigation of the CH₃NH₃PbI₃ crystal growth on bare ZnO-NPs film
11
12 shows that the presence of hydroxide groups and residual acetate ligands on the surface of ZnO
13
14 lead to deprotonation of perovskite crystals,^[134] an issue which can partly be overcome via
15
16 suitable doping^[135] or via sintering the films at higher temperature^[136] to remove defect states.
17
18 Another remedy is to add a buffer layer such as PC₆₁BM between ZnO and perovskite which has
19
20 shown to effectively reduce charge recombination at ZnO-perovskite interface and improved
21
22 PCE from ~6.4% to ~10.2%,^[134] however the best performance of ZnO/buffer-layer PSCs is still
23
24 reported in planar device architectures (PCE 15.9%)^[137] that will be discussed in a subsequent
25
26 section of planar PSCs. Nevertheless, the performance in ZnO based PSCs is improved by either
27
28 employing pure (PCE ~ 10–11%)^[138] or doped one-dimensional nanorods (PCE ~ 14.35%),^[139]
29
30 and their planar (PCE up to 15.7%)^[140] or inverted planar device architectures (PCE ~16.1%)^[122].

31
32
33
34
35
36
37
38 PSCs based on SnO₂, unlike its ZnO counterparts, have shown great success with an
39
40 average PCE as high as ~16% (photocurrent density (J_{SC}) ~22.8 mA/cm², open circuit voltage
41
42 (V_{OC}) ~1.11 V and fill factor (FF) ~0.64) owing to their high electronic mobility.^[141] The highest
43
44 performance using SnO₂ nanocrystals, till date, is achieved in inverted PSCs in conjunction with
45
46 NiO as HSC (PCE 18.8%) which also showed remarkably stable performance for 30 days at high
47
48 humidity conditions.^[142]

49
50
51
52
53 CdS quantum dots and Nb₂O₅ are two other ESC materials employed in PSCs owing to
54
55 their higher electronic conductivity and significantly higher CB and demonstrated
56
57 PCE ~11.2%^[143] and 8.8%, respectively.^[144] In addition, binary oxides such as SrTiO₃,^[145]
58
59
60
61
62
63
64
65

1
2
3
4 ^{146]}BaSnO₃ and Zn₂SnO₄ have been reported in PSCs.^[146] It is important to note that SrTiO₃ has
5
6 nearly similar conduction band edge (CB) as that of CH₃NH₃PbI₃, i.e., -3.9 eV(vs. vacuum)
7
8 where electron injection might be an issue; and therefore, CH₃NH₃PbI_{3-x}Cl_x with CB at ~-3.8 eV
9
10 (vs. vacuum) is more favored for electron injection. Similarly, BaSnO₃ having a similar crystal
11
12 structure as that of MAPbI₃ is employed in PSCs that demonstrated PCE ~12.3%, higher than
13
14 that of a reference device made using TiO₂ (PCE ~11.1%).^[147] However, the PSCs employing
15
16 BaSnO₃ showed higher charge recombination at high bias voltage and also a very high
17
18 hysteresis. Another successful material that offers high electron mobility (10–30 cm²V⁻¹s⁻¹)^[148] is
19
20 Zn₂SO₄. Till date, the best performance in Zn₂SO₄ PSCs is reported when a thin flat layer is
21
22 deposited over flexible substrates (PET/ITO) via low temperature processing resulting in PCE
23
24 ~14.85%.^[149] This high performance is achieved by developing a pin-hole free flat perovskite
25
26 layer over a Zn₂SO₄ flat film via spin coating at a temperature ~100°C which also makes it
27
28 compatible with roll-to-roll processing.
29
30
31
32
33
34
35

36 6.1.1 Doped and Composite ESC Materials

37 Doping have been known as an effective method to modify electronic bands structure of
38
39 MOS in organic solar cells^[150] which routinely resulted in improved PV parameters, particularly,
40
41 the V_{OC}.^[151] In mesoscopic PSCs, doping has shown to improve charge transport properties
42
43 eventually overcoming the interfacial recombination and hysteresis and also have demonstrated
44
45 an increase in the V_{OC} in these device.^[135, 152-156] In such cases, the CB is tuned by suitably
46
47 doping a metal ion, such as Y³⁺, Al³⁺, Nb⁵⁺, and Mg²⁺ etc., into crystal lattice of MOS ESC
48
49 (typically TiO₂, ZnO or SnO₂).^[152, 153, 157, 158]
50
51
52
53

54 A crucial aspect during doping is to optimize the dopant concentration because addition
55
56 of impurities induces strains in the TiO₂ crystal which increases grain boundaries within the
57
58 TiO₂. Nb doping by Kim et al^[155] showed that while 0.5% Nb doping in TiO₂ resulted in
59
60
61
62
63
64
65

1
2
3
4 improved optical properties, a further increase in dopant concentration to 1 and 5% lowered the
5
6 device performance. The 0.5% doping resulted in V_{OC} as high as 990 mV, ~40 mV higher than
7
8 pure TiO_2 analogues, higher J_{SC} and FF and demonstrated a final PCE ~13.4% notably higher
9
10 than pure TiO_2 (~12.9%).
11
12

13
14 Doping has also shown to reduce charge recombination at MOS/perovskite interface by
15
16 reducing the surface defects of the ESC and also played a role in improving perovskite
17
18 crystallization behavior. In a report by Qin et al,^[159] 0.5% Y^{3+} doped TiO_2 although resulted in
19
20 15% improved J_{SC} , surprisingly no change in V_{OC} is observed. Other possibilities to modify the
21
22 ETL crystal structures are through incorporation of Nb^{5+} and Ga^{3+} or coating with a thin layer of
23
24 an insulating oxide such as ZrO_2 or $CaCO_3$, strategies that have demonstrated potential to alter
25
26 electron injection dynamics by modifying the interface properties in DSCs.^[160]
27
28
29

30
31 The ESC – $CH_3NH_3PbX_3$ interface is a possible recombination center which not only
32
33 suppresses the FF in PSCs but often also results in inferior V_{OC} . Herein, surface coating of
34
35 scaffold layer is a remedy to avoid charge recombination.^[161] For example, Han et al^[162] reported
36
37 modification TiO_2 ETL in PSCs using an ultrathin MgO layer (1 –2 nm) on TiO_2 NPs that
38
39 extended carrier lifetime (τ_n). The V_{OC} increased from ~840 mV (PCE 11.4%) to ~1000 mV
40
41 (PCE 12.7%) when the MgO layer thickness is systematically increased. Despite the
42
43 improvement in V_{OC} the J_{SC} decreased while increasing the insulating over-layer thickness
44
45 beyond a critical threshold due to reduced electron injection owing to large bandgap of MgO
46
47 monolayer (7.8 eV) compared to TiO_2 (3.2 eV). Similar strategy adopted in ZnO MOS, a
48
49 material known for its surface defects^[129] and to decompose perovskite crystals during thermal
50
51 annealing,^[134] resulted in PCE ~4.3% and ~15.4% in ZnO/CdS NPs^[163] and ZnO-NRs/ TiO_2 -
52
53 NP^[164] core-shell architectures, respectively. The ZnO surface modification not only resulted in
54
55
56
57
58
59
60
61
62
63
64
65

performance improvement due to improved light absorption, passivation of the notorious defect states, and improved charge injection efficiency from $\text{CH}_3\text{NH}_3\text{PbI}_3$ to ETL, but also, more importantly, eliminated the perovskite degradation on its surface and reduced the anomalous hysteresis significantly. A similar progress is also shown in WO_3 - TiO_2 core-shell architectures resulted in $\sim 11.2\%$ PCE where a highly porous WO_3 ETL is post-treated with a thin TiO_2 NP layer (**Fig. 12**).^[165]

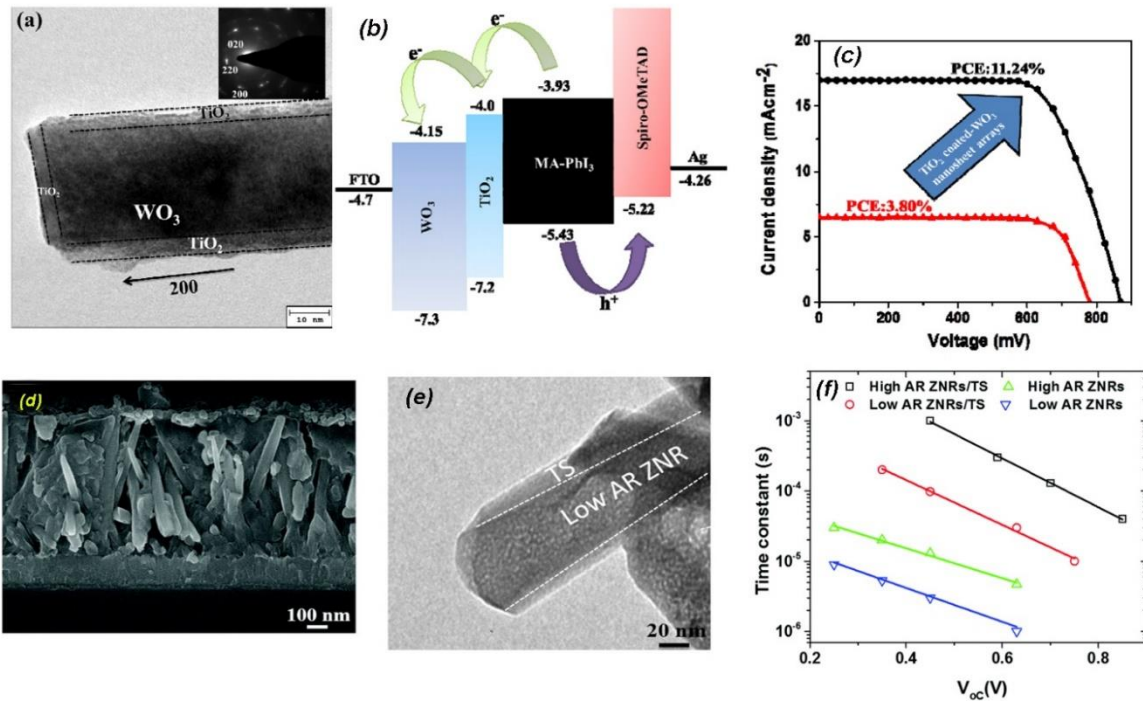


Fig. 12: (a) TEM image of WO_3 - TiO_2 core-shell nanorod, (b) energy level diagram of the $\text{WO}_3/\text{CH}_3\text{NH}_3\text{PbI}_3/\text{HTM}/\text{Ag}$ device exhibiting a favored electron injection and hole extraction, (c) a characteristic current-voltage curve of a pure WO_3 and a WO_3 - TiO_2 core-shell analogue,^[165] (d) cross-sectional view of device employing ZnO nanorods coated with TiO_2 (ZNRs), (e) TEM image of a ZNR with TiO_2 shell (TS), and (f) charge recombination lifetime of four different ETL-based PSCs, employing various ratio of ZNR and TS.^[164] Figures reproduced with permission from the referred articles.

6.1.2 One-dimensional and three-dimensional electron selective contacts

The electron transport through a material strongly depends on its morphology; the transport is anisotropic for one- and three-dimensional nano-architectures such as wires, flowers and hierarchical structures. Available evidences suggest that charge separation and transport in PSCs take place within perovskite, perovskite-ESC and perovskite-HSC interfaces; therefore,

morphology of the selective contacts are detrimental for the interfacial recombination and hence the PCE.^[166] The diffusion lengths of electron and hole in hybrid perovskites are over $\sim 1 \mu\text{m}$ ^[167] with orders of magnitude higher electron mobility than materials used for ESC and HSC (Table 1), which makes the charge recombination significant at the interfaces. This put stringent conditions, particularly on ESC, to be a material of high charge mobility and defect-free. Besides the inferior electronic mobility of the typically employed TiO_2 NPs, another crucial issue is their poor pore-filling due to labyrinthine mesoporous morphology which could be resolved by employing one-dimensional materials with more porous morphology such as nanotubes (NTs), nanowires (NWs), nanorods (NRs) or hierarchical structures (HS).

Table 2: Values are taken from ref^[168] if not stated otherwise.

Material/Morphology	Diffusion Length (μm)	Diffusion coefficient ($\text{cm}^2 \text{s}^{-1}$)	Charge mobility ($\text{cm}^2 \text{V}^{-1} \text{s}^{-1}$)
$\text{CH}_3\text{NH}_3\text{PbI}_3$	14.0 ± 5.1	1.59 – 2.41	56.4 to 93.9 ^[168, 169]
$\text{CH}_3\text{NH}_3\text{PbBr}_3$	6.0 ± 1.6	0.50 to 1.44	19.4 – 56.1
$\text{CH}_3\text{NH}_3\text{PbI}_x\text{Cl}_{3-x}$	~ 8 times higher than $\text{CH}_3\text{NH}_3\text{PbI}_3$ ^[167]	~ 2.5 times higher than $\text{CH}_3\text{NH}_3\text{PbI}_3$ ^[167]	~ 2.5 times higher than $\text{CH}_3\text{NH}_3\text{PbI}_3$ ^[167]
TiO_2 (spherical)	10 – 90 ^[170]	$\sim 10^{-5}$ – 10^{-4} ^[171]	1×10^{-7} , ^[127, 172]
TiO_2 (1-D)		2 order of magnitude higher than NPs ^[171]	2 order of magnitude higher than NPs ^[171]
Spiro-OMeTAD	--	--	4×10^{-5} Ref ^[173]
P3HT			$\sim 10^{-4}$ – 10^{-3} , ^[174]

Alternative morphologies to NPs, which are known for inferior electronic transport and large grain boundary density, have been widely adopted to improve charge kinetics at the interfaces. Such morphologies improved charge collection in PSCs, particularly those made using ZnO. The state-of-the-art PCE of TiO_2 NP and 1D nanostructures is 21.2% (although 22.1% is published in NREL efficiency chart, the details of the device are not given) and 14%, respectively, whereas in ZnO these values are 15.7% and 16.1%, respectively (**Table**

1
2
3
4 **3)**,clearlydemonstrating the beneficial effects in the latter in removing surface defect when
5
6 employing 1D nanostructures. A detailed account of such various key-reports is listed in **Table**
7
8 **3**.The first report on TiO₂ NRs PSCs was by Kim et al^[175] who employed highly crystalline NRs,
9
10 a material that offers two orders of magnitude higher electron mobility than their NP
11
12 counterparts, and reported a PCE ~9.4% (J_{SC} ~15.6 mA/cm²). Surface passivation of the ESC
13
14 interface (TiO₂nanorods) by a thin TiO₂ layer grown via atomic layer deposition resulted in
15
16 further improvement in PCE (13.45%),^[176] which is also, to the best of our knowledge, the best
17
18 PCE by a pure TiO₂ NR PSC. In addition to the pristine TiO₂ NRs, their doped analogues such as
19
20 Mg-, Sn- and Nb-doped are also employed in PSCs resulting in PCE ~4.17%,^[152] 7.5%,^[153] and
21
22 6.3%,^[154] respectively. In addition to TiO₂ NRs, ZnO NRs ESC (thickness ~600 nm) have also
23
24 demonstrated a PCE ~14.35%, achieved in their surface modified architectures by over coating a
25
26 thin TiO₂ layer (<10 nm). The efficiency is slightly lower in pure ZnO NRs (13.4%) prepared by
27
28 magnetron sputtering (thickness <200 nm),^[177] which is the best PCE in pure ZnO NRs.
29
30 However, the best performance (~16.1%) of ZnO NRs based PSCs is achieved in their nitrogen-
31
32 doped nanostructures and also by optimizing its aspect ratio, enhancing electron density, and
33
34 substantially reducing their work function than conventional ZnO NRs.^[178] The results showed
35
36 that surface modification to overcome intrinsic defects sites on ZnO and their suitable doping
37
38 have the potential to further improvement. These examples demonstrate that for an efficient
39
40 selective contact, surface properties and energy level alignment with perovskite should also be
41
42 taken into account besides its electrical properties.
43
44
45
46
47
48
49
50
51
52

53 The nanorods are typically grown via a highly acidic synthesis route making is
54
55 challenging for large scale fabrication. An acid free synthesis of TiO₂ NRs is also reported
56
57 resulting in PCE ~11.1%.^[179] Furthermore, other morphologies such as nanocones
58
59
60
61
62
63
64
65

(NCs)^[180] synthesized using a green-method have also been employed as ESC resulting in PCE ~11.9% (thickness >1 μm). These NCs provided additional advantages of superior charge collection and also enhanced absorbance owing to the greater perovskite loading in their relatively wider voids than NRs (Fig 12).^[181] The superior charge collection can be attributed to the fact that NCs provide larger surface to volume ratio compared to other 1D morphologies and thereby improve charge separation or the presence of electrostatic force that acts as a driving force for electrons collection within NCs with enhanced carrier lifetime (**Fig. 13**).^[180, 182]

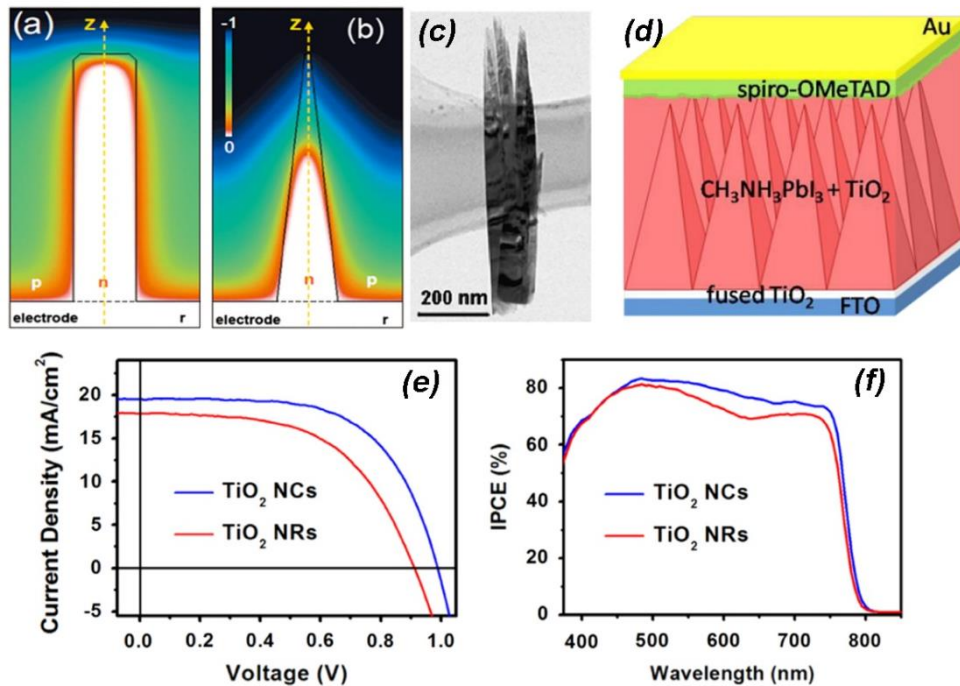


Fig. 13: (a & b) Electric potential contours of n-type nanorod and nanocone in a p-type matrix. Herein, for the electric potential created due to the p-n junction. For nanocones the electrostatic potential varies in both axial and radial directions whereas it remains constant for nanorods in axial direction. This potential variation creates an electric field in nanocones along the axial direction which acts as a driving force for electrons in nanocones eventually resulting in improved electronic transport.^[180, 182] (c) is a TEM image of a nanocone employed in PSCs whereas (d) is a schematic of a full PSC fabricated using NCs, (e and f) are I-V and IPCE spectra of two PSCs fabricated using NCs and NRs.^[180]

Nanowires (NWs) as an ESC material have also shown remarkable performance in PSCs leading to a maximum PCE ~14.2% using a dendritic morphology (thickness ~250 nm),^[183] an improvement from initial ~4.9% and ~12.8%, using ~1.5 μm thick TiO₂ NWs^[184] and <500 nm

1
2
3
4 thick TiO₂ NWs.^[185] TiO₂ Nanotubes (NTs) have also been an ESC material of choice in PSCs
5
6 owing to their directed electron transport and hollow morphology.^[186, 187]The state-of-the-art
7
8 PCE 14.8% is reported by Qin et al^[187] via efficient pore-filling of NTs. Future route to improve
9
10 performance of NT based PSCs could be to employ SnO₂ NTs which offer high electronic
11
12 mobility.^[41]
13
14

15
16 Another strategy to engineer the ESC interface with 1D materials is to employ composite
17
18 nanostructures which typically resulted in high PCE >14%. A surface treatment of low mobility
19
20 MOS such as TiO₂ with a high mobility SnO₂ or an insulator such as MgO to remove surface
21
22 traps or alternatively, reduction in surface defects of ZnO by TiO₂ thin layer has already been
23
24 established with few successful architectures such as ZnO/CdS NR (~4.3%)^[163], SnO₂ NWs/TiO₂
25
26 shell (~14.2%),^[188] WO₃/TiO₂ (~11.2%),^[165]MgO coated TiO₂(~15.3%) and core-shell ZnO-TiO₂
27
28 (~15.3%)^[164].Three dimensional (3D) nanostructures are employed to simultaneously offer high
29
30 surface area, improved light harvesting and also superior electron transport,^[189, 190] as evidenced
31
32 by their inception in PSCs (PCE ~9%).^[191]In a such report involving in inverse-opal like
33
34 multifunction TiO₂ scaffold (~200 nm)synthesized via a simple solution processing aPCE
35
36 ~13.1% is reported which is higher than a TiO₂NP analogue (~11%).^[192] These novel structures
37
38 alleviated the deposition of a compact layer that is typically required to block holes reaching the
39
40 FTO and thereby made the device fabrication easier. Other unconventional 3D morphologies
41
42 employed are branched shaped M13-virus enabled ETL (PCE ~7.5%)^[190] and 3D
43
44 TiO₂nanodendrites (PCE ~13.2%)^[189].
45
46
47
48
49
50
51

52 53 6.1.3 Bi-layered mesoporous scaffolds

54
55 So far, the two important factors, such as low interfacial recombination at ESC/perovskite
56
57 or FTO/ESC, have been achieved in separate materials or via cumbersome surface modification
58
59 of MOS. ZnO although provide high electron mobility its energy offset with perovskite and its
60
61
62
63
64
65

1
2
3
4 poor hole blocking characteristics hinder its further progress in PSCs. Similarly, TiO₂, which has
5
6 shown to effectively block holes reaching FTO and thereby achieving a remarkable progress in
7
8 its mesoporous or planar architectures, still suffers from intrinsic lower electron mobility (**Table**
9
10 **1**). To overcome this issue and to develop an easy to fabricate ESC combining the two crucial
11
12 parameters, Xu et al.^[193] proposed a simple TiO₂/ZnO bilayer architecture thereby combining
13
14 good blocking behavior and electrical conductivity in a single ESC. The bilayer ESC resulted in
15
16 PCE ~17.2% with negligible hysteresis which is a significant improvement when compared to
17
18 corresponding PSCs employing a single ESC (TiO₂ ~10.2% and ZnO ~13.2%). The bilayer not
19
20 only demonstrated efficient charge extraction but also no dark current thereby establishing an
21
22 efficient hole blocking behavior. A similar performance enhancement is also observed in
23
24 inverted PSCs where a ZnO/PCBM bilayer ESC has shown remarkable PCE ~14.2%,
25
26 significantly higher than a pristine ZnO or PCBM counterpart.^[194]
27
28
29
30
31
32
33

34 6.1.4 Compact layer to avoid interfacial recombination

35 High performance PSCs typically employ a thin compact hole blocking layer (CL, <50
36
37 nm) underneath the mesoporous scaffold (200 –300 nm) on conducting substrates to avoid a
38
39 direct contact between HSC and transparent conductive oxide which may otherwise induce short
40
41 circuit in the device eventually resulting in a low FF. The interfacial charge recombination may
42
43 become even intense as perovskite layer itself act as a hole transporter^[195] and a physical barrier
44
45 between FTO and CH₃NH₃PbX₃ is important. The function of CL is conceived to be hole
46
47 blocking only, although there are arguments that it can also act as an ESC.^[7, 196] Nevertheless, the
48
49 compact layer has shown to significantly improve the performance of PSCs by minimizing
50
51 charge recombination, particularly, in cases when the mesoporous TiO₂ layer or perovskite layer
52
53 is characterized by nano size pinholes.^[27, 197]
54
55
56
57
58
59
60
61
62
63
64
65

1
2
3
4 A crucial aspect while preparing CL is optimizing its thickness as demonstrated by Hong
5 et al.^[198] and Wang et al.^[199] Although it is reported that performance of PSCs increases with
6 increasing CL thickness (from 0 to 90 nm)^[199] because a thicker layer has lesser pinholes which
7 suppress interfacial recombination, it increases transport resistance within the film. Nevertheless,
8 an optimized selective contact thickness is crucial to efficient block shunting within the device
9 and also not to increase electron transport resistance.
10
11
12
13
14
15
16
17
18
19

20 **6.2 Planar selective contacts and improved charge extraction at interfaces**

21 Planar heterojunction architecture of PSCs resembles thin film solar cells or polymer
22 solar cells (OPVs) where an absorber layer is employed between flat electron and hole selective
23 contacts, making it a planar heterojunction cell unlike mesoporous scaffolds based PSCs which
24 are more like a bulk heterojunction device.^[7] The elimination of mesoporous TiO₂ scaffold is
25 beneficial when commercial scale production is concerned as planar architecture eliminates two-
26 step processing of the mesoporous layer, i.e., coating and subsequent high temperature sintering.
27 This marks them as a preferred device design in PSCs, particularly after their high PCE report
28 (19.3%, **Table 3**)^[11] which is closer to the state-of-the-art mesoporous architecture counterpart
29 (22.1 %). Although from a production related cost viewpoint the planar architecture seems to be
30 adopted as the ultimate device design, it is rather challenging (at least at the moment) when the
31 stability (next important parameter to efficiency) is taken into account. Whereas the mesoporous
32 architecture delivered a certified efficiency 22%,^[80] the value, for a planar rival, is only 15.6%
33 (certified)^[80]. However uncertified PCE >20% is recently reported.^[125] Nonetheless, in the high
34 efficiency planar vs mesoporous PSCs, a distinction is hard to draw, not only because the planar
35 layers often resemble a thin nanoporous layer, but also, almost all high performing PSCs with
36 mesoporous ESC also employ a compact (flat) thin layer underneath and a ~200 nm thick
37
38
39
40
41
42
43
44
45
46
47
48
49
50
51
52
53
54
55
56
57
58
59
60
61
62
63
64
65

1
2
3
4 capping layer on top of mesoporous-perovskite junction (a mixture of bulk heterojunction and
5
6 planar configuration).^[45]
7
8

9 The pre-requisites for high efficiency planar PSCs are (i) pin-hole free thin selective
10 contacts and (ii) high quality perovskite films to maximize light absorption,^[200] minimize charge
11 recombination and reduce defect densities at the ESC-perovskite interface. The fact that
12 perovskite itself is characterized by ambipolar charge transport puts more stringent conditions on
13
14 the selective contacts to block opposite charges (holes and electrons) reaching the substrate or
15 metal contact, respectively. It would otherwise results in significant deterioration of device
16 performance as shown by Liu et al.^[9] Whereas an inhomogeneous perovskite layer (50 –400 nm)
17 with voids demonstrated inferior PCE (8.6%), a uniform, even, and pin-hole free perovskite layer
18 by dual source evaporation demonstrated nearly doubled PCE (15.4%). The dual source
19 evaporation process is not compatible with mass production as it is both time and energy
20 consuming. This brings into account simple vapor assisted perovskite deposition (VASP) method
21 to produce high quality perovskite films as shown by Chen et al.^[11](PCE 12.1%) and Li et al.^[201]
22 (PCE 16.8%). The latter also manifested remarkably low *JV*-hysteresis, an anomalous typical
23 behavior in planar PSCs.^[202, 203] A further improvement in device performance is made by Zhou
24 et al.^[11]where optimized selective contacts enabled efficient charge injection and extraction in
25 addition to light absorption and carrier generation in perovskite layer. They employed a surface
26 modified ITO with lower work function, Yttrium doped TiO₂ (Y-TiO₂) for efficient charge
27 extraction and transport, and Co- and Li- co-doped spiro-OMeTAD and reported PCE ~19.3% at
28 1 sun condition with nearly unity external quantum efficiency owing to extreme transparency
29 offered by modified ESC and FTO interface. However, this particular device showed *JV*-
30 hysteresis.
31
32
33
34
35
36
37
38
39
40
41
42
43
44
45
46
47
48
49
50
51
52
53
54
55
56
57
58
59
60
61
62
63
64
65

1
2
3
4 The best performance in planar PSCs ($PCE \geq 20\%$) is recently reported by Momblona et
5
6 al.^[125] in a fully vacuum processed PSC and Anaraki et al.^[82] using SnO_2 as a selective contact
7
8
9 (**Table 3**). Herein, the perovskite layer was employed between fully organic ESC and HSCs, all
10
11 prepared via vacuum processing, resulting in high quality films, as shown in **Fig. 14**. This
12
13 important report highlights two key findings: Firstly, contrary to the general perception, that
14
15 larger perovskite crystals favor high PCE, this reports employs small perovskite grains and yet
16
17 demonstrate high PCE 18% (average, 20% in a champion device), suggesting that the nature of
18
19 grain boundaries and defects within the perovskite layer are the primary performance
20
21 determining factors. This affirms a previous report that the benign grain boundaries in perovskite
22
23 films do not create sub-bandgap states.^[204] Secondly, it compares p-i-n and n-i-p architecture,
24
25 where exactly same materials (except metal back contact) shows large difference in performance
26
27 (**Fig. 14**). This is due to the fact that in p-i-n architecture, HTM (employed in this study) forms
28
29 poor contact at the front contact (ITO), whereas in n-i-p architecture, a good contact is formed as
30
31 metal contact is thermally evaporated over HTM. Similarly, the PSCs made using SnO_2 (PCE
32
33 20.7%)^[82] as a selective contact resulted in one of the highest V_{OC} 1.21 V (for $\text{CH}_3\text{NH}_3\text{PbI}_3$),
34
35 close to its thermodynamic limit^[77, 84] of 1.32 V.
36
37
38
39
40
41
42
43
44
45
46
47
48
49
50
51
52
53
54
55
56
57
58
59
60
61
62
63
64
65

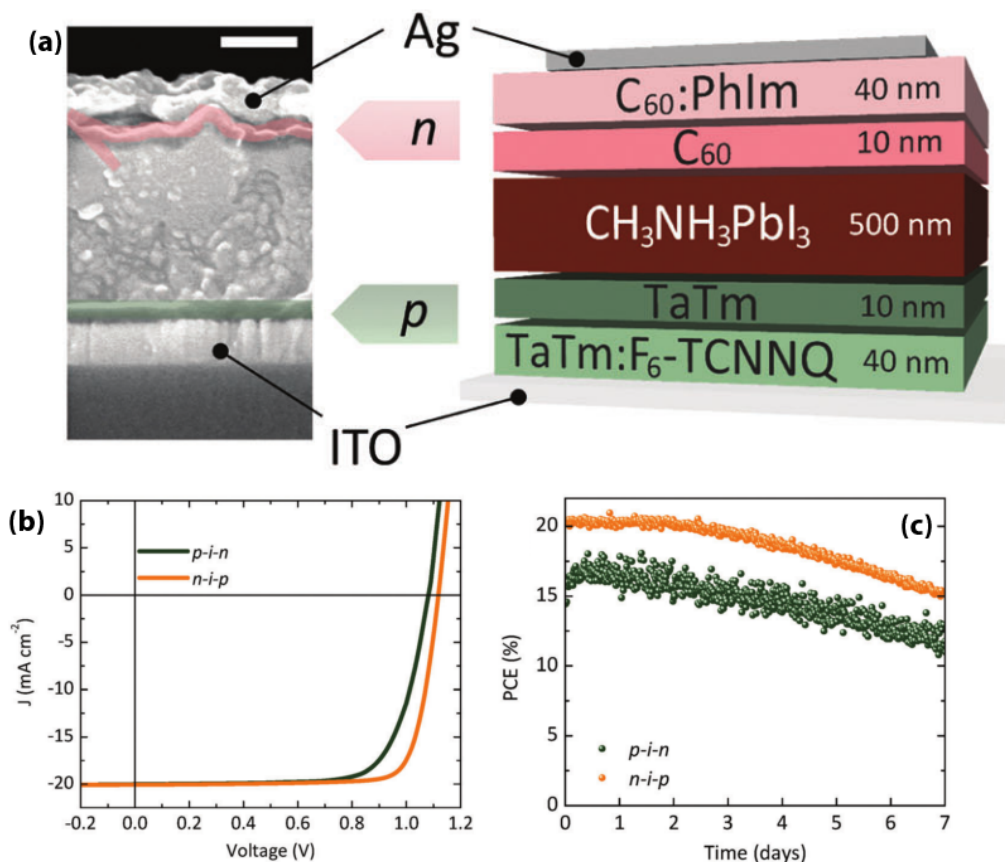


Fig 14: (a) A cross-section view and schematics of a completed p-i-n solar cell (scale bar 200 nm), (b) J-V curves for the n-i-p and p-i-n solar cells under standard test conditions (both devices employ the same materials, just the order is changed), and (c) PV performance as a function of time under approximated 100 mW cm^{-2} illumination. Figure reproduced with permission from reference ^[125]. Copyright of The Royal Society of Chemistry.

Alternatives to TiO_2 such as ZnO ^[18], SnO_2 ^[205] and ZnO-SnO_2 composites^[206] are also employed that resulted in remarkable PCE $\sim 15.7\%$, 18% and 15.2% , respectively. The efficiency of ZnO planar PSCs is further improved to 15.9% via modifying ZnO energy levels by introducing oxygen vacancies in which it resulted in improved electron extraction.^[207] A similar performance rise is witnessed when suitable conduction band alignment to SnO_2 compact layer resulted in a remarkable PCE $>18\%$ with almost no I-V hysteresis.^[205] Additionally, a bi-layer design where ZnO CL over TiO_2 suppressed interfacial recombination at ESC/perovskite interface and resulted in over 17% PCE.^[193] Similarly, progress in flexible planar PSCs is also remarkable.^[48] PCE 13.5% is reported in high quality TiO_2 compact layer prepared via e-beam at

1
2
3
4 T < 80°C.^[208] The highest performance (PCE 15.6%) in flexible planar PSCs is however achieved
5
6 using a thin ZnO layer.^[209]
7
8

9 6.2.1 Inverted perovskite solar cells: Case for organic and inorganic interfaces

10 Inverted PSCs, also called p-i-n type PSCs, employ a p-type organic or inorganic layer on
11
12 conducting substrates to collect holes whereas electrons are collected from the back contact
13
14 (**Fig.1**).^[210] These designs are particularly interesting as, contrary to their n-i-p rival, high quality
15
16 selective contacts can be fabricated at low temperature and also they often do not show *JV*-
17
18 hysteresis (**Fig.10**).
19
20
21

22
23 The charge separation in these devices is conceived to be due to the presence of internal
24
25 electric field at the perovskite and HSC or ESC interface, and the electrons are injected to the
26
27 LUMO of ESC, viz. PC₆₁BM whereas the holes are transferred to conducting substrate via HSC,
28
29 i.e., PEDOT:PSS (donor-acceptor mechanism). This is validated by the steady state
30
31 photoluminescence (PL) measurements by Sun et al^[211] who compared PL quenching of
32
33 CH₃NH₃PbI₃, CH₃NH₃PbI₃/PEDOT:PSS and CH₃NH₃PbI₃/PC₆₁BM bilayers. The bilayers
34
35 showed 3 and 4 times higher PL quenching respectively, compared to a perovskite layer itself
36
37 validating the improved charged separation at bilayer interface. Surprisingly, unlike
38
39 the ambipolar charge transport properties of perovskite,^[212] and the reports that it can work with a
40
41 single interface only,^[28, 213-215] the devices in this report did not work with single interface
42
43 probably due to the less efficacious perovskite/PEDOT:PSS interface compared to
44
45 perovskite/spiro-OMeTAD analogue and also due to energy mismatch between perovskite and
46
47 back contact (Al) as shown in **Fig. 15b** which hinders efficient exciton dissociation in the
48
49 absence of PC₆₁BM. This can also be confirmed from a plot of PL intensity versus temperature
50
51 that the exciton binding energy is ~20 meV, indicating that an electric field is still required for
52
53
54
55
56
57
58
59
60
61
62
63
64
65

efficient exciton dissociation. The energy level difference between perovskite and ESC is ~ 0.27 eV which is ~ 10 times higher than the required energy for charge separation (**Fig. 15 c**).

From an initial PCE $\sim 3.9\%$ in their first report,^[216] the p-i-n planar device now demonstrate a state-of-the-art PCE $\sim 18.8\%$ ($V_{OC} \sim 1.12V$, $J_{SC} \sim 21.8 \text{ mA/cm}^2$, FF $\sim 77\%$) as shown in **Table 3**.^[142] The best performing device (FTO/NiO/MAPbI₃/C₆₀/SnO₂/Ag) also showed a stable power output of 18.5%. Various reports employing PEDOT:PSS^[217, 218] or NiO_x^[122, 219, 220] as HTL (See **Fig. 16** and **Table 3**) reported PCE $>17\%$ in PSCs with minor or no hysteresis making them one of the successful device designs so far, although there are concerns on their stability. The remarkable improvement in these devices has been due to improvement dense and pinhole free perovskite layers that enable complete light absorption^[218, 219] as well as selection of charge selective contacts which are mostly adapted from polymer solar cells such as PEDOT:PSS and fullerene derivatives, i.e., PCBM.

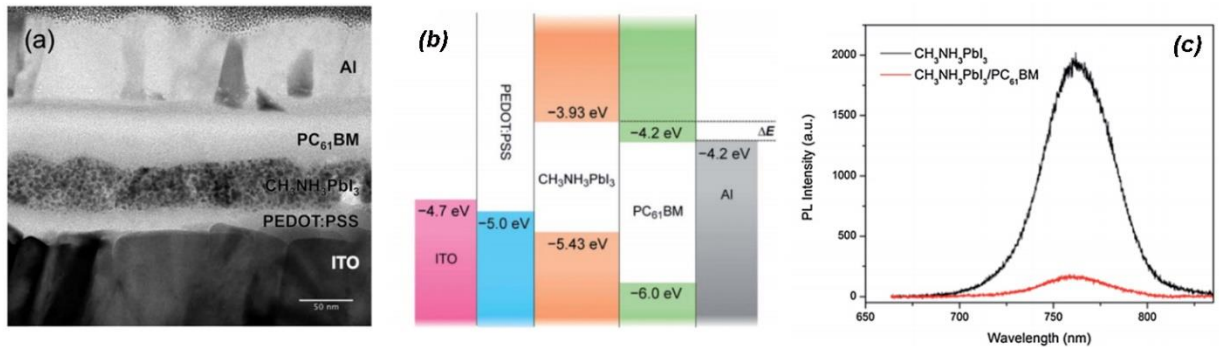


Fig. 15: (a) A cross-section TEM of a typical inverted PSC (p-i-n) employing PEDOT:PSS and PC₆₁BM as HSC and ESC, respectively, (b) schematic showing energy level diagram of ITO, PEDOT:PSS, CH₃NH₃PbI₃, PC₆₁BM and Al. (c) Steady-state PL spectra for CH₃NH₃PbI₃ and CH₃NH₃PbI₃/PC₆₁BM ($\lambda_{ex} = 600 \text{ nm}$) showing efficient charge separation when a PC₆₁BM layer is employed. Figure is reproduced with permission from ref.^[211]

A typical problem in these devices is the poor contact formed between fullerene derivatives when conjugated directly with metal back contact. This brings into account additional buffer layers such as PFN (polyelectrolyte poly[(9,9-bis(3'-(N,N-dimethylamino) propyl)-2,7-

fluorene)-alt-2,7-(9,9-dioctylfluorene)], BCP (bathocuproine), and LiF to improve Ohmic contact and eventually the charge transfer at the interface.^[216, 221, 222] In such a report, You et al.^[222] reported a moisture assisted perovskite growth to synthesize a thick absorber layer and showed a remarkable PCE ~17.1%. A buffer layer of PFN is employed to support efficient charge extraction to back contact which enabled a FF as high as 0.80.^[222] Other such works include a thin layer of MoO₃ in conjunction with PEDOT:PSS that resulted in PCE ~15% by improving hole collection efficiency^[223] and C in conjunction with CuSCN with C₆₀+BCP as ESC that resulted in PCE >16.8%.^[32] The buffer layers are also employed at the ETL/perovskite or ETL/TCO interface. For example, fullerene derivatives (IC₆₀BA, PC₆₁BM, C₆₀) have also shown to enhance performance of PSCs when employed in conjunction with ETL (Bis-C₆₀),^[224] a thin ZnO layer in conjunction with PCBM resulted in PCE ~16.8% and also enhanced the stability of the device significantly.^[225] In addition, thin buffer layers of MOS such as ZnO and TiO_x are also employed in order to improve device operational stability.^[137, 226]

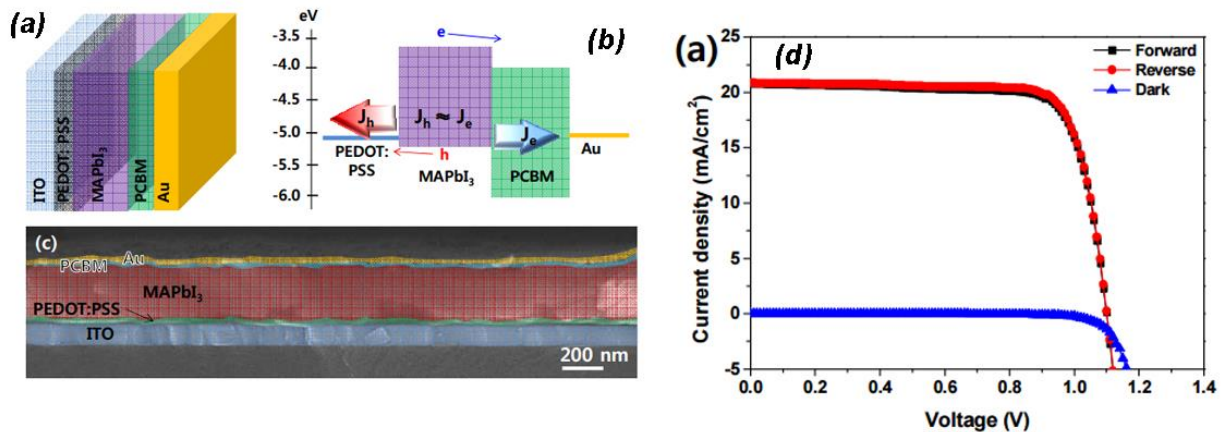


Fig. 16: A schematic showing device architecture and band energy diagram of an inverted planar MAPbI₃ PSC (a & b), (c) the SEM cross-sectional image of representative device showing a perovskite layer of thickness ~300 nm, (d) J-V curves of a representative inverted PSC with respect to forward and reverse scan direction demonstrating no hysteresis.^[31] Figures reproduced with permission from the reference.

Table 3: Photovoltaic parameters of perovskite solar cells employing various types of MOS as electron transport layer. Only the keyreports are included in the table for comparison. The table is categorized according to device architecture and within each category according to the type of ESC employed.

Device architecture	ESC/ Morphology	ESC Thickness (nm)	Method of deposition (perovskite)	Subst rate	Perovskite	HSC	J _{sc} (mA/cm ²)	V _{oc} (V)	FF	η (%)	Ref	
Mesoporous or Mesoscopic	c-TiO ₂ /m-TiO ₂ NPs	150 nm	Single step	FTO	C _{Sx} (MA _{0.17} FA _{0.83}) _(100-x) Pb(I _{0.83} Br _{0.17}) ₃	Li- and Co doped Spiro	23.5	1.15	0.78	21.2	Saliba et al. ^[12]	
	c-TiO ₂ /m-TiO ₂ NPs	~200 nm	Single step	FTO	PbI/FAI ₂ , MABr/PbBr ₂	Spiro-OMeTAD	24.6	1.16	0.73	20.8	Bi et al. ^[25]	
	c-TiO ₂ /m-TiO ₂ NPs	~200 nm	VASP	FTO	FA _{0.81} MA _{0.15} PbI _{2.51} Br _{0.45}	Spiro-OMeTAD	23.4	1.14	0.76	20.5 (19.5) cert*	Li et al. ^[227]	
	c-TiO ₂ /m-TiO ₂ NPs	--/~300 nm	Sequential deposition	FTO	FAPbI ₃	PTAA	24.7	1.06	0.77	20.2	Yang et al. ^[23]	
	c-TiO ₂ /m-TiO ₂ NPs	30 nm/ 200 nm	Sequential deposition	FTO	CH ₃ NH ₃ PbI ₃ And CH ₃ NH ₃ PbBr ₃	FDT ^a	22.7	1.15	0.76	20.2	Saliba et al. ^[24]	
	c-TiO ₂ /m-TiO ₂ NPs	40 nm/ 230 nm	Sequential deposition	FTO	MAPbI ₃ .DMSO	Spiro-OMeTAD	23.83	1.09	0.76	19.7	Ahn et al. ^[228]	
	c-TiO ₂ /m-TiO ₂ NPs	~150 nm	Single step	FTO	((FAPbI ₃) _{0.85} (MAPbBr ₃) _{0.15})	Spiro-OMeTAD	22.3	1.1	0.70	18.8	Aitola et al. ^[229]	
	c-TiO ₂ /m-TiO ₂ NPs	70 nm/ 300 nm	2-step spin coating	FTO	CH ₃ NH ₃ Pb(I _{1-x} Br _x) ₃	PTAA	19.6	1.1	0.76	16.5	Jeon et al. ^[10]	
	(Include mono and binary MOS and their various morphologies, composite and bilayer structures)	TiO ₂ (0D+1D+2D)	30 nm/ 150 nm	Single step	FTO	CH ₃ NH ₃ PbI ₃	Spiro-OMeTAD	22.6	1.05	0.70	16%	Wu et al. ^[230]
		TiO ₂ Nanotubes	420 nm	Two step spin coating	FTO	CH ₃ NH ₃ PbI ₃	Spiro-OMeTAD	22.6	1.0	0.64	14.8	Qin et al. ^[187]
TiO ₂ Nanowires		220 nm	One step spin coating	FTO	CH ₃ NH ₃ PbI ₃	Spiro-OMeTAD	20.3	0.99	0.70	14.2	Wu et al. ^[183]	
TiO ₂ NRs		~1.5 μm	Two-step spin coating	FTO	CH ₃ NH ₃ PbI ₃	Spiro-OMeTAD	19.8±0.7	0.97±0.01	0.72 ± .35	13.45±0	Mali et al. ^[176]	
TiO ₂ Nanowires		430 nm	Sequential deposition	FTO	CH ₃ NH ₃ PbI ₃	Spiro-OMeTAD	18.2	1.05	0.67	12.8	Tao et al. ^[185]	
TiO ₂ NRs		~1.8 μm	Single step	FTO	CH ₃ NH ₃ PbI _{3-x} Cl _x	Spiro-OMeTAD	21.8	0.8	0.68	11.8	Li et al. ^[231]	
TiO ₂ Nanocones		150 nm	Two step spin coating	FTO	CH ₃ NH ₃ PbI ₃	Spiro-OMeTAD	18.2	0.94	0.67	11.4	Peng et al. ^[181]	
Nb-doped TiO ₂ NRs		~600 nm	Single step	FTO	CH ₃ NH ₃ PbI _x Br _{3-x}	Spiro-OMeTAD	16.6	0.89	≈0.52	7.5	Yang et al. ^[153]	
Sn-doped TiO ₂ NRs		>600 nm	Sequential deposition	FTO	CH ₃ NH ₃ PbI ₃	Spiro-OMeTAD	14.9	0.74	0.52	6.3	Zhang et al. ^[154]	
3D TiO ₂		400 nm	Sequential deposition	FTO	CH ₃ NH ₃ PbI ₃	Spiro-OMeTAD	22.9	0.92	0.62	13.2	Lin et al. ^[189]	

14
15
16
17
18
19
20
21
22
23
24
25
26
27
28
29
30
31
32
33
34
35
36
37
38
39
40
41
42
43
44
45
46
47
48
49
50
51
52
53
54
55
56
57
58
59
60
61
62
63
64
65

	TiO ₂ /ZnO bi layer	--	Spin coating	FTO	CH ₃ NH ₃ PbI ₃	Spiro-OMeTAD	20.8	1.08	0.71	16.1	Xu et al. ^[193]	
	ZnO NPs	~25 nm	Sequential deposition	ITO	CH ₃ NH ₃ PbI ₃	Spiro-OMeTAD	20.4	1.03	0.75	15.7	Liu et al. ^[18]	
	ZnO NRs	40-160 nm	Sequential deposition	FTO	CH ₃ NH ₃ PbI ₃	Spiro-OMeTAD	22.4	1.04	0.57	13.4	Liang et al. ^[177]	
	N:ZnO NRs	0.6 –1.1 μm	Sequential deposition	ITO	CH ₃ NH ₃ PbI ₃	Spiro-OMeTAD	21.5	0.96	0.70	16.1	Mahmood et al. ^[130]	
	Al-doped ZnO NRs	~600 nm	--	FTO	CH ₃ NH ₃ PbI ₃	Spiro-OMeTAD	~20	~0.91	~0.58	10.7	Dong et al. ^[158]	
	ZnO-NR/TiO ₂ core-shell	600 – 700 nm	Sequential deposition	FTO	CH ₃ NH ₃ PbI ₃	Spiro-OMeTAD	22	1	0.7	15.4	Liu e al. ^[164]	
	ZnO NRs-TiO ₂ NPs	~600 nm	Two step spin coating	FTO	CH ₃ NH ₃ PbI ₃	Spiro-OMeTAD	19.4	1.05	0.70	14.35%	Son et al. ^[139]	
	SnO ₂ NPs	60 nm	Sequential deposition	FTO	CH ₃ NH ₃ PbI ₃	Spiro-OMeTAD	22.83	1.11	0.64	16	Ke et al. ^[141]	
	SnO ₂ NWs	300 nm	Sequential deposition	FTO	CH ₃ NH ₃ PbI ₃	Spiro-OMeTAD	21.2	1.02	0.65	14.2	Han et al. ^[188]	
	CdS	30 nm	Sequential deposition	FTO	CH ₃ NH ₃ PbI ₃	Spiro-OMeTAD	16.1	1.05	0.66	11.2%	Liu et al. ^[143]	
	SrTiO ₃	--	Sequential deposition	FTO	CH ₃ NH ₃ PbI ₃	Spiro-OMeTAD	18.08	0.97	0.57	10%	Wang et al. ^[146]	
	BaSnO ₃	~300 nm	Sequential deposition	FTO	CH ₃ NH ₃ PbI ₃	Spiro-OMeTAD	16.8	1.03	0.71	12.3	Zhu et al. ^[147]	
	Zn ₂ SO ₄	~100 nm/ ~300 nm	Sequential deposition	FTO	CH ₃ NH ₃ PbI ₃	Spiro-OMeTAD	13.78	0.83	0.61	7.02	Oh et al. ^[232]	
	Zn ₂ SO ₄ NFs (C-L+m-L)	~700 nm	Sequential deposition	FTO	CH ₃ NH ₃ PbI ₃	Spiro-OMeTAD	12.68	0.99	0.59	7.38	Mali et al. ^[233]	
	Zn ₂ SO ₄ NPs	--/~ 200 nm	2-step spin coating	PET/ITO	CH ₃ NH ₃ PbI ₃	PTAA	21.4	1.05	0.66	14.85	Shin et al. ^[149]	
	WO ₃ -TiO ₂ core-shell	~700 nm	Sequential deposition	FTO	CH ₃ NH ₃ PbI ₃	Spiro-OMeTAD	17	0.87	0.76	11.24	Mahmood et al. ^[165]	
	Device architecture	ESC/ Morphology	CL Thickness (nm)	Method of deposition (ESC/perovskite)	Subst rate	Perovskite	HSC	J_c (mA/cm²)	V_{oc} (V)	FF	η (%)	Ref
	Planar (n-i-p) on glass	c-TiO ₂	<50 nm	Vapor deposition	FTO	CH ₃ NH ₃ PbI _{3-x} Cl _x	Spiro-OMeTAD	21.5	1.07	0.67	15.4	Liu et al. ^[9]
		c-TiO ₂	<50 nm	Sol. processing	FTO	CH ₃ NH ₃ PbI _{3-x} Cl _x	Spiro-OMeTAD	17.6	0.84	0.58	8.6	Liu et al. ^[9]
		c-TiO ₂	--	Sol. processing	FTO	CH ₃ NH ₃ PbI _{3-x} Cl _x	Spiro-OMeTAD	20.3	0.89	0.64	11.4	Eperon et al. ^[200]
		c-TiO ₂	<50 nm	VASP ^b	FTO	CH ₃ NH ₃ PbI ₃	Spiro-OMeTAD	20.8	0.94	0.68	12.1	Chen et al. ^[11]

14
15
16
17
18
19
20
21
22
23
24
25
26
27
28
29
30
31
32
33
34
35
36
37
38
39
40
41
42
43
44
45
46
47
48
49
50
51
52
53
54
55
56
57
58
59
60
61
62
63
64
65

substrates	c-TiO ₂	<50 nm	LP-VASPC ^c	FTO	CH ₃ NH ₃ PbI _{3-x} Cl _x	Spiro-OMeTAD	21.7	1.04	0.75	16.8	Li et al. ^[201]	
	Y-TiO ₂ ^d	<50 nm	Sol. processing	PEIE-ITO ^e	CH ₃ NH ₃ PbI _{3-x} Cl _x	Li-,Co-doped Spiro-OMeTAD	22.7	1.13	0.75	19.3	Zhou et al. ^[11]	
	c-ZnO	~25 nm	Sol. processing	ITO	CH ₃ NH ₃ PbI ₃	Spiro-OMeTAD	20.4	1.03	0.75	15.7	Liu et al. ^[18]	
	c-ZnO	40 nm	Sputtering/Sol. processing	ITO	CH ₃ NH ₃ PbI ₃	Spiro-OMeTAD	21.8	1.00	0.73	15.9	Tseng et al. ^[207]	
	c-SnO ₂	<40 nm	Sol. Processing/ALD	FTO	Cs _x (MA _{0.17} FA _{0.83}) _{100-x} Pb(I _{0.83} Br _{0.17}) ₃	Li- and Co doped Spiro	22.6	1.17	0.76	20.7	Anaraki et al. ^[82]	
	c-SnO ₂	--	Sol. processing	FTO	CH ₃ NH ₃ PbI ₃	Spiro-OMeTAD	19.9	1.06	0.58	12.1	Song et al. ^[206]	
	c-SnO ₂	~30 nm	ALD/ Sol. processing	FTO	(FAPbI ₃) _{0.85} (MAPbBr ₃) _{0.15}	Spiro-OMeTAD	21.3	1.19	0.74	18.1	Baena et al. ^[205]	
	c-SnO ₂ (T 70°C)		sequential deposition	ITO	CH ₃ NH ₃ PbI ₃	Spiro-OMeTAD	19.5	1.08	0.62	13	Song et al. ^[234]	
	TiO ₂ -ZnO bi layer	~30 nm each	Sol-gel/Sol. processing	FTO	CH ₃ NH ₃ PbI ₃	Spiro-OMeTAD	20.8	~1.08	0.75	17.2	Xu et al. ^[193]	
	ZnO-SnO ₂ composite	--	Sol. processing	FTO	CH ₃ NH ₃ PbI ₃	Spiro-OMeTAD	19.5	1.07	0.73	15.2	Song et al. ^[206]	
Planar (n-i-p) on flexible substrates	C60/phlm	10/40 nm	Vacuum processing	ITO	CH ₃ NH ₃ PbI ₃	TaTm/F ₆ -TCNNQ	22.1	1.14	0.80	20.3	Momblona et al. ^[125]	
	c-TiO ₂	~100 nm	Sol. processing	IZO-PET ^f	CH ₃ NH ₃ PbI ₃	Spiro-OMeTAD	17.6	~1	0.7	12.3	Dkhissi et al. ^[235]	
	c-TiO ₂	~60 nm	e-beam/Sol. processing	PET/ITO	CH ₃ NH ₃ PbI _{3-x} Cl _x	poly(triaryl amine) doped PTAA	20.5	0.89	0.73	13.4	Qiu et al. ^[208]	
	c-ZnO	40 nm	Spin coating	PEN/ITO	CH ₃ NH ₃ PbI ₃	PTAA	18.7	1.1	0.76	15.6	Heo et al. ^[209]	
	c-ZnO	--	Sputtering/sol. Processing	W. glass, ^f flexible	CH ₃ NH ₃ PbI ₃	Spiro-OMeTAD	19.3	0.98	0.69	11.7	Tavakoli et al. ^[236]	
	c-ZnO	≤50 nm	Sol. processing	PET/ITO	CH ₃ NH ₃ PbI ₃	Spiro-OMeTAD	13.4	1.03	0.74	10.2	Liu et al. ^[18]	
	c-TiO ₂ -Al ₂ O ₃	50/350 nm	Spin coating	Ti foil	CH ₃ NH ₃ PbI _{3-x} Cl _x	Spiro-OMeTAD + PEDOT:PSS	17	0.98	0.61	10.3	Troughton et al. ^[237]	
	Device architecture	ESC		Method of CL	Substrate	Perovskite	HSC	Jsc (mA/cm²)	Voc (V)	FF	η(%)	Ref
		NO ETL	--	Sol. Processing (DS)	ITO	CH ₃ NH ₃ PbI ₃	Spiro-OMeTAD	~17.5	1.01	~0.66	13.5	Liu et al. ^[28]

14
15
16
17
18
19
20
21
22
23
24
25
26
27
28
29
30
31
32
33
34
35
36
37
38
39
40
41
42
43
44
45
46
47
48
49
50
51
52
53
54
55
56
57
58
59
60
61
62
63
64
65

ESC Free	NO ETL	--	Sol. Processing (DS)	Cs ₂ CO ₃ -ITO	CH ₃ NH ₃ PbI ₃	Spiro-OMeTAD	19.9	1.07	0.71	15.1	Hu et al. [238]
Meso-superstructures solar cells (employing insulating scaffolds) MSSC-PSCs	c-TiO ₂ /Al ₂ O ₃ (T >400 °C)	~50/~200 nm	Sol. processing	FTO	CH ₃ NH ₃ PbI _{3-x} Cl _x	Spiro-OMeTAD	17.8	0.98	0.63	10.9	Lee et al. ^[7]
	c-TiO ₂ /Al ₂ O ₃ (T~150 °C)	<50/~20 nm	Sol. processing	FTO	CH ₃ NH ₃ PbI _{3-x} Cl _x	Spiro-OMeTAD	18	1.02	0.67	12.3	Ball et al. ^[27]
	TiO ₂ -GRO/ Al ₂ O ₃ bi-layer	~100/~400 nm	Sol. processing	FTO	CH ₃ NH ₃ PbI _{3-x} Cl _x	Spiro-OMeTAD	21.9	1.04	0.73	15.6	Wang et al. ^[239]
	c-TiO ₂ /Al ₂ O ₃	--/ >300 nm	Sol. processing	FTO	CH ₃ NH ₃ PbI _{3-x} Cl _x	PDI	1.08	1.3	0.4	0.56	Edri et al. ^[91]
	c-TiO ₂ /Al ₂ O ₃	--	Sol. processing	FTO	CH ₃ NH ₃ PbBr _{3-x} Cl _x	p-doped CBP	4.0	1.5	0.46	2.7	Edri et al. ^[87]
	c-TiO ₂ /ZrO ₂	--/ >300 nm	Sol. Processing (DS)	FTO	CH ₃ NH ₃ PbI ₃	Spiro-OMeTAD	17.3	1.07	0.59	10.8	Bi et al. ^[240]
c-TiO ₂ /m-Al ₂ O ₃	--/~200 nm	Spin coating	FTO	CH ₃ NH ₃ PbI _{3-x} Cl _x	Spiro-OMeTAD	21.5	≈1.07	0.71	15.9	Wojciechowski et al. ^[26]	
Device architecture	Device Architecture	Thickness (active layers)	Method of ESC/perovskite	Subst rate	Perovskite	HSC	J_{sc} (mA/cm²)	V_{oc} (V)	FF	η(%)	Ref
HSC-free PSCs	c-ZnO/P/C	55nm	Spin coating/sequential deposition	FTO	CH ₃ NH ₃ PbI ₃	HTM free	20	0.81	0.54	8.7	Zhou et al. ^[241]
	c-TiO ₂ /TiO ₂ /P/MWCNTs	--	Spin coat/drop cast	FTO	CH ₃ NH ₃ PbI ₃	HTM free	18	0.88	0.8	12.7	Wei et al. ^[242]
	c-TiO ₂ /TiO ₂ /ZrO ₂ /P/C	100nm, 1/2/10 μm	Spray pyr., sc. Print./ drop cast.	FTO	(FA) _{0.6} (MA) _{0.4} PbI ₃	HTM free	20.9	0.92	0.67	12.9	Hu et al. ^[214]
	c-TiO ₂ /TiO ₂ /P/Graphene (MW)	--/200/400 nm, >10 μm	Spin coating/-	FTO	CH ₃ NH ₃ PbI ₃	HTM free	16.7	0.94	0.73	11.5	Yan et al. ^[243]
	c-TiO ₂ /TiO ₂ /ZrO ₂ /P/C	100nm, 1/2/10 μm	Spray coating, screen pr../ drop casting	FTO	(5-AVA) _x (MA) _{1-x} PbI ₃	HTM free	22.8	0.86	0.66	12.8	Mei et al. ^[13]
	c-TiO ₂ /TiO ₂ /ZrO ₂ /P/C	100nm, 1/2/10 μm	Spray coating, screen pr../ drop casting	FTO	(5-AVA) _x (MA) _{1-x} PbI ₃	HTM free	22.9	0.87	0.67	13.4%	Yang et al. ^[244]
Inverted Perovskite	PTAA doped with F4-TCNQ ^g	<100 nm	spin coat./double step	ITO	CH ₃ NH ₃ PbI ₃	PCBM+ C ₆₀ +BCP	~22	1.07	0.77	18.3	Bi et al. ^[218]
	PEDOT:PSS	<50 nm	Spin coating	ITO	CH ₃ NH ₃ PbI ₃	PCBM	20.9	1.1	0.78	18.1	Heo et al. ^[31]

14
15
16
17
18
19
20
21
22
23
24
25
26
27
28
29
30
31
32
33
34
35
36
37
38
39
40
41
42
43
44
45
46
47
48
49
50
51
52
53
54
55
56
57
58
59
60
61
62
63
64
65

solar cells (p-i-n)	PEDOT:PSS		Spin coating/ single step	FTO	CH ₃ NH ₃ PbI _{3-x} Cl _x	PCBM	22.4	0.92	0.82	18	Nie et al. ^[217]
	PEDOT:PSS	--	Spin coating	ITO	CH ₃ NH ₃ PbI ₃	PCBM/PFN	20.3	1.05	0.8	17.1	You et al. ^[222]
	PEDOT:PSS	20 nm	Spin coating	ITO	CH ₃ NH ₃ PbI _{3-x} Cl _x	PCBM/ZnO	22	1.02	0.74	16.8	Zhang et al. ^[225]
	PEDOT:PSS	~20 nm	Spin coating	ITO	CH ₃ NH ₃ PbI ₃	PC ₆₁ BM	10.8	0.91	0.76	7.4	Sun et al. ^[211]
	PEDOT:PSS	<50 nm	Spin coating	ITO	CH ₃ NH ₃ PbI ₃	C ₆₀ /BCP	10.3	0.60	0.63	3.9	Jeng et al. ^[216]
	PEDOT:PSS	<50 nm	Spin coating/ALD	ITO	CH ₃ NH ₃ PbI ₃	ZnO NWs	≈21	1.02	≈77	≈16.5	Chang et al. ^[245]
	PEDOT:PSS	<50 nm	Spin coating	ITO	CH ₃ NH ₃ PbI ₃	PCBM/ZnO NC	20.5	0.97	0.80	15.9	Bai et al. ^[137]
	NiO _x	20 nm	Spin coating	ITO	CH ₃ NH ₃ PbI ₃	C ₆₀ -Bis-C ₆₀	21.8	1.03	0.78	17.6	Zhang et al. ^[219]
	NiO _x	<50 nm	--	ITO	CH ₃ NH ₃ PbI ₃	PC ₆₁ BM/LiF	20.2	1.06	0.81	17.3	Park et al. ^[220]
	NiO	< 50 nm	60 – 100 nm	FTO	CH ₃ NH ₃ PbI ₃	SnO ₂ /C ₆₀	21.8	1.12	0.77	18.8	Zhu et al. ^[142]
	NiO _x	80 nm	Spin coating	ITO	CH ₃ NH ₃ PbI ₃	ZnO	21	1.01	0.76	16.1	You et al. ^[122]
	CuI	--	Spin coating	ITO	CH ₃ NH ₃ PbI ₃	PCBM	21.1	1.04	0.62	13.3	Chen et al. ^[246]
	CuSCN	57 nm	Spin coating	ITO	CH ₃ NH ₃ PbI ₃	C ₆₀ /BCP	21.9	1.00	0.76	16.6	Ye et al. ^[32]
Device architecture	ESC	Thickness (CL/scaffold) nm	Method of CL	Subst rate	Perovskite	HSC	J_{sc} (mA/cm²)	V_{oc} (V)	FF	η(%)	Ref
	TiO ₂	~50/>500 nm	Dip coating	Stainless steel	CH ₃ NH ₃ PbI ₃	Spiro-OMeTAD	10.2	0.66	0.49	3.3	Qiu et al. ^[247]
Fiber or wire shaped PSCs	TiO ₂	--	Electrochemical anodization	Ti foil	CH ₃ NH ₃ PbI ₃	Spiro-OMeTAD	11.97	0.73	0.44	3.85	Lee et al. ^[248]
	ZnO	--	Dip coating	Stainless steel	CH ₃ NH ₃ PbI ₃	Spiro-OMeTAD	15.3	0.66	--	3.8	He et al. ^[249]

^a**FDT**: 2',7'-bis(4-methoxyphenyl)amino)spiro[cyclopenta[2,1-b:3,4-b']dithiophene-4,9'-fluorene

^b**VASP**: Vapor assisted solution process

^c**LP-VASP**: Low pressure-vapor assisted solution process

^d**Y-TiO₂**: Yttrium doped TiO₂

^e**PEIE-ITO**: poly-ethyleneimineethoxylated (PEIE) doped ITO

^f**IZO-PET**: Indium doped zinc oxide coated polyethylene terephthalate

^g**F4-TCNQ**: tetrafluoro-tetracyanoquinodimethane (F4-TCNQ)

^h**DCIP**: direct contact and intercalation process

6.3 Engineering of selective contacts: manipulating defects and charge dynamics

A major challenge to achieving high PV parameters in PSCs is the interfacial recombination, particularly, at the ESC-perovskite interface, primarily due to low mobility materials such as TiO₂ and ZnO and their surface defects. Thanks to the ambipolar charge transport in perovskite films which opened possibility of insulating oxide scaffolds such as Al₂O₃ and ZrO₂ to be employed in PSCs (also called Meso-superstructured solar cells, MSSCs) and resulted in high PV parameters, especially, higher V_{OC}.^[7, 26, 123] Not only the insulating scaffolds helped in perovskite crystallization but also had dually advantageous effect on charge transport properties of the PSCs. In a comparative study of TiO₂ vs Al₂O₃ based PSCs (TiO₂ ESC PCE ~7.6%, V_{OC} ~0.8 V); Al₂O₃ PSCs, PCE ~10.9%, V_{OC} ~1.13 V)^[7] the latter showed effective charge transfer and longer carrier lifetime, as confirmed via photoinduced absorption (PIA) spectroscopy and small-perturbation transient photocurrent decay measurements (**Fig. 16**) resulting in higher J_{sc} and nearly 200 mV increased V_{OC} in a similar device configuration. The ~10 times faster lifetime in Al₂O₃ based PSCs is due to the fact that electrons are carried by the perovskite layer itself, a material with several orders of higher electron mobility than TiO₂, whereas the ~200 mV higher V_{OC} is due to the removal of sub-band gap states when TiO₂ is replaced with Al₂O₃. The higher V_{OC} is due to the fact that, in TiO₂, the structural disorderly induced sub-bandgap states that bring its Fermi level (E_F) much lower than its conduction band create charge storing capability. The TiO₂ ESC under illumination thereby acts store charges in it likewise a capacitor (which is called chemical potential) and limits the V_{OC}.

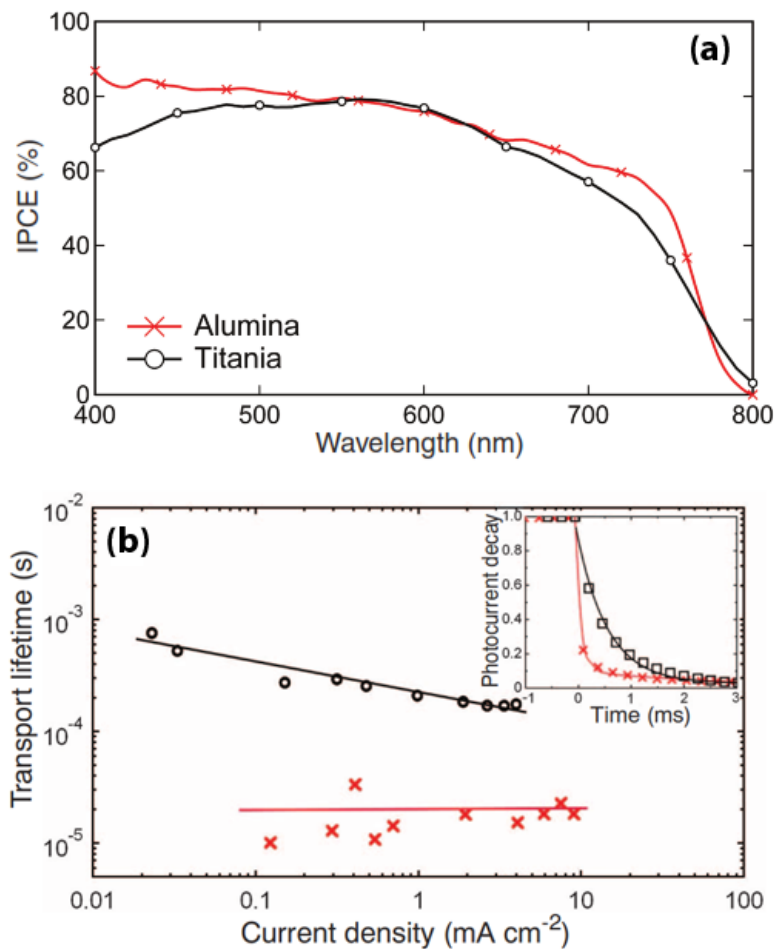


Fig. 17: (a) IPCE action spectrum of an Al_2O_3 and TiO_2 based and perovskite-sensitized solar cell, and (b) charge transport lifetime determined by small-perturbation transient photocurrent decay measurement of TiO_2 PSCs (black circles) and Al_2O_3 PSCs (red crosses). Inset shows normalized photocurrent transients for Al_2O_3 cells and TiO_2 cells. Figure are reproduced with permission from the reference^[7]. Copyright of AAAS.

The working mechanism of a MSSC is similar to that of a planar PSC where charges are transported via perovskite itself. This is because a perovskite layer is considered as an intrinsic semiconductor with sub-bandgap trap states (predominantly the positive under-coordinated Pb^+ or Pb^{2+} species), the distribution and occupancy of which is largely influenced by the selective contact (or scaffold material) and its polarity. The negative charge on the Al_2O_3 layer due to presence of aluminol groups fills up these trap states and brings the Fermi level closer to the conduction band. Hutter et al.^[250] observed an order of magnitude higher trap density ($6 \times 10^{16} \text{cm}^{-3}$)

3) for planar $\text{CH}_3\text{NH}_3\text{PbI}_3$ films than $\text{CH}_3\text{NH}_3\text{PbI}_3/\text{Al}_2\text{O}_3$ rivals (10^{15} cm^{-3}), despite the much smaller crystal size of the latter. This evidences that the presence of insulating scaffold not only influence the crystal morphology but also, the electronic properties of the resultant film. However, one must note that (i) the MSSCs only demonstrate high performance when a capping layer of perovskite exists above $\text{CH}_3\text{NH}_3\text{PbI}_3/\text{Al}_2\text{O}_3$, which makes a preferred gradient for electron collection, and (ii) the $\text{CH}_3\text{NH}_3\text{PbI}_3/\text{Al}_2\text{O}_3$ films demonstrate significantly lower charge carrier mobility and PL quantum efficiency (PLQE).^[251]

ZrO_2 as a scaffold layer that has achieved PCE > 10%.^[240] However, notable PCE (>12%) is typically reported in a bi-layer architecture (**Fig.18**) where an insulating layer of ZrO_2 is employed on top of mesoporous TiO_2 (**Table 3**).^[252] Such architecture offers additional advantage as it does not employ an organic HTM and instead use thick mesoporous hydrophobic carbon layer thereby yielding a stable device,^[13] as will be discussed in stability section of this article. The best performing MSSC architecture, reported so far, is 15.9% efficient employing a low temperature (<150 °C) processed scaffold.^[26] Another notable performance from same group for MSSC demonstrated PCE ~15.6% in a bi-layer design employing TiO_2 -RGO/ Al_2O_3 bi-layer where the inclusion of graphene flake facilitated superior charge extractions and lowered R_s .^[239]

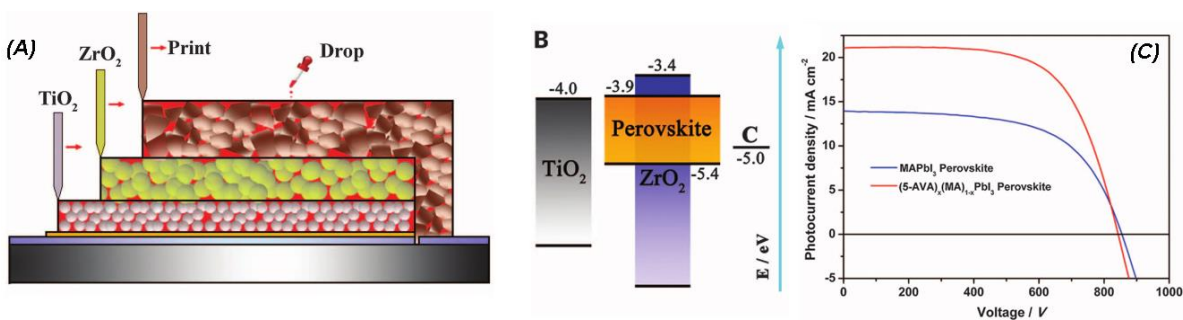


Fig. 18: A typical architecture of monolithic PSCs also called HSC-free PSCs. It utilizes an insulating spacer (typically ZrO_2) between ESC and back contact (typically carbon, also conceived to be hole selective contact here) as shown in (A), Fig. (B & C) shows energy level diagram and also a J-V curve of a PSCs shown in (A).^[252] Figure reproduced with permission from the reference. Copy right of AAAS.

6.4 Single interfacial perovskite solar cells

6.4.1 Electron selective contact free PSCs

The PSCs, likewise many common organic solar cells, also initially employed a tri-layer architecture for charge extraction where an absorber is sandwiched between two selective contacts (**Fig. 1**) which facilitate efficient charge extraction, modify work function of TCO, and reduce interfacial recombination. However, the subsequent research that showed that pristine $\text{CH}_3\text{NH}_3\text{PbI}_3$ or $\text{CH}_3\text{NH}_3\text{PbI}_3/\text{Al}_2\text{O}_3$ has higher electron mobility than $\text{CH}_3\text{NH}_3\text{PbI}_3/\text{TiO}_2$ indicated that an efficient device can, in principal, be made without an ESC.^[7, 253] It is important to note that the low exciton binding energy (2- 5meV)^[254] of perovskite enables thermal dissociation of >98% of the photogenerated excitons at room temperature which can be extracted if only one of the selective contacts is present. This is also supported by the fact that PSCs work as a n-i-p junction device with two key serially connected interfaces; i.e., perovskite/ESC and perovskite/HSC, where the device might work with presence of only one junction.^[255]

This led to unconventional single interface architectures of PSCs: (i) ESC-free, where a perovskite layer is directly deposited on bare TCO or surface modified TCO, and (ii) HSC-free where a back contact is directly deposited on perovskite absorber layer without a HTM layer. For the ESC-free PSCs, Liu et al^[28] first reported PCE 13.5% when a dense ~300 nm thick $\text{CH}_3\text{NH}_3\text{PbI}_3$ is deposited on a bare ITO. Important is to note the energy level mismatch (~ 0.8 eV) between perovskite and ITO which restricted the performance. Towards this, Hu et al^[238] successively reduced this energy mismatch by ~0.4 eV (**Fig. 19**) via surface modification of ITO with Cs_2CO_3 and demonstrated PCE ~15.1% (PV parameters are in **Table 3**). In a similar attempt to reduce energy mismatch at FTO-perovskite interface Ryu et al.^[256] modified FTO surface with PEI (polyethyleneimine), which is widely employed in polymer solar cells to modify work function of FTO by introducing self-assembled dipoles,^[257] and reported PCE >15%

in a device configuration FTO/PEI/PCBM/CH₃NH₃PbI₃/PTAA/Au. Although the device is not ESC free rather it is a metal oxide-free architecture, it is still advantageous over their mesoporous analogues as n-type organic thin films can be prepared at much lower temperature. The use of just a self-assembled monolayer of fullerene derivatives deposited directly on FTO reduces significantly efficiency and avoids the photocurrent decrease observed when ESC is removed.^[120]

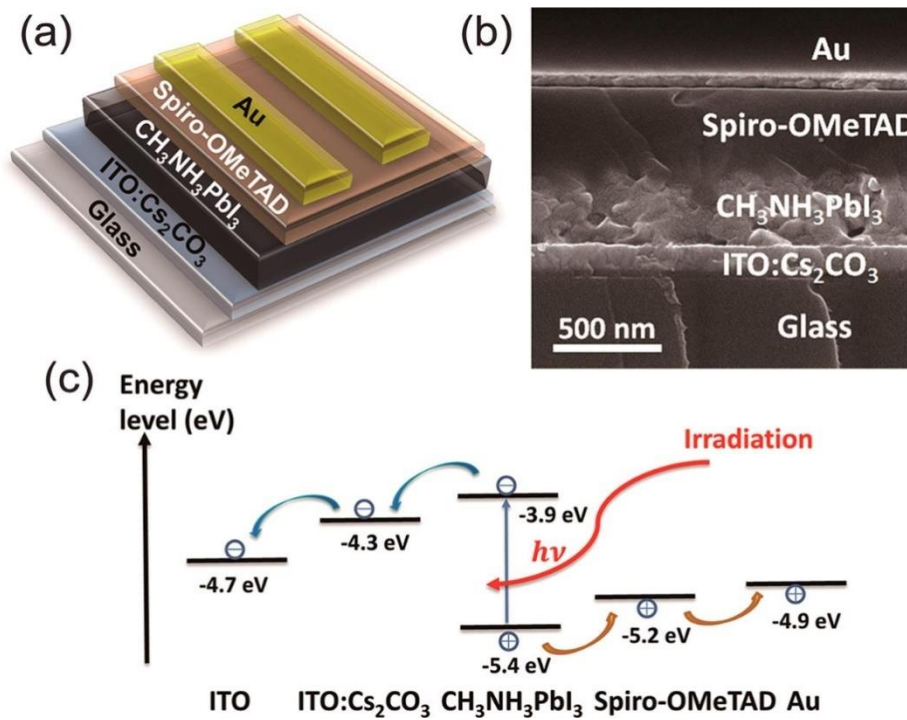


Fig. 19. Device architecture of an ESC free PSC where perovskite is deposited on top of a surface modified ITO. (a) Schematic of the device structure. (b) SEM cross-sectional image of a perovskite solar cell based on Cs₂CO₃-modified ITO substrate, and (c) schematic showing energy level diagram of various device components. Figure are reproduced with permission from the reference.^[238]

6.4.2 Hole selective layer free device architectures

A conventional PSCs offers numerous challenges prior to its commercial deployment; it employs expensive HSC (Spiro-OMeTAD, ≈500 \$) and back contact (Au).^[48, 258] Furthermore, the organic HSCs are humidity sensitive and the metal back contacts typically require vacuum based deposition incompatible with roll-to-roll (R2R) production. The market acceptance of

1
2
3
4 PSCs will require their mass production compatible ambient processing, cost-effectiveness so as
5
6 to reach grid parity (<\$0.05 kWh)^[259] and a stable operational lifetime of devices (>20 years).
7
8

9 HSC-free PSCs offer remedy to these various challenges as they eliminate both the HSC
10 and back contact. The first PSC (architecture: c-TiO₂/m-TiO₂/ZrO₂/perovskite/C) replacing both
11 the HSC and the metal back contact, likewise monolithic DSCs,^[260] and fabricated via mass
12 production compatible protocols reported PCE ~6.6%.^[261] The ZrO₂ layer blocks electrons
13 reaching the carbon back contact as also evidenced in a report by Mei et al which demonstrated a
14 remarkable PCE ~12.8% and a stable performance under 1000 h of light soaking in a fully-
15 printable PSC.^[252] The same group further improved the performance in monolithic PSCs to
16 13.4% by optimizing the size of TiO₂ and thereby the pore size and pore volume which allowed a
17 greater perovskite infiltration in the scaffold.^[244] Similarly, performance enhancement from
18 11.4% to 12.9% is also reported by optimizing perovskite composition from pure MAPbI₃ to
19 FA_{1-x}MX_xPbI₃ (FA- and MA::3:2) which resulted in a broader absorption up to ~840 nm.^[214]
20
21
22
23
24
25
26
27
28
29
30
31
32
33
34
35

36 The monolithic or HSC-free PSCs typically result in a low FF (typically <0.7) owing to a
37 poor perovskite/C interface due to the fact that carbon film has a higher sheet resistance
38 compared to an Au (**Table 3**).^[262] To overcome this, Yan et al^[243] employed single and multi-
39 layered graphene (SG and MG) as HSC resulting in PCE ~6.7 and ~11.5%, respectively. While
40 the SG formed an Ohmic contact, the MG formed a Schottky junction resulting in superior hole
41 extraction rate ~5.1 ns⁻¹ than the former (3.7 ns⁻¹ for SG). A further increase in performance,
42 particularly the FF, is reported by employing multi-wall carbon nanotubes (MWCNTs, PCE
43 ~12.7% and FF~0.8) (**Fig.20**).^[242] Notably, the devices showed a hysteresis free performance
44 compared to a carbon black and graphite based analogues. An optimized perovskite/C interface
45
46
47
48
49
50
51
52
53
54
55
56
57
58
59
60
61
62
63
64
65

is also reported by directly hot-pressing free-standing thermoplastic carbon which resulted in a remarkable PCE ~13.5%, one of the highest till date for HSC-free PSCs.^[263]

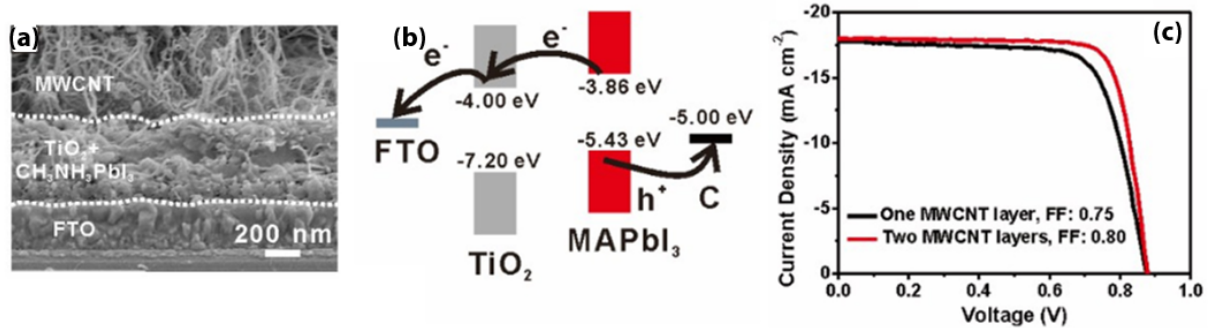


Fig. 20: A common architecture of monolithic PSCs that does not include any insulating layer between ESC and back contact Fig (D).^{[252][252]312[251]}Fig. (E & F) shows energy levels of (D) and J-V curves of such device showing the best FF till date.^[243]Copyright Wiley-VCH Verlag GmbH & Co. KGaA. Reproduced with permission.

Interestingly, the HSC-free PSCs may or may not employ an intermediate insulating layer between ESC and carbon/perovskite (Fig. 20 a-c). This is because the typically employed carbon (carbon black or graphite) has lower conductivity and inferior electronic transport compared to carbon nanotubes, the former's hole extraction rate is lower. Absence of an insulating layer in such case will further increase the interfacial charge recombination, as demonstrated by Mei et al.^[252]The performance dropped from 12.8% to 4.2% when ZrO₂ layer is not employed compared. However, as SWCNTs and MWCNTs are characterized by a superior hole extraction,^[243] directional charge transport and also has shown improved perovskite/C interface,^[242] it may not require an insulating layer for high performance. This is perhaps the reason that the HSC-free or monolithic PSCs with CNT derivatives as back contact do not employ an insulating scaffold layer. It is important to note that the only report (to the best of our knowledge) containing conducting carbon without an insulating spacer (ZrO₂) is by Zhou et al^[241] with a PCE ~8.7% on rigid substrates and ~4% for flexible polymer analogues.

Also, CNTs are a p-type material at ambient conditions and the energy level difference between HOMO of CNTs and VB of perovskite (Fig. 20 b) acts as a driving force for hole

1
2
3
4 injection.^[262] This can also be validated from the fact that a perovskite/CNT film showed 44
5
6 times enhanced charge transfer compared to a bare perovskite film when investigated using PL
7
8 quenching experiment.^[262] The working of monolithic or HSC-free PSCs is conceived be similar
9
10 to heterojunction solar cells.^[215] The balanced electron and hole transport in perovskite
11
12 crystals^[212, 264] explains the charge transport in perovskite film prior to separation at the selective
13
14 contact/s. There are also arguments that the diffusion length in perovskite is not solely
15
16 responsible for charge collection in HSC-free PSCs. Instead the charge transport may take place
17
18 due to drift owing to the built-in electric field ca. 0.9 V^[241] –1.2 V^[265], provided charge
19
20 generation/separation takes place near the depletion layer.^[266]
21
22
23
24
25

26 6.4.3 Monolithic PSCs with a hole selective contact

27 There are PSCs in monolithic configuration that employ alternative HSC to spiro-
28
29 OMeTAD such as CuPc,^[267] PTAA,^[268] NiO^[269] and TPDI^[173] and have achieved PCE 16, 15.3,
30
31 15.3 and 15.5%, respectively, however, as they do not fall under the HSC-free category, their
32
33 performance is not exclusively discussed here. Nevertheless, such designs are suitable when high
34
35 stability and performance in monolithic based PSCs is desired, as they do not employ a humidity
36
37 sensitive spiro-OMeTAD as HTM. We refer reader to a recent review by Bakr et al for more
38
39 comprehensive understanding of various such architectures.
40
41
42
43
44
45
46

47 6.5. Low temperature processing of selective contacts on flexible substrates

48 When it comes to the market applications, four key features of any PV technology
49
50 determine its market success, i.e., cost, efficiency, stability or lifetime and the added
51
52 functionality.^[22] The added functionalities such as transparency, flexibility and aesthetics
53
54 become particularly important when the PVs have to be installed for indoor, portable or
55
56 integrated applications such as in indoor electronics, wearables, and solar windows etc.^[128] Since
57
58
59
60
61
62
63
64
65

1
2
3
4 PSCs have shown to work in low or diffused light,^[270] and have demonstrated PCE >15% in
5
6 flexible devices^[271, 272] with fair indoor stability,^[273, 274] it makes them a preferred choice for
7
8 indoor and portable applications, outperforming the DSCs (~8.5%) and OPVs (~11.5%).^[128, 275]
9
10 Flexible PSCs are also important as they can be prepared on plastic and metallic substrates which
11
12 are ~30% and ~90% cheaper than glass substrates.^[276]
13
14

15
16 The flexible PSCs are mostly developed at T<150°C on conducting plastic substrates
17
18 such as polyethylene terephthalate (PET), polyethersulfone (PES), polyethylene naphthalate
19
20 (PEN) or polycarbonate (PC) and metallic substrates such as titanium, stainless steel and nickel
21
22 foil.^[128, 277] For details on flexible PSCs, we refer to a comprehensive review by Di Giacomo et
23
24 al.^[48] In brief, among the devices made on conducting plastic substrates, PCE ~15.3 and 14.9%
25
26 have been achieved using PET-ITO^[272] employing a TiO₂ NP ESC and PEN-ITO^[278] with
27
28 ZnSnO₄ ESC, respectively. An excellent PV performance and bending stability is also reported
29
30 for f-PSCs when the PET substrates is incorporated with Ag-mesh and a transparent conducting
31
32 polymer (PH1000), resulting in PCE ~14% as shown in **Fig 21 (a –h)**. The best performance in
33
34 f-PSCs to date is reported using ZnO thin ESC in an architecture
35
36 PEN/ITO/ZnO/MAPbI₃/PTAA/Au (PCE ~15.6%, Table 2).^[209] However, while employing ZnO
37
38 as an ESC, one must note that a low temperature processed ZnO often induces more defect sites
39
40 in PSCs leading to a thermal degradation of perovskite.^[279] Similarly, flexible PSCs employing a
41
42 p-type organic layer has also yielded PCE over 12% (PET-
43
44 ITO/PEDOT:PSS/perovskite/PCBM/Au).^[274]
45
46
47
48
49
50
51
52
53
54
55
56
57
58
59
60
61
62
63
64
65

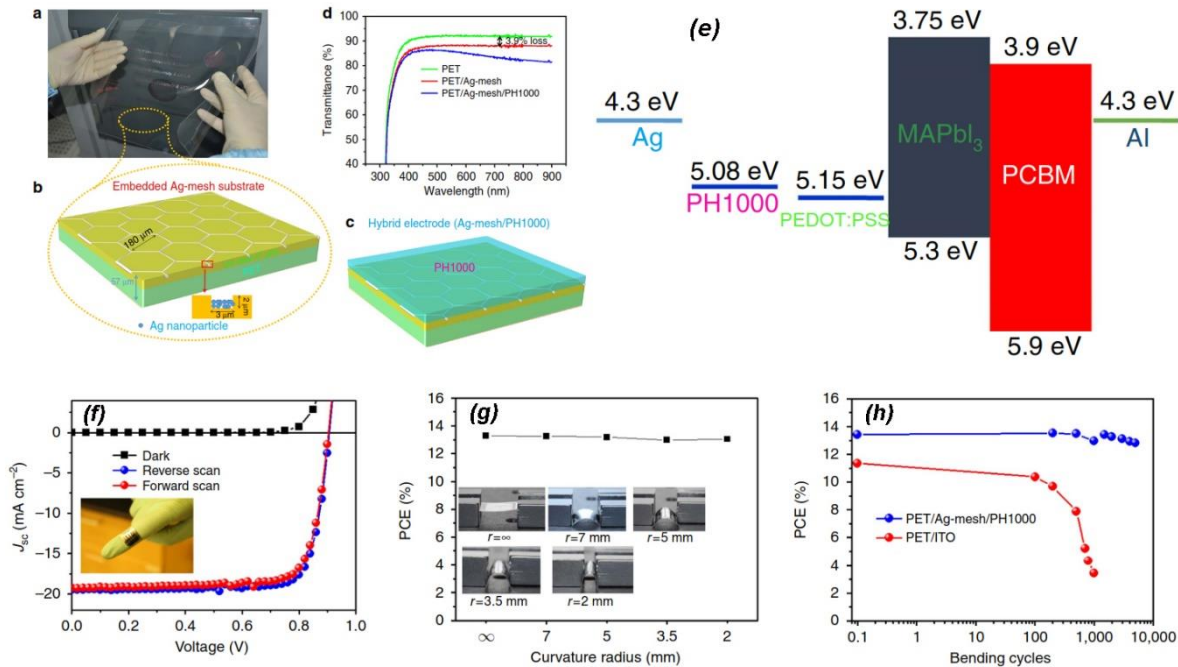


Fig. 21: A modified PET electrode incorporated with a transparent conducting polymer (PH1000) and Ag mesh. (a) is a real image of such a substrate, (b) and (c) show the details of Ag-mesh incorporation and also deposition of PH1000 on PET to develop a hybrid PET/Ag-mesh/PH1000 electrode, (d) transmission spectra of bare PET, PET/Ag-mesh, PET/Ag-mesh/PH1000-based substrates, (e) corresponding energy-level diagram of the various material components employed, (f) J–V curves in reverse and forward scan of the best performing flexible PET/Ag-mesh/PH1000/PEDOT:PSS/MAPbI₃/PCBM/Al solar cell (Inset shows picture of a f-PSC). The device showed no hysteresis upon changing scan directions, (g) bending stability of f-PSC within a specified radius of ∞, 7, 5, 3.5 and 2 mm. The inset shows the real images of the corresponding bending radii, respectively, and (h) PCE of flexible PSCs as a function of bending cycles at a radius of 5 mm. Figure is reproduced with permission from ref.^[271] Copyright of Macmillan Publishers Limited.

On the other hand, flexible PSCs made on opaque metallic foils have shown PCE >10% using Ti foil^[237, 280] and much less for a stainless steel counterpart (<4%)^[247]. The significantly higher performance in Ti foil is understood as a better interaction between TiO₂ ESC and also the native TiO_x layer at the substrate resulting in efficient charge extraction at the interface. However, the key issue here is the requirement of a back contact with high transparency so that maximum light can reach to the absorber layer. Therefore, the typically employed relatively thicker Au layer (~100 nm) is replaced by a thin ITO layer mixed with CNT or Ag mesh.^[280]

1
2
3
4^{281]}Nevertheless, the highest performance (PCE ~10.3%) in such devices has been achieved on
5
6
7 Ti-foil with an insulating scaffold (Al_2O_3) as shown in.^[237]
8
9

10 11 6.5.1 Fiber shaped or unconventional PSCs

12 Inspired from the progress in fibrous DSCs and the need for integrated wearable energy
13 generation and storage devices, fiber or wire shaped PSCs are also witnessed recently.^[247, 248, 282]
14

15 Although the performance (PEC <4%) is much lower than the predecessors, the DSCs (PCE
16 ~9%)^[283], numerous research opportunities exist, particularly in terms of ESC-perovskite
17 interface optimization. Such un-conventional PV designs are of particular interest as they, when
18 incorporated as electronic textile, pave way to wearable PV technology and modern electronics.
19 Here the advantage PSCs offered over DSCs is the absence of liquid electrolyte despite the
20 latter's high PCE.
21
22

23 A first report on wire-shaped PSCs (w-PSCs) by Qiu et al^[247] in 2014 reported ~200 μm
24 thick device on a stainless steel wire and a PCE ~3.3% ($J_{\text{SC}} \sim 10 \text{ mA/cm}^2$ and $V_{\text{OC}} \sim 650 \text{ mV}$).
25 Although the performance is much below liquid electrolyte based DSCs, it is higher than their
26 solid-state DSCs (PCE ~2.6%)^[284] and polymer counterparts (PCE ~2.6%)^[285]. In another report,
27 He et al.^[249] introduced obelisk-like vertically aligned ZnO nanorods at low temperature (<100
28 °C) enabled faster charge extraction ($J_{\text{SC}} \sim 15 \text{ mA/cm}^2$) and a PCE ~3.8%. To further improve the
29 performance, strategies need to be developed for a thick pin-hole free perovskite layer so as to
30 avoid a contact between ESC and HSC. Nonetheless, the w-PSCs demonstrated the ability to be
31 transformed into electronic-textile of size up to few cm^2 , the first demonstration of a perovskite
32 fabric. Future researches to improve performance of w-PSCs should consider improving the
33 contact between ESC and core substrate, transparency of back contact (as w-PSCs are back
34 illuminated due to opaque core material), control over perovskite morphology to avoid ESC-

1
2
3
4 HSC shunting, physical encapsulation for humidity stability, and enhancing their resilience
5
6 during twisting or bending.
7
8
9

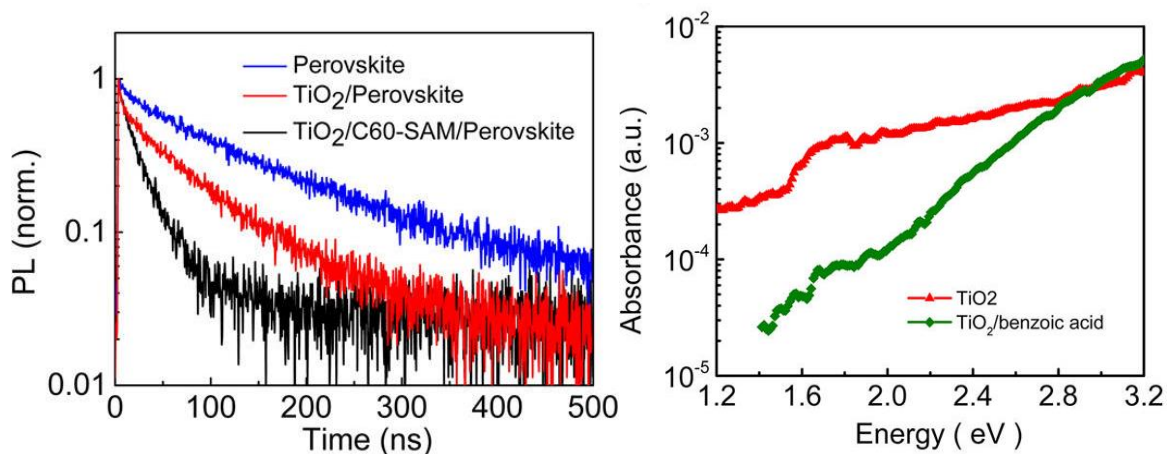
10 11 **7 Interfacial modifiers to improve PV performance of perovskite solar cells**

12 Towards the two pre-requisites of a high performing PV device, i.e., light absorption and
13
14 a complete charge collection, the $\text{CH}_3\text{NH}_3\text{PbX}_3$ offers a high absorption coefficient in the visible
15
16 spectrum ($\sim 10^5 \text{ cm}^{-1}$) which consequent high density of carriers. However, the charge extraction
17
18 is often challenging even in films of thickness $< 300 \text{ nm}$. This is due to the various recombination
19
20 processes within the perovskite film and especially at device interfaces, as we have commented
21
22 in section 3.
23
24
25
26
27

28 Strategies to overcome the various recombination involve depositing perovskite over a
29
30 lead iodide (PbI_2) monolayer,^[286] post-treating $\text{CH}_3\text{NH}_3\text{PbI}_3$ film with di-ammonium iodide,^[55]
31
32 and manipulating the perovskite crystal growth via a polymer matrix.^[54] Similarly, interface
33
34 modification is also carried out at the ESC-perovskite interface, at HSC-perovskite interface, at
35
36 ESC/TCO interface, and at perovskite-metal interface in order to enhance the charge transfer
37
38 efficiency. **Table 4** lists the PV improvement in various such devices. The modifiers employed
39
40 include thin insulating oxide layers, i.e., Al_2O_3 , self-assembled layer (SAM) of fullerene
41
42 derivatives, inorganic materials such as CsBr and CsCl, small molecules, thiols ligands, and
43
44 polymers.
45
46
47
48
49

50 TiO_2 remains the most common selective contact material till date which is known for
51
52 sub-bandgap states arising from under-coordinated surface Ti(IV) ions in its lattice and its
53
54 surface defects. The TiO_2 based PSCs often demonstrate non-radiative recombination. A thin
55
56 layer of fullerene derivatives^[59, 120, 287] or PCBM^[288] and PCBA^[289] have shown to increase
57
58 electron injection into ESC. Wojciechowski et al.^[59] demonstrated via PL decay and
59
60
61
62
63
64
65

1
 2
 3
 4 photothermal deflection spectroscopy that the traps states are significantly passivated when the
 5
 6 TiO_2 layer is functionalized with a fullerene derivative SAM. Not only an efficient charge
 7
 8 extraction is observed from the PL decay, the slope of the absorption at the band edge
 9
 10 (corresponding to Urbach energy) also evidenced significant improvement in TiO_2 lattice
 11
 12 disorder (**Fig.22**). Furthermore, electroluminescence spectra of samples provide a direct evidence
 13
 14 of the 5 to 10 folds' reduction in non-radiative recombination at the interface. Another key issue
 15
 16 is the low charge mobility of TiO_2 which often hinders electron collection leading to hysteresis in
 17
 18 the device. This is overcome by introducing a PCBM overcoating, a material of several orders of
 19
 20 higher electronic mobility that reduced the dark current at the interface and improved the
 21
 22 hysteresis-free performance.^[33, 290] Without the PCBM coating, the TiO_2 based devices require
 23
 24 pre-polarization for efficient charge extractions, which would otherwise leads to large hysteresis
 25
 26 in the PSCs made using them.^[33, 291]
 27
 28
 29
 30
 31
 32
 33
 34



51
 52
 53
 54
 55
 56
 57
 58
 59
 60
 61
 62
 63
 64
 65

Figure 22. (Left) Normalized PL decays of perovskite films interfaced with TiO_2 only and TiO_2 functionalized with a C_{60} -SAM, and (right) photo-thermal deflection spectra of TiO_2 based films and a mimic of C_{60} -SAM (benzoic acid). Figures are reproduced with permission from ref.^[59] Copyright of American Chemical Society.

Similarly, improvement at HSC-perovskite interface, such as by introduction of Mo-IPA (Molybdenum iso-propoxide) assisted perovskite layer fabrication, resulted in VBM (Valence band maximum) alignment of perovskite with spiro-OMeTAD and a more efficient hole

1
2
3
4 extraction. ^[292]The interfacial layers also demonstrated stability improvement, especially under
5
6 the UV-light due to interface modification. ^[293, 294] Research has also been carried out to improve
7
8 perovskite metal interface to obtain smoother and more compact junction and to avoid series
9
10 resistance at the metal electrode side, ^[61] and at FTO/ESC contact by creating a negative dipole to
11
12 alter the work function of the substrate which enhances the electrostatic potential across the
13
14 device. ^[57, 295]
15
16
17
18
19
20
21
22
23
24
25
26
27
28
29
30
31
32
33
34
35
36
37
38
39
40
41
42
43
44
45
46
47
48
49
50
51
52
53
54
55
56
57
58
59
60
61
62
63
64
65

Table 4: An account of various interfacial modifiers employed in perovskite solar cells.

Interface to be modified	Modifier	Device architecture	Voc(V)		Jsc (mA/cm ²)		FF		PCE (%)	
			Test Cell	Ref. cell	Test Cell	Ref. cell	Test Cell	Ref. cell	Test Cell	Ref. cell
ESC-perovskite	4-Cl-PhCOOH, PhCOOH	FTO/c-,m-TiO ₂ / FA _x MA _{1-x} PbI _{3-y} Br _y /Spiro/Au	1.07	1.05	22.28	21.64	0.77	0.76	18.43	17.4
ESC-perovskite	PCBA ^{*a}	FTO/c-TiO ₂ / CH ₃ NH ₃ PbI ₃ /Spiro/Ag	1.16	1.08	21.38	14.94	0.72	0.63	17.76	10.3
ESC-perovskite	PbO monolayer	FTO/c-TiO ₂ / CH ₃ NH ₃ PbI _{3-x} Cl _x /Spiro/Au	1.02	0.98	21.96	20.5	0.76	--	17.03	≈1
ESC-perovskite	La ₂ O ₃	FTO/c-,m-TiO ₂ / CH ₃ NH ₃ PbI ₃ /Spiro/Au	1.01	0.90	20.84	18.73	0.66	0.75	15.81	11.3
ESC-perovskite	C ₆₀ -SAM	FTO/c-TiO ₂ / CH ₃ NH ₃ PbI _{3-x} Cl _x /Spiro/Au	1.02	0.90	21.7	18.6	0.67	0.46	15.0	7.6
ESC-perovskite	PCBM	FTO/ZnO NRs/ CH ₃ NH ₃ PbI ₃ /Spiro/Au	0.96	0.81	22.06	18.57	0.55	0.53	11.67	7.9
HSC-perovskite	DEA ^{*b}	FTO/NiO/DEA/Perovskite/PCBM/PN4N/Ag	0.95	0.94	20.90	17.71	0.80	0.65	15.90	10.9
HSC-perovskite	GeO ₂	ITO-PEDOT:PSS/ CH ₃ NH ₃ PbI _{3-x} Cl _x /PCBM/Ag	0.96	0.89	21.55	18.57	0.74	0.67	10.97	15.3
HSC-perovskite	Mo-IPA ^{*c}	FTO/c-TiO ₂ / CH ₃ NH ₃ PbI ₃ /Spiro/Au	0.90	0.91	22.06	20.86	0.57	0.59	10.8	12.3
Metal/perovskite-PCBM	Doped Bphen ^{*d}	ITO-PEDOT:PSS/ CH ₃ NH ₃ PbI ₃ /PCBM/Ag	0.95	0.88	21.89	20.06	0.75	0.59	15.87	10.7
Metal-perovskite	C ₆₀ -N	ITO-PEDOT:PSS/ CH ₃ NH ₃ PbI ₃ /PCBM/Ag	--	--	--	--	--	--	15.5	7.5
Metal-perovskite	TPB ^{*e}	FTO/c-TiO ₂ / CH ₃ NH ₃ PbI ₃ /Au	0.81	0.74	13.26	11.68	0.58	0.61	6.26	5.2

^{*a} [6,6]-phenyl-C61-butyric acid (PCBA)

^{*b} Diethanolamine

^{*c} Molybdenum isopropoxide

^{*d} N,N,N',N'-Tetraphenyl-benzidine (TPB)

^{*e} 4,7-diphenyl-1,10-phenanthroline (Bphen) doped with bis(2-methyl-dibenzo-[f,h]quinoxaline) (Ir(MDQ)₂(acac))

8 Interfaces towards stability of perovskite solar cells

When it comes to practical deployment of the solar cell technology, the stability becomes as important as their initial PCE.^[300] Although PSCs have shown exceptional PV performance in almost all of their device architectures, they are known to degrade when exposed to outdoor conditions such as humidity, temperature, UV light, light soaking and under the effect of an electric field.^[40, 301, 302] The predominant reasons for instability are intrinsic: (i) structural instability that arises from the fact that the materials constituting a perovskite crystal are chemically unstable and are subjected to a phase change under the effect of atmospheric

1
2
3
4 factors,^[6, 39, 303] and (ii) change in current-voltage profile upon applying an electric bias which
5
6 could either be attributed to the ferroelectric polarization of the MAX₃ or due to ion movement
7
8 of halide ions (see the section 3 for details).^[202, 304] It is noteworthy that although moisture affects
9
10 the long term performance of PSCs, a controlled moisture environment during device fabrication
11
12 is crucial to obtain high photoluminescence and a high PCE.^[305] The origin of this effect is
13
14 attributed to a reduction in trap states due to the partial solvation of the MA ion and “self-
15
16 healing” of the perovskite crystal.^[306] However, over a long term exposure, water ingress into
17
18 PSC decomposes perovskite crystal due to its water solubility.^[307]
19
20
21
22

23
24 Numerous articles suggesting improving chemical stability or elimination of hysteresis in
25
26 PSCs by chemically modifying the CH₃NH₃PbX₃ or by controlling the external factors such as
27
28 water and oxygen ingress in a device, putting UV-filters, and device encapsulation^{[39, 40, 252, 308,}
29
30 ^{309]}or incorporating the perovskite film in a polymer matrix.^[310] However, there have been
31
32 significant contribution to degradation from the interfacing contacts too. It is evidenced that
33
34 replacement of most common HSC in n-type PSCs, i.e., spiro-OMeTAD by humidity resistant
35
36 counterparts such as PTAA^[268] and inorganic counterparts^[246, 267] or in p-type PSCs, replacement
37
38 of organic HSC, i.e., PEDOT:PSS by NiO^[219, 311] enhanced device stability significantly. Reports
39
40 on the role of interfaces determining perovskite stability^[36, 312, 313] are also seen recently. As the
41
42 structural stability of perovskite and also the effect of external atmospheric factors are well
43
44 documented, herein we limit our discussion within the scope of this article, i.e., the case for the
45
46 interfaces namely, ESC/perovskite and HSC/perovskite towards device stability. This is
47
48 particularly important after the reports that interfaces are also crucial for long term stability^{[314,}
49
50 ^{315]} and a recent demonstration that a perovskite layer itself could be stable when exposed to
51
52
53
54
55
56
57
58
59
60
61
62
63
64
65

1
2
3
4 humidity and light and it is rather the interface properties that induces degradation within the
5
6 devices as the characteristics of the interface changes over time.^[316]
7
8

9 **8.1 Degradation at ETL/perovskite interface (mesoporousvs planar)**

10 So far, the most common employed MOSs in mesoporous PSCs are TiO₂ and ZnO.
11
12 Whereas the former has been known to degrade when exposed to UV light^[37] and also induce
13 surface degradation^[36] in its NPs morphology, the latter has been known to deprotonate
14 perovskite layer due to the presence of hydroxide groups on its surface.^[134, 279] Yet mesoporous
15 architecture offers better stability than their planar rivals because the perovskite crystal
16 decomposes upon degradation leaving discontinued film with increased grain boundaries,^{[313,}
17
18 ^{316]}and in such cases, the mesoporous layer helps maintaining stable charge transport channels.
19
20 TiO₂ NPs are also known to induce instability in the device when expose to UV-radiation due to
21 light induced adsorption of surface adsorbed oxygen.^[37] The presence of oxygen sites (Ti₃⁺) on
22 TiO₂ surface may act as traps which are activated in presence of oxygen. One could argue stable
23 performance of the same materials in DSSCs in presence of UV light; however, it is important to
24 note that in DSSCs, these surface traps are pacified by acetonitrile in liquid
25 electrolyte.^[317] Replacing TiO₂ with Al₂O₃ in PSCs has shown a stable performance for 1000 h
26 when exposed to UV-light. This phenomenon also induce instability in planar PSCs, although the
27 rate of observed degradation is relatively slower than PSCs with a mesoporousTiO₂.^[37]
28
29
30
31
32
33
34
35
36
37
38
39
40
41
42
43
44
45
46

47 Alternatively, TiO₂nanorods (NRs) showed greater stability compared to NP based or
48 even planar analogues, in un-encapsulated PSCs^[35] or even their sealed analogues.^[36] PSCs
49 withthree types of TiO₂(**Fig. 23**), fabricated and sealed in an inert atmosphere, showed different
50 degradation profile at similar testing conditions.^[36] Fastest degradation is observed in planar
51 PSCs that retained only <10% of initial PCE after 2500 h followed by a NPs based device that
52 retained nearly 50% of original PCE. However, NRs based devices surprisingly showed slight
53
54
55
56
57
58
59
60
61
62
63
64
65

1
2
3
4 improvement in performance as shown in **Fig. 23 (d)** and also in **Table 5**. It shows that besides
5
6 humidity, the nature of interface to be one of the dominating factors for instability.^[16, 40, 302, 313]
7
8
9 As the devices were sealed in an inert atmosphere and the effect of humidity is negligible, and
10
11 therefore, one would expect as similar degradation behavior for all three device types. The XRD
12
13 analysis of replica of the aged devices (after 2500 h) showed that whereas, the NRs based PSCs
14
15 retained >80% of initial perovskite phase fraction (calculated from the major XRD peaks of
16
17 $\text{CH}_3\text{NH}_3\text{PbI}_3$ at $2\theta \sim 14.4$ and $\sim 28.8^\circ$), NPs based and planar PSCs showed drastic diminishing of
18
19 perovskite, probably due to the fact that the ESC films here induces surface degradation of
20
21 perovskite film by reacting with it unlike NRs that seems to avoid it. This could be related to
22
23 more thermodynamically stable rutile NRs than anatase NPs, and (ii) the different surface energy
24
25 of NRs owing to their different size and crystallinity (NRs are single crystalline and have a larger
26
27 volume $\sim 4.7 \times 10^6 \text{ nm}^3$) than NPs (polycrystalline and significantly smaller volume
28
29 $\sim 8.2 \times 10^3 \text{ nm}^3$). However, regarding the different degradation rate of planar and mesoporous TiO_2
30
31 NPs based PSCs, is not fully understood so far.
32
33
34
35
36
37
38
39
40
41
42
43
44
45
46
47
48
49
50
51
52
53
54
55
56
57
58
59
60
61
62
63
64
65

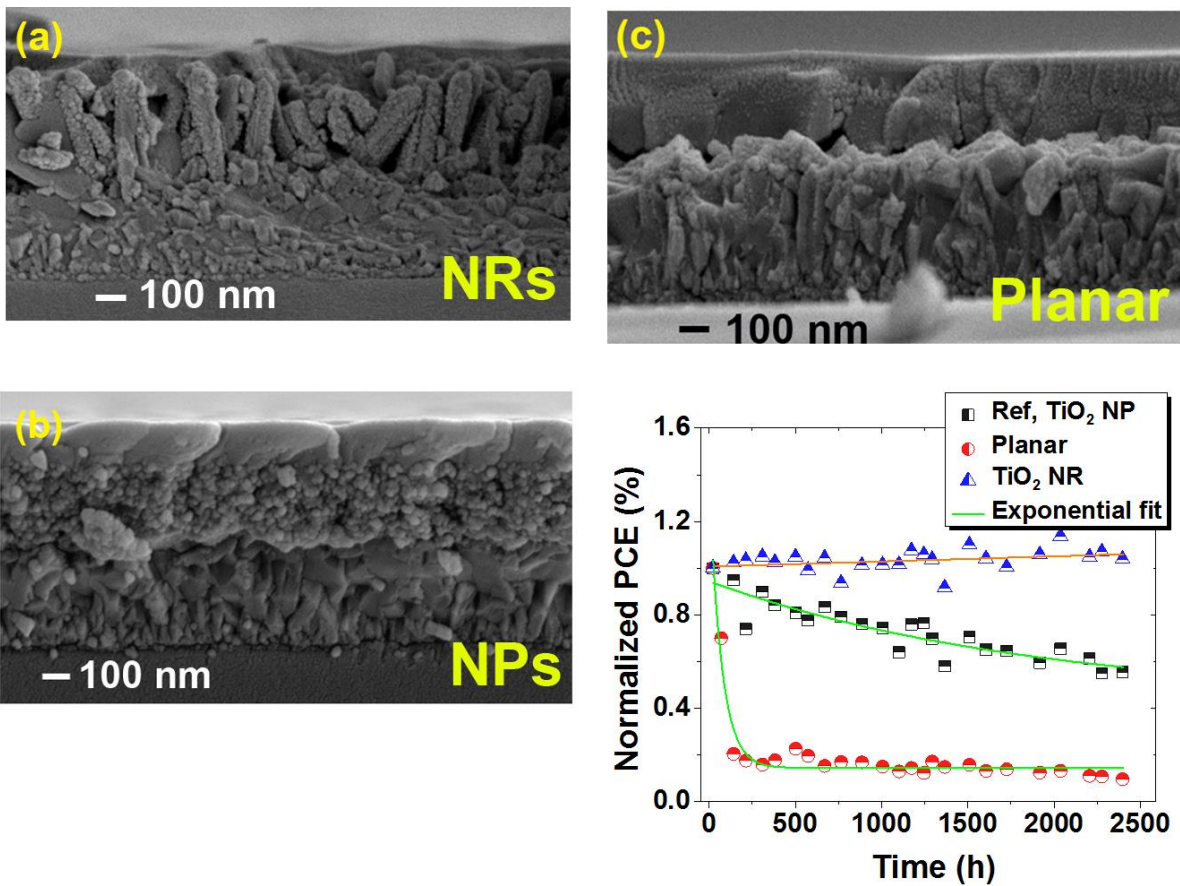


Fig. 23: Cross sectional view of PSCs employing three types of interfaces: (a) TiO₂nanorods, (b) TiO₂ compact layer (a planar PSC configuration), and (c) TiO₂ NP layer using commercial their commercial paste. (d) Normalized PV performance of the three PSCs (encapsulated) stored in dry air (Rel. H <30% at room temperature and in dark). Figures reproduced with permission from Ref.^[36]Copyright of American Chemical Society.

Efforts to modify the characteristics of the ESC interface has demonstrated improvement in stability of PSCs. Ito et al^[318] modified the surface of TiO₂ by coating a thin layer of Sb₂S₃ and observed improvement in photostability of device without encapsulation. Incorporation of Sb₂S₃ between perovskite and TiO₂ avoided surface degradation of CH₃NH₃PbI₃ crystals. A similar report,^[319] where surface passivation of TiO₂ by a thin layer of CdS suppressed interface defects and reduced charge recombination, showed relatively stable performance during 12 h of light soaking compared to a bare TiO₂ analogue.

1
2
3
4 Similarly, replacement of TiO₂ NPs with alternatives such as ZnO NRs,^[320] and
5
6 Zn₂SnO₄^[321] have also demonstrated improved stability thereby evidencing that the interfacing
7
8 material matters in long term durable performance of PSCs(**Table 5**). While the TiO₂ based PSCs
9
10 showed ~50% power drop only after 10 days, Zn₂SnO₄ PSCs retained 86% of initial PCE even
11
12 after 30 days of testing. The Zn₂SnO₄ favored well crystallized perovskite morphology with
13
14 significantly larger grains (~2 μm) which avoided moisture attack on grain boundaries, a
15
16 susceptible site to degradation.^[217, 322] Another possible reason of stable performance could be
17
18 the stronger bonding between CH₃NH₃PbI₃ and Zn₂SnO₄ than between CH₃NH₃PbI₃ and TiO₂
19
20 that improved the interface characteristics.
21
22
23
24
25
26
27
28

29 8.1.1 Stability of planar PSCs

30 The planar PSC have showed drastic degradation not only under light soaking^[323] but
31
32 also during their shelf-life testing.^[36] The degradation was drastic under light soaking resulting in
33
34 complete power drop in the devices. An 80 –90% performance drop is observed for their
35
36 unencapsulated laboratory scale devices^[35] as well as their encapsulated large area modules.^[36] in
37
38 these devices. While one could argue that the drop in the PV performance in the former could be
39
40 due to the presence of humidity, the latter were sealed in a glove box and the contribution from
41
42 humidity is negligible. It is therefore conceivable that the interface (c-TiO₂-perovskite) is highly
43
44 reactive with perovskite crystals. Other possible reasons are the photo-degradation of c-TiO₂ due
45
46 to surface adsorbed oxygen in presence of UV-light, as discussed before, and also its surface
47
48 defects. A recent work by Li et al^[124] report UV-stable performance of a planar PSC by
49
50 incorporating an interface modifier, i.e., cesium bromide (CsBr) between c-TiO₂ and perovskite
51
52 which not only improved the photocatalytic activity of ESC but also reduced interfacial defect
53
54 sites. The reportsuggests a reduction in reactivity of TiO₂ upon incorporation of CsBr thereby
55
56
57
58
59
60
61
62
63
64
65

1
2
3
4 affirming our understanding that a planar device can, in principle, degrade in absence of
5
6 humidity.^[36] Based on the findings of this report and the previous work that encapsulated planar
7
8 and mesoporous-TiO₂ PSCs degraded in absence of humidity,^[36] it seems conceivable that the
9
10 highly reactive TiO₂-perovskite interface plays a dominant role towards instability. This can also
11
12 be understood from the fact that when a thick less reactive insulating oxide layer (ZrO₂, ~2 μm)
13
14 is employed on top of TiO₂, the PSCs showed one of the highest stability (1000 h under light
15
16 soaking) till date.^[252]
17
18
19
20

21 **8.2 Interface effect and stability in flexible PSCs**

22 Flexible PSCs are more prone to degradation as an uneven substrate surface, such as in
23
24 the case of PET-ITO, may result in distortion of perovskite film morphology above it as also
25
26 evidenced by Schmidt et al.^[324] creating an additional degradation channel. Towards a robust and
27
28 highly conductive substrate, Li et al.^[271] reported an Ag-embedded substrate modified with a
29
30 polymer conductor (PH1000) to support low sheet resistance which is also mechanically robust
31
32 as it employs a protective layer of PET (~57 μm) which retained not only at room temperature
33
34 (92% of original performance, PCE~14%), but also, more importantly at higher temperature ~45
35
36 °C (75% of original PCE). Interestingly the stability is higher than that of a reference device
37
38 made on rigid ITO (90% at room temperature and 69% on 45 °C).
39
40
41
42
43
44

45 **8.3 Stability at ITO and back contact interfaces**

46 The degradation can also take place at ITO- or metal back contact. The PSCs with
47
48 organic selective contacts, i.e., PEDOT: PSS, which is acidic, react with ITO surface that leads
49
50 to corrosion. This can be avoided by modifying ITO surface. For example, HSC-free *f*-PSCs
51
52 without a PEDOT:PSS layer demonstrated ~6 times higher stable performance than a
53
54 rival.^[325] Similarly, the degradation due to metal contact is overcome via incorporating a
55
56 Cr₂O₃/Cr interlayer between perovskite and metal contact and pre-treating the PET/ITO substrate
57
58
59
60
61
62
63
64
65

with dimethylsulphoxide resulted in an air stable performance (**Fig. 24**).^[274] It is important to note that the device is extremely thin ($\sim 3 \mu\text{m}$) and showed a stable performance compared to that of a glass ITO based PSCs.

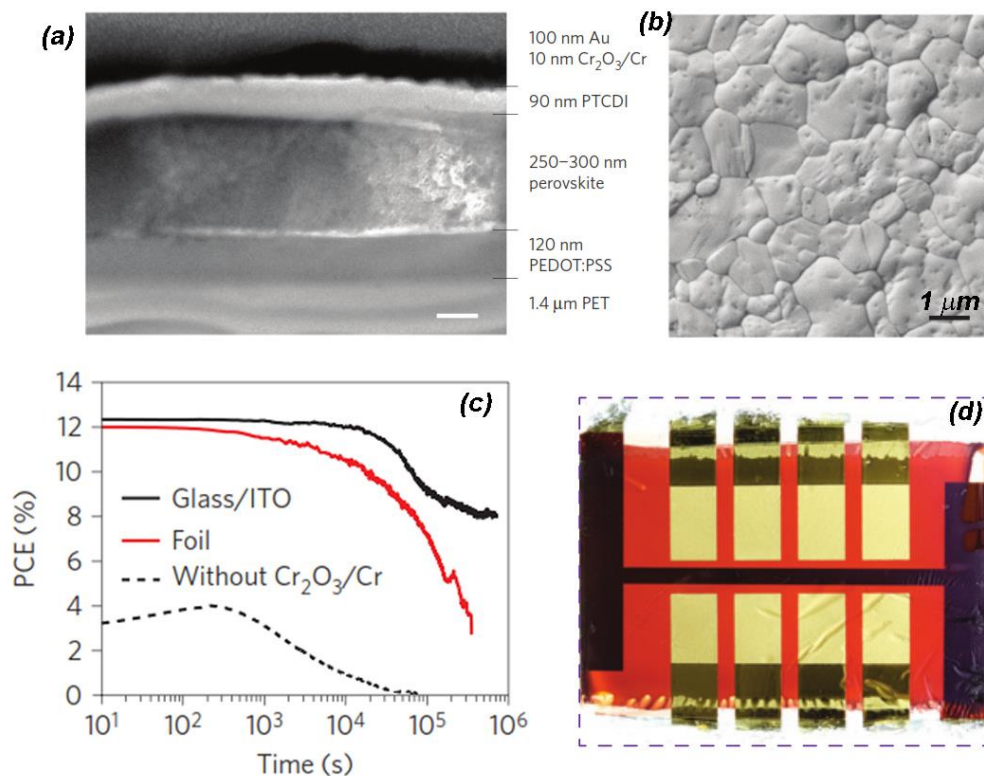


Fig 24: An ultrathin flexible PSC ($\sim 3 \mu\text{m}$). **(a)** Cross-sectional view of a full f-PSC exhibiting uniform and well-separated layers of active materials. Scale bar, 100 nm, **(b)** SEM image of perovskite morphology film on PEDOT:PSS-coated foil. Scale bar, 1 μm, **(c)** stability testing of f-PSCs employing Cr₂O₃/Cr barrier layer and modified PET-ITO (red line) compared with pristine flexible (dashed line) and glass ITO based (black line) counterparts. The pristine flexible PSC showed drastic drop in PCE, and **(d)** a photograph of f-PSC. Figure reproduced with permission from reference ^[274].

Table 5: Stability tests carried out for various types of PSCs. Unless specified, otherwise the abbreviation used in device configuration column corresponds to following: c-T = compact TiO₂, m-T = mesoporous TiO₂ (NPs), MAX₃ = CH₃NH₃PI₃ (X= Cl, Br, I), S = Spiro, P= P3HT, C= Carbon, A=Al₂O₃, Z= ZrO₂, P:P=PEDOT:PSS, Sealed = S, Not Sealed = NS. The performance of the devices is measured at standard test conditions.

Device architecture	Interfacial material		Device fabrication conditions	Stability test conditions	Test duration and/device encapsulation?	Initial PCE (%)	Percentage of PCE change (%)	Reference
	ESC	HSC						
Mesoporous	C,m-TiO ₂	Spiro	Rel. H 50%, ambient air and temperature	Rel. H 15%, dry air, room temperature	2400 h (NS)	10.2	-15%	Yin et al. ^[313]
	C,m-Zn ₂ SnO ₄	Spiro	NA	Dark, dry air, room temperature	~700h (NS)	13.3	-26%	Bera et al. ^[321]
	ZnO-NRs	Spiro	NA	Ambient, room temperature	500h (NS)	5	-14%	Bi et al. ^[320]
	c-TiO ₂	Spiro	Inert atmosphere	Rel. H 40%, dry air, room temperature	1300 h (NS)	12.1	-95%	Fakharuddin et al. ^[35]
	c-T/TiO ₂ NRs	Spiro	Inert atmosphere	Rel. H 40%, dry air, room temperature	1300 h (NS)	5.8	-40%	Fakharuddin et al. ^[35]
	c-T/TiO ₂ NRs-TiCl ₄	Spiro	Inert atmosphere	Rel. H 40%, dry air, room temperature	1300 h (NS)	12.2	+14%	Fakharuddin et al. ^[35]
	c-T/TiO ₂ -NPs/CdS	Spiro	Ambient	Light soaking, ambient	12 h (NS)	9	-20%	Hwang et al. ^[319]
	c-T/TiO ₂ NPs	Spiro	Inert atmosphere	R. H <40%, room temperature	2500 h (S)	7.9	-40%	Fakharuddin et al. ^[36]
	c-T/TiO ₂ NRs	Spiro	Inert atmosphere	R. H <40%, room temperature	2500 h (S)	10.5	+5%	Fakharuddin et al. ^[36]
c,m-TiO ₂	TPDI	--	Ambient, 25 –30 °C, R. H. 40 –50%	720 h	13%	-5%	Zhang et al. ^[173]	
Planar n-i-p	c-TiO ₂	Spiro	Inert atmosphere	R. H <40%, room temperature	2500 h (S)	5.8	-95%	Fakharuddin et al. ^[36]
	c-T/CsBr	Spiro	Inert atmosphere	UV-light (360 nm) at 523 mWcm ⁻²	20 min (NS)	16.1	-30%	Li et al. ^[124]
HTM free	C,m-TiO ₂ /ZrO ₂	HTL free	Ambient	Ambient, light soaking at AM 1.5	1008 h (NS)	10.5	+1%	Mei et al. ^[252]
Inverted planar (p-i-n)	PC ₆₁ BM	PEDOT:PSS	Inert atmosphere	Ambient, 20 °C, R. H. 30%	50 m (NS)	11.7	-99%	Zhang et al. ^[325]
	PCBM	PEDOT:PSS	Inert atmosphere	Inert atmosphere, room temperature	500 h (NS)	14	-10%	Li et al. ^[271]
	PCBM	PEDOT:PSS	Inert atmosphere	Inert atmosphere, 45 °C	~100 h (NS)	14	-31%	Li et al. ^[271]
	PCBM	PEDOT:PSS	Inert atmosphere	Inert atmosphere, 70 °C	≈100 h (NS)	14	-85%	Li et al. ^[271]

14
15
16
17
18
19
20
21
22
23
24
25
26
27
28
29
30
31
32
33
34
35
36
37
38
39
40
41
42
43
44
45
46
47
48
49
50
51
52
53
54
55
56
57
58
59
60
61
62
63
64
65

	PCBM	CPE-K	Inert atmosphere	Ambient ≈ 20 °C, R. H. $\approx 40\%$	120 m (NS)	12.5	-60%	Choi et al. ^[326]
	PCBM	PEDOT:PSS	Inert atmosphere	Ambient, ≈ 20 °C, R. H. $\approx 40\%$	120 m (NS)	12.5	-99%	Choi et al. ^[326]
	PCBM	CuI	Inert atmosphere	Ambient	350 h (NS)	13.6	-10%	Chen et al. ^[246]
	ZnO	PEDOT:PSS	--	Ambient, 30 °C, R. H. 60%	≈ 1000 h	16.1	-20%	Chang et al. ^[245]
	C ₆₀ /BCP	CuSCN	Inert atmosphere	Ambient air, in dark	40 h (NS)	16.6	-(10–15)%	Ye et al. ^[32]
	ZnO	NiO _x	Ambient	Ambient, 25 °C, R. H. 30–50%	1440 h	16.1	-5%	You et al. ^[122]
	PC ₆₁ BM	Cu:NiO _x	--	Ambient	240 h (NS)	≈ 15	-(5–8)%	Kim et al. ^[327]
Device architecture	Device configuration		Device fabrication conditions	Stability test conditions	Test duration and/device encapsulation?	Initial PCE (%)	Percentage of PCE change (%)	Reference
Flexible PSCs	PET-ITO/MAI ₃ /PC ₆₁ BM/Al		Inert atmosphere	Ambient, 20 °C, R. H. 30%	50 m (NS)	9.7	-30%	Zhang et al. ^[325]
	PET-ITO/MAI ₃ /PC ₆₁ BM/Al		Inert atmosphere	Ambient, 20 °C, R. H. 30%	300 m (NS)	9.7	-99%	Zhang et al. ^[325]
	PET-ITO/Ag-mesh/PH1000/P:P/MAI ₃ /PCBM/Al		Inert atmosphere	Inert atmosphere, room temperature	500 h (NS)	14	-8%	Li et al. ^[271]
	PET-ITO/Ag-mesh/PH1000/P:P/MAI ₃ /PCBM/Al		Inert atmosphere	Inert atmosphere, 45 °C	≈ 100 h (NS)	14	-25%	Li et al. ^[271]
	PET-ITO/Ag-mesh/PH1000/P:P/MAI ₃ /PCBM/Al		Inert atmosphere	Inert atmosphere, 70 °C	≈ 100 h (NS)	14	-77%	Li et al. ^[271]
	PET/P:P:MAI ₃ /PCBM/PTCDI ^{*b} /Cr ₂ O ₃ -Cr/Au/PU ^{*c}		Inert atmosphere	Ambient	≈ 10 h (NS)	≈ 12	-20%	Kaltenbrunner et al. ^[274]

^a**CPE-K**: Poly[2,6-(4,4-bis-potas-siumbutanylsulfonate-4H-cyclopenta-[2,1-b;3,4-b']-dithiophene)alt-4,7-(2,1,3-benzothiadiazole)]

^b**PTCDI**: N, N-dimethyl-3,4,9,10-tetracarboxylic perylenediimide

^c**PU**: Polyurethane

8.4 Degradation at HTM/perovskite interface

Since the inception of PSCs, most designs employ an organic hole transporting layer (~300 nm), typically small molecules (spiro-OMeTAD), conducting polymers (P3HT, PTAA and PANI etc.), and inorganic HTMs (CuPc, NiO, CuO etc.), as a hole selective contact.^[328] Despite the fact that the most successful device till date employ inorganic HSCs these organic charge selective contacts are sensitive to moisture and oxygen and thereby induce degradation in PSCs.^[14, 252, 308, 329, 330, 331, 332] A common example is the widely employed spiro-OMeTAD doped with Li-salt (Li-TFSI) which, owing to its extremely hygroscopic nature, tends to react with humidity.^[333, 334] Apart from extrinsic degradation routes, it has been recently reported how the chemical reaction between *spiro*-OMeTAD⁺ and migrating I⁻ from the perovskite absorber progressively reduces the hole transporting material conductivity and deteriorates solar cell performance.^[118] The research activities seeking stable PSCs from an HSC perspective can be classified as: (i) dopant free HSCs,^[333] (ii) inorganic^[335, 336] or organic alternatives^[14, 332, 337] to the commonly used hygroscopic spiro-OMeTAD, (iii) post-modification of HSC or encapsulation to protect the device from humidity^[273, 274, 294, 308, 331], and (iv) by adding new less reactive additives to spiro-OMeTAD^[330, 338]. However, as the focus of the present article is on the role of interfaces only, we limit our discussion to the reports where a modification in HSC/perovskite interface increased the stability in the device. We present case studies from two type of devices here; firstly a mesoporous architecture employing an HSC (**Fig. 1a**) and secondly a p-i-n planar architecture (**Fig. 1 f**) that employs an HSC on conducting substrates, also called an inverted planar PSC.

Despite the fact that highest efficiency PSCs employ spiro-OMeTAD as a HSC, it is known to degrade in presence of moisture, primarily due to the presence of Li-salt dopant in it.

1
2
3
4 Replacement of spiro-OMeTAD with alternative HTMs such as 5, 10, 15-triphenyl-5H-
5
6 diindolo[3, 2-a:3', 2'-c]carbazole(TPDI) has shown to increase the PCE from 15.1% to
7
8 15.5%.^[173]In the absence of Li-TFSI as a dopant in both HTLs, the devices showed PCE ~10.8
9
10 and ~13.6%, respectively. It is important to note that TPDI is a HSC with two order of
11
12 magnitude higher hole mobility (μ_h for TPDI $3.5 \times 10^{-3} \text{ cm}^2 \text{V}^{-1} \text{s}^{-1}$) than spiro-OMeTAD (μ_h for
13
14 TPDI $4 \times 10^{-5} \text{ cm}^2 \text{V}^{-1} \text{s}^{-1}$).^[173]Besides the higher PCE, the PSCs employing a pristine TPDI also
15
16 showed enhanced air-stability; the PCE only dropped by 5% for pristine TPDI based PSCs and
17
18 ~17% for their doped analogues. The use of an iridium complex instead of the commonly Co
19
20 complex additive used to enhance the conductivity of spiro-OMeTAD also has a significant
21
22 beneficial effect in the long term stability.^[339]Other alternatives to spiro-OMeTAD are inorganic
23
24 NiO, and CuSCN which can be employed in mesoporous PSCs.
25
26
27
28
29
30

31 Inverted PSCs also called planar heterojunction PSCs suffer from significant degradation
32
33 primarily arising from their organic ESC and HSC components. The design typically employs
34
35 either a thin PCBM layer, an ESC which is sensitive to moisture, and PEDOT:PSS as a HSC
36
37 which is acidic in nature and also known to degrade in the presence of humidity.^[210] Despite the
38
39 fact that incorporation of organic ESC and HSC routinely resulted in PCE as high as 15 –17%
40
41 (**Table 3**), the devices often degrade drastically even during their shelf-life testing thereby
42
43 putting a question mark on their commercial deployment. Thanks to the optimization of these
44
45 selective contacts, inverted planar PSCs started to show signs of stable performance recently.^{[122,}
46
47 ^{246, 314, 327, 340]} Firstly, interface engineering at ESC via (i) replacing organic PCBM by inorganic
48
49 ESC such as NiO^[122, 220, 341] and NiO_x:Cu^[327] and (ii) post-treatment of PCBM or anorganic-
50
51 inorganic bi-layer design such as PC₆₁BM/TiO_x^[226] and PC₆₁BM/ZnO^[137, 225] demonstrated
52
53 significantly enhanced stability in these device (**Table 5**). These inorganic counterparts
54
55
56
57
58
59
60
61
62
63
64
65

demonstrated stable performance in presence of humidity and also are not corrosive to the substrates underneath.

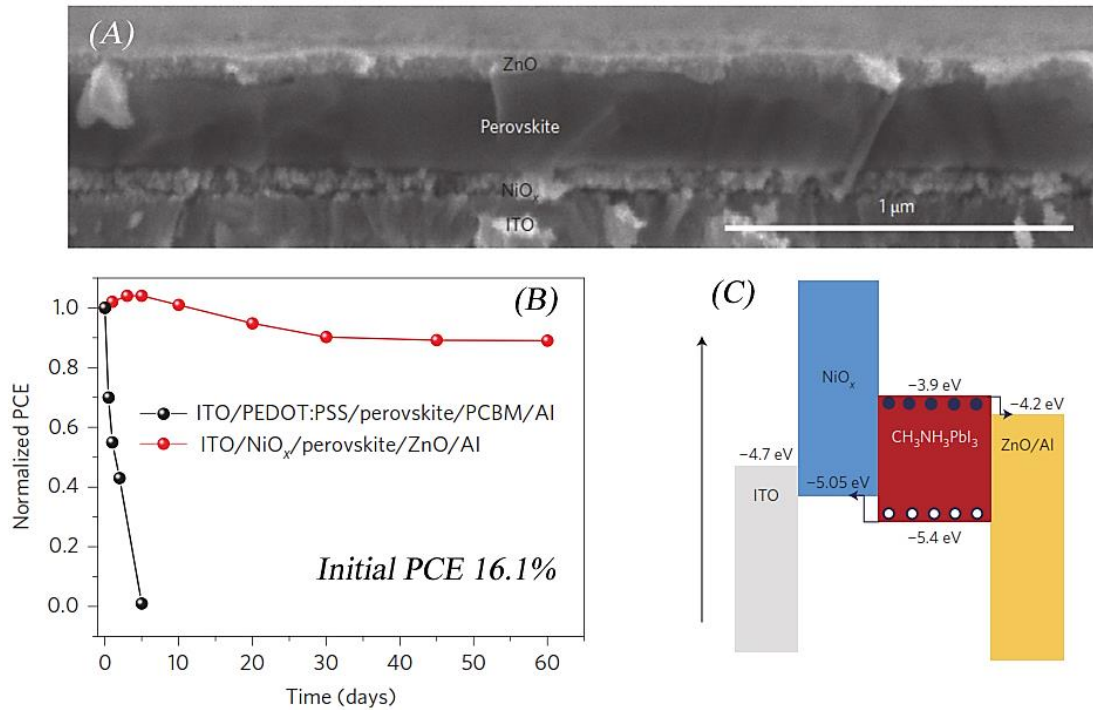


Fig. 25: (a) Cross-sectional image of an inverted planar PSC employing inorganic ESC and HSC (the unfinished Al electrode is not included) with the structure glass/ITO/NiO_x/perovskite/ZnO, (b) air stability of device and a reference PSC employing organic selective contacts, and (c) schematic showing energy levels of materials components of the air-stable inverted planar PSC. Figure reproduced with permission from reference.^[122]

Towards the stability of HSC layer in inverted PSCs, replacing the typically employed humidity sensitive and acidic organic selective contact (PEDOT:PSS, PH ≈ 2)^[342] with an air-stable inorganic counterpart such as NiO^[219, 311, 343], CuSCN,^[32, 336, 344] MoO₃,^[223] and Cu:NiO_x^[327] has also shown enhanced stability. It is important to note that PEDOT:PSS film itself reacts with humidity and form new complexes (water-PEDOT:PSS) which alter its energy levels and thereby hole extraction efficiency of a device. Inorganic HSCs have demonstrated significantly high stability in this class of PSCs; for example, CuSCN based PSCs showed a stable performance for 40 h.^[32] Similarly, Cu:NiO_x based PSCs showed stable performance and retained >90% of initial PCE after 240 h compared to a PEDOT:PSS based PSCs (PCE dropped by 70%). The details of

1
2
3
4 many such alternatives is given in **Table 5**. One of the best stability in such devices is reported
5
6 when both the inorganic selective contacts are replaced with inorganic counterparts (**Fig. 25**),
7
8 resulting in PCE 16.1% and also a significantly stable performance for 60 days.^[122]
9

10
11 Another possible degradation route is the reaction between perovskite and metal back
12 contact (Ag) which corrodes Ag. Incorporation of an intermediate layer such as ZnO^[225] and
13
14 Cr₂O₃-Cr^[274] has shown to form an effective barrier to overcome such degradation. Nevertheless,
15
16 one of the highest stability in inverted planar PSCs is shown in devices replacing both the
17
18 organic components simultaneously. You et al.^[122] reported a fully MOS based inverted planar
19
20 device which retained >90% of initial PCE even after 60 days of shelf life testing and at room
21
22 temperature light soaking contrary to an organic counterpart that degraded in merely 5 days. The
23
24 MOS based inverted PSCs also showed a remarkable PCE ≈16.1% at standard test conditions.
25
26
27
28
29

30
31 As PSCs have demonstrated a photoconversion energy as high as other commercial solar
32
33 devices (CdTe, CIGS, polycrystalline Si), one of the key^[345] challenges is achieving their long
34
35 term stable performance when exposed to outdoor conditions. It can be seen from **Table 3 and 5**
36
37 that PSCs are fabricated with a wide variety of materials and design architectures, many of which
38
39 are intrinsically unstable. It can also be noted that even the similar PSC architectures fabricated
40
41 at different laboratories resulted in different stability which is due to the fact that the durability of
42
43 these devices largely depends on the purity of starting materials, fabrication methods and
44
45 conditions, and also the characteristics of the device interfaces. Unlike silicon and thin film solar
46
47 cells where decades of research has brought them to deliver a stable performance over 20 years
48
49 with negligible intrinsic degradation, these materials resembles OPVs where instability mostly
50
51 arises from the materials components itself such as photo-oxidation, change in morphologies
52
53 over time, and interfacial degradation.^[346] We therefore believe that stability protocols of PSCs
54
55
56
57
58
59
60
61
62
63
64
65

1
2
3
4 are more likely to follow the consensus being developed for OPVs^[346] and DSCs^[22] as the device
5
6 degradation involves chemical modifications. For a detailed overview of the protocols that may
7
8 be adopted while reporting stability of PSCs, we refer to the comprehensive reports highlighting
9
10 various ISOS protocols to be adopted while measuring and reporting operational stability (indoor
11
12 and outdoor).^[22, 300, 346, 347] Although so far, not many reports have followed any standard
13
14 protocol while reporting stability of PSCs, we recommend that the perovskite community should
15
16 follow few considerations while reporting such data. Most importantly the overestimation in PV
17
18 performance of PSCs due to anomalous hysteresis and their erroneous efficiency reporting
19
20 (missing IV data for reverse and forward scan, stabilized maximum power output and statistical
21
22 analysis) must be carefully looked at.^[348] For a reliable device characterization, we suggest a
23
24 measurement protocol developed by Zimmermann et al.^[349] The protocol is derived from standard
25
26 *J-V* measurements, power point tracking and stabilized PV parameters as well as characteristics
27
28 extracted from time resolved current density-voltage measurements. The PSCs research
29
30 community needs to report stabilized PV performance for both scan directions and preferably the
31
32 *J-V* curves at various scan conditions (delay time, scan rate etc.) in order to provide a clearer
33
34 picture of device performance. We recommend a recently published checklist while reporting the
35
36 PV performance.^[350] (ii) while reporting the stability of PSCs, the protocols such as those for
37
38 dark or indoor testing (ISOS-D-1, shelf-life, ISOS-D-2, high temperature storage, and ISOS-D-3,
39
40 damp heat) or those for outdoor (ISOS-O-1-3)^[346] must be followed so that a consensus on the
41
42 stability is made and a true picture of device performance is obtained.
43
44
45
46
47
48
49
50
51

52
53 It is important to note that the PSCs are subjected to stress when continuously exposed to
54
55 incident light. A standard light soaking protocol (humidity, temperature and power of incident
56
57 light) should therefore be considered while reporting such tests. This will be a critical test in
58
59
60
61

1
2
3
4 PSCs provided the fact that perovskite materials polarize when exposed to light inducing
5 hysteresis in the device. We recommend that stability tests need to be divided in to materials'
6 stability (ESC, HSC, perovskite, back contact, transparent electrode and interfaces) and device
7 operation stability under various atmospheric conditions. One can also note that most of the
8 stability tests carried out on PSCs (**Table 5**) are with un-encapsulated devices, a practice that
9 should not be carried out particularly while using TiO₂ based PSCs. This is due to the fact that
10 TiO₂ owing to its oxygen vacancies behaves differently in an environment with less or no
11 oxygen^[37] and therefore the performance of sealed and open devices could largely differ. Also
12 important to note that the stability of flexible PSCs, if their intended deployment is for indoor
13 applications, will have to follow less stringent conditions as they will not be exposed to
14 continuous light soaking.
15
16
17
18
19
20
21
22
23
24
25
26
27
28
29
30
31
32

33 **9. Conclusions and future outlook**

34
35 In this article we have addressed the importance of the charge selective contacts and their
36 interfaces in perovskite solar cells (PSCs) and provided an overview of the different types of
37 interfaces and how they determine device operation and stability. The electron selective contact
38 (ESC) and hole selective contact (HSC) layers are deployed in PSCs in different architectures
39 from planar to nanostructured. As can be seen in **Fig. 26**, there has been tremendous progress in
40 terms of efficiency, scalability and stability of PSCs. We see the application of perovskite in
41 different architectures, wide variety of designs including flexible solar cells on plastic and
42 metallic substrates, their large area modules and also different applications such as in batteries,
43 and light emitting diodes etc.
44
45
46
47
48
49
50
51
52
53
54
55
56

57 The archetypical materials as ESCs are metal oxides, most commonly TiO₂, SnO₂, ZnO
58 and other metal-oxides, including many doped variations and combinations of these.
59
60
61
62
63
64
65

1
2
3
4 Additionally, we find organic ESCs in inverted solar cells using PCBM or C₆₀, however, recently
5 use of organic molecules (and semiconductors) is also demonstrated (Ref.^[125] of this article).
6
7 Even ESC-free PSCs have been fabricated. The same is observed for the HSC, where the
8 standard is the organic spiro-OMeTAD, but many other organic, inorganic, small molecules and
9 polymers counterparts have also been successfully implemented (See Ref.^[351] of this
10 manuscript). The reason for this large variety is manifold: Historically the PSCs started as
11 extremely thin absorber cell, where the dye of a dye-sensitized solar cells (DSSCs) had been
12 replaced by an inorganic thin absorber layer, the methyl ammonium lead halide perovskite.
13
14 Consequently, the material of choice was mesoporous TiO₂ and spiro-OMeTAD as used in solid-
15 state DSSCs. However, since then many different device architectures have been demonstrated,
16 and it is clear, that the PSCs are not excitonic solar cells as dye-sensitized and organic solar cells.
17
18 Therefore, it can be expected that other ESCs and HSCs optimized for excitonic solar cells will
19 adapt better to the PSCs.
20
21
22
23
24
25
26
27
28
29
30
31
32
33
34
35

36 PSCs resemble in its function more thin film inorganic solar cells; however, they present
37 some new features that have not been previously observed in other photovoltaic technologies as
38 ion migration, accumulation capacitance or inductive loops. In contrast to organic and other
39 hybrid solar cell, the ESC and HSC in PSCs only need to function as charge selective layers.
40
41 Exciton splitting at this interface is not necessary. Especially the standard HSC spiro-OMeTAD
42 is probably not ideal, as it has a relative low charge carrier mobility forming amorphous films
43 and only functions well when doped with additives. Furthermore, recently an irreversible
44 chemical reaction between spiro-MeOTAD⁺ and migrating I⁻ is reported at perovskite/HSC
45 interface which leads to deterioration in device performance and instability.^[118]
46
47
48
49
50
51
52
53
54
55
56
57
58
59
60
61
62
63
64
65

1
2
3
4 Currently it is not clear, what the ideal interfacial layers to the perovskite are, however, it
5
6 can be assumed that for different device architectures different materials are ideal. Even more, it
7
8 can be assumed that the different perovskite preparation methods – leading to different
9
10 perovskite films – also show optimized performance with different interfacial layers, which is
11
12 even more the case for different chemical perovskite compositions. Currently, most PSCs are
13
14 primarily optimized in terms of efficiency. However, other aspects will play a major role for
15
16 industrial fabrication and commercialization. Next to solar cells stability, which strongly depend
17
18 on the interfacial layers, also fabrication issues will have strong impact on the choice of
19
20 interfacial layers. This is particularly important as perovskite film morphology depends on the
21
22 underneath layer (scaffold, in case of Al₂O₃). Ideally low temperature processing routes will be
23
24 used, which will allow roll-to-roll fabrication on flexible substrates. The solar cells stability will
25
26 also strongly depend on these layers as replacement of organic selective contacts with inorganic
27
28 ones have shown significant stable performance for inverted planar architectures. Therefore, next
29
30 to the optimized electronic properties the interfacial layers also need be stable and ideally serve
31
32 as protection layers for the perovskite.
33
34
35
36
37
38
39
40
41
42
43
44
45
46
47
48
49
50
51
52
53
54
55
56
57
58
59
60
61
62
63
64
65

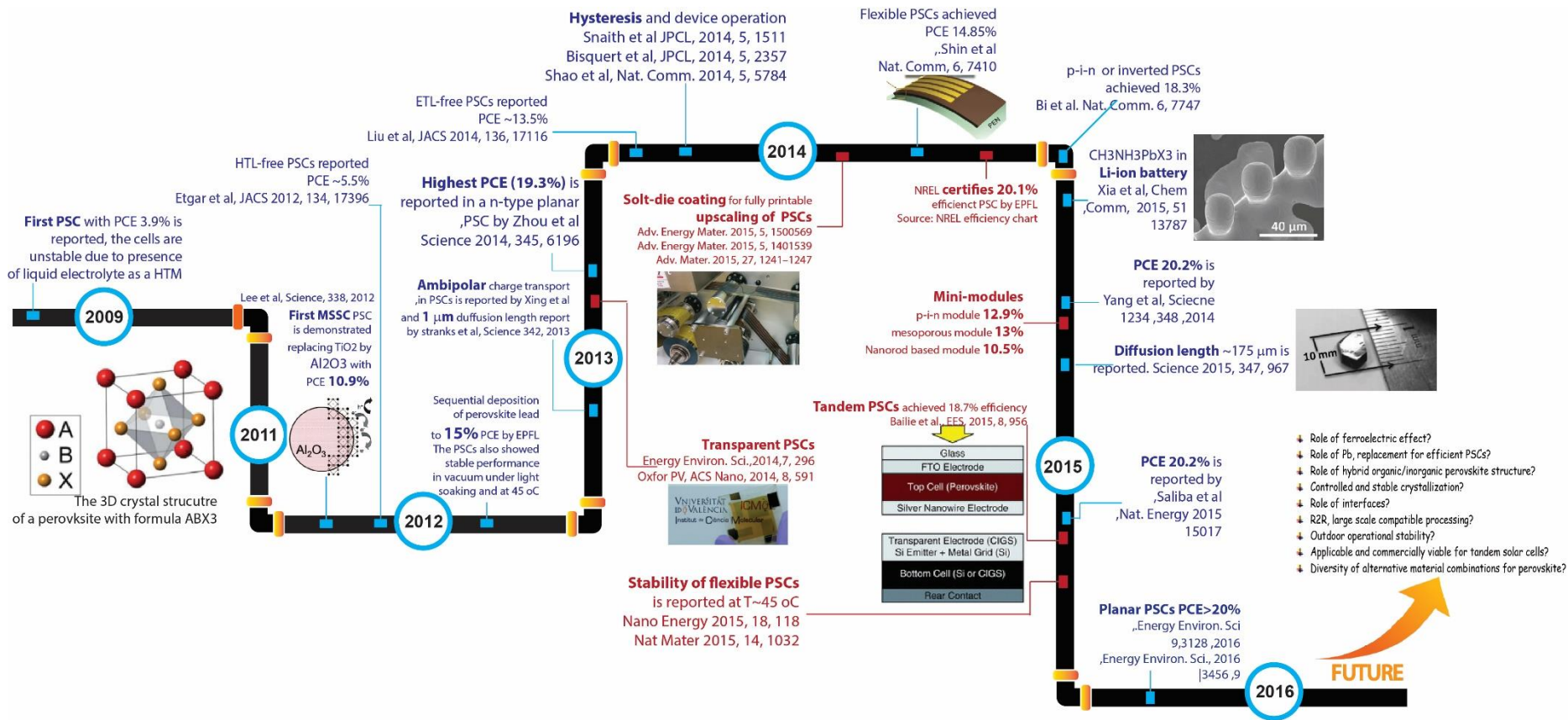


Fig. 26: A timeline showing key developments in perovskite solar cells since their inception in 2009. The notes above the line (in blue text) shows developments towards efficiency and also understanding of device working mechanism whereas the notes below the line (red text) shows milestones towards scalability and stability. The text in black on the right (future) shows key questions that need to be addressed to completely understand the working of these devices for a commercially deployable device.

1
2
3
4 The interfacial selective contacts also have a strong effect on the often observed
5 hysteresis phenomenon. The most common selective contact, TiO₂, often demonstrate a
6 hysteretic effect. There are a number of explanations to this hysteretic effect, such as
7 ferroelectric behavior, ion migration, interfacial capacitive effects and trapping processes.
8
9 However, the effect strongly depends on the interfacial layers, device architecture (planar or
10 mesoporous/nanostructured), the materials, and the perovskite processing, etc. For example, in
11 devices with PCBM or C₆₀ as interfacial layer replacing or just covering the TiO₂ layer, this
12 effect is much smaller, sometimes even negligible. This indicates that hysteresis strongly
13 depends on the nature of the interface and its interaction with the perovskite layer. It seems that
14 high efficiency and stable devices show less of this hysteretic effect. Therefore, it could be that
15 hysteresis is indicating limitations of the cells and possibilities exist to avoid it by optimizing the
16 processing parameters, device architectures and interfacial layers which in this case would also
17 lead to high efficiency and maybe also an improved stability.
18
19
20
21
22
23
24
25
26
27
28
29
30
31
32
33
34
35

36 For highly efficient PSCs, we need perovskite film between charge selective layers,
37 which suppresses interfacial recombination. Surface traps at the interfaces act as recombination
38 centers and need to be avoided and the physical mechanism of charge accumulation have to be
39 completely understood. This makes a good “matching” between the materials necessary, which
40 concerns not only the energetic levels, but also is important for structural alignment at the
41 interface. Finally, most selective interfacial layers have a relative low charge carrier mobility. In
42 this case, they should be as thin as possible, still leading to compact, pin-hole free layers to have
43 minimal transport resistance.
44
45
46
47
48
49
50
51
52
53
54

55 Also the ideal device architectures of the interface to the perovskite layer is not yet
56 completely decided. Record PSC have been obtained with mesoporous TiO₂, nevertheless a very
57
58
59
60
61
62
63
64
65

1
2
3
4 significant progress in the performance of planer solar cells has been made over the last year, and
5
6 very recently, without TiO₂(Ref.^[125] of this article). Usually metal oxides such as TiO₂, SnO₂,
7
8 ZnO and doped variations of them or also binary metal oxides are used, while TiO₂ is by far the
9
10 most common material. However, currently it seems completely open, whether it is really the
11
12 best material. Even though PSCs based on mesoporous TiO₂ films currently hold the efficiency
13
14 record, it is also not clear whether this mesoporous scaffold is really needed for efficient
15
16 crystallization of the perovskite film. An issue without a scaffold might be the device stability,
17
18 which seems to improve in cells with nanostructured metal-oxides as these might be able to
19
20 protect the perovskite layer. It has been shown very early on already that also an insulating
21
22 mesoporous scaffold (Al₂O₃) can be used to replace the mesoporous TiO₂ film due to the
23
24 ambipolar nature of the perovskite layer. In this case, the mesoporous layer just acts as
25
26 crystallization layer and scaffold for the perovskite. High efficiency and stability achieved in
27
28 PSCs using insulating scaffolds such as Al₂O₃ and ZrO₂ would open up extensive investigation.
29
30 The nature of the perovskite film also allows having just one selective contact and having a metal
31
32 contact directly on the perovskite on the other side. This ESC or HSC free p-n type devices do
33
34 function astonishing well, but do not show the same performance and stability as p-i-n type
35
36 devices, where both sides have the selective contacts. Also important to note that a hysteresis-
37
38 free behavior is yet to be observed in these single interface devices, but it has been reduced with
39
40 surface treatments.
41
42
43
44
45
46
47
48
49

50 Towards long term stability and commercialization, PSC technology is advancing in
51
52 order to follow the standard developed by International Electrochemical Committee IEC 61646
53
54 (thin-film terrestrial PV modules–design qualification and type approval), although it seems that
55
56 qualifying other standards such as IEC 61215 (crystalline silicon terrestrial PV modules–design
57
58
59
60
61
62
63
64
65

1
2
3
4 qualification), and IEC 62108 (concentrator photovoltaic (CPV) modules and assemblies—design
5 qualification and type approval) might take longer to be accomplished.^[300] For PV technologies
6
7 such as OPVs, DSCs and PSCs, the IEC 61646 seems more suitable, nonetheless, to reach a
8
9 deployable stage the PSCs have to undergo outdoor exposure tests at maximum power output,
10
11 UV-protection tests, thermal cycling tests (-40 – 85 °C, 200 cycles), damp heat (85 °C, R.H 85%
12
13 for 1000 h), and light soaking (1 sun, ~80 °C). Although initial reports on stability are
14
15 encouraging, PSCs still have a long way to reach a deployable PV technology. PSCs
16
17 manufacturing companies such as Oxford Photovoltaics have made important announcements
18
19 towards stability and deployment in upcoming years. Nonetheless, to achieve long term
20
21 operational stability, stable selective contacts are as important as perovskite layer itself.
22
23
24
25
26
27
28

29 It remains exciting, what progress will be made, and how the understanding of different
30
31 observed features increases and leads to improved device efficiency and stability. As indicated in
32
33 **Fig. 26**, there are still a number of open questions. Answering these will help us to gain deeper
34
35 understanding, which will pave the way to commercialization. It is very likely that we have not
36
37 yet found the “ideal” interface, promoting efficient charge extraction from the perovskite, not
38
39 creating or even passivating surface traps at the interface, and improving the device stability.
40
41 Maybe there is not “one” material, but different pathways which might be successful. The most
42
43 exciting physics happens at the interfaces, so a better understanding of the details of the
44
45 interfacial process will also give us more information on current limitations and ideas how to
46
47 overcome these.
48
49
50
51
52
53
54
55

56 **10 Acknowledgments**

57 A.F acknowledges Alexander von Humboldt Foundation for the postdoctoral research
58
59 fellowship. R.J. acknowledges the Ministry of Education (KPT), Govt. of Malaysia, for the
60
61
62
63
64
65

1
2
3
4
5
6
7
8
9
10
11
12
13
14
15
16
17
18
19
20
21
22
23
24
25
26
27
28
29
30
31
32
33
34
35
36
37
38
39
40
41
42
43
44
45
46
47
48
49
50
51
52
53
54
55
56
57
58
59
60
61
62
63
64
65

fundamental research grant (RDU140126) on perovskite solar cells and thank the Vice Chancellor, Professor Dato' Dr. DaingNasir Ibrahim, and Dy. Vice Chancellor (Research & Innovation), Professor Mashitah Mohd Yusoff to support Nanostructured Renewable Energy Materials Laboratory. The authors from INAM-UJI acknowledge the support from Generalitat Valenciana under project PROMETEOII/2014/020 and from MINECO of Spain Government under project MAT2016-76892-C3-1-R.

11 References

- [1] M. Era, S. Morimoto, T. Tsutsui, S. Saito, *Applied Physics Letters* 1994, 65, 676; H. Oshima, K. Miyano, Y. Konishi, M. Kawasaki, Y. Tokura, *Applied Physics Letters* 1999, 75, 1473; D. B. Mitzi, K. Chondroudis, C. R. Kagan, *IBM Journal of Research and Development* 2001, 45, 29; D. B. Mitzi, C. D. Dimitrakopoulos, L. L. Kosbar, *Chemistry of Materials* 2001, 13, 3728.
- [2] S. Mathews, R. Ramesh, T. Venkatesan, J. Benedetto, *Science* 1997, 276, 238; C. R. Kagan, D. B. Mitzi, C. D. Dimitrakopoulos, *Science* 1999, 286, 945; B. B. Van Aken, T. T. M. Palstra, A. Filippetti, N. A. Spaldin, *Nature Materials* 2004, 3, 164.
- [3] A. Kojima, K. Teshima, Y. Shirai, T. Miyasaka, *J. Am. Chem. Soc.* 2009, 131, 6050.
- [4] J. Wu, Z. Lan, J. Lin, M. Huang, Y. Huang, L. Fan, G. Luo, *Chemical Reviews* 2015, 115, 2136; G. Calogero, A. Bartolotta, G. Di Marco, A. Di Carlo, F. Bonaccorso, *Chemical Society Reviews* 2015, 44, 3244; J. D. Roy-Mayhew, I. A. Aksay, *Chemical Reviews* 2014, 114, 6323; A. Hagfeldt, G. Boschloo, L. Sun, L. Kloo, H. Pettersson, *Chem. Rev.* 2010, 110, 6595.
- [5] J. H. Im, C. R. Lee, J. W. Lee, S. W. Park, N. G. Park, *Nanoscale* 2011, 3, 4088.
- [6] H. S. Kim, C. R. Lee, J. H. Im, K. B. Lee, T. Moehl, A. Marchioro, S. J. Moon, R. Humphry-Baker, J. H. Yum, J. E. Moser, M. Grätzel, N. G. Park, *Scientific Reports* 2012, 2.
- [7] M. M. Lee, J. Teuscher, T. Miyasaka, T. N. Murakami, H. J. Snaith, *Science* 2012, 338, 643.
- [8] J. Burschka, N. Pellet, S. J. Moon, R. Humphry-Baker, P. Gao, M. K. Nazeeruddin, M. Grätzel, *Nature* 2013, 499, 316.
- [9] A. Gugliuzza, A. Basile, *Membranes for Clean and Renewable Power Applications*, 2013.
- [10] N. J. Jeon, J. H. Noh, Y. C. Kim, W. S. Yang, S. Ryu, S. I. Seok, *Nature Materials* 2014, 13, 897.
- [11] H. Zhou, Q. Chen, G. Li, S. Luo, T. B. Song, H. S. Duan, Z. Hong, J. You, Y. Liu, Y. Yang, *Science* 2014, 345, 542.
- [12] M. Saliba, T. Matsui, J.-Y. Seo, K. Domanski, J.-P. Correa-Baena, M. K. Nazeeruddin, S. M. Zakeeruddin, W. Tress, A. Abate, A. Hagfeldt, M. Grätzel, *Energ. Environ. Sci.* 2016.
- [13] A. Mei, X. Li, L. Liu, Z. Ku, T. Liu, Y. Rong, M. Xu, M. Hu, J. Chen, Y. Yang, M. Grätzel, H. Han, *Science* 2014, 345, 295.
- [14] X. Li, M. Ibrahim Dar, C. Yi, J. Luo, M. Tschumi, S. M. Zakeeruddin, M. K. Nazeeruddin, H. Han, M. Grätzel, *Nature Chemistry* 2015, 7, 703.
- [15] P. F. Ndione, W. J. Yin, K. Zhu, S. H. Wei, J. J. Berry, *Journal of Materials Chemistry A* 2015, 3, 21940.
- [16] G. Niu, X. Guo, L. Wang, *Journal of Materials Chemistry A* 2015, 3, 8970.
- [17] M. H. Kumar, N. Yantara, S. Dharani, M. Graetzel, S. Mhaisalkar, P. P. Boix, N. Mathews, *Chemical Communications* 2013, 49, 11089; C. Roldán-Carmona, O. Malinkiewicz, A. Soriano, G. Mínguez Espallargas, A. Garcia, P. Reinecke, T. Kroyer, M. I. Dar, M. K. Nazeeruddin, H. J. Bolink, *Energy and Environmental Science* 2014, 7, 994; Y. Yang, J. You, Z. Hong, Q. Chen, M. Cai, T. B. Song, C. C. Chen, S. Lu, Y. Liu, H. Zhou, *ACS Nano* 2014, 8, 1674; M. Dianetti, F. Di Giacomo, G. Polino, C. Ciceroni, A. Liscio, A. D'Epifanio, S. Licoccia, T. M. Brown, A. Di Carlo, F. Brunetti, *Solar Energy Materials and Solar Cells* 2015, 140, 150.
- [18] D. Liu, T. L. Kelly, *Nature Photonics* 2014, 8, 133.
- [19] F. Di Giacomo, V. Zardetto, A. D'Epifanio, S. Pescetelli, F. Matteocci, S. Razza, A. Di Carlo, S. Licoccia, W. M. M. Kessels, M. Creatore, T. M. Brown, *Advanced Energy Materials* 2015, 5.
- [20] G. Y. Margulis, M. G. Christoforo, D. Lam, Z. M. Beiley, A. R. Bowering, C. D. Bailie, A. Salleo, M. D. McGehee, *Advanced Energy Materials* 2013, 3, 1657; G. E. Eperon, V. M. Burlakov, A. Goriely, H. J. Snaith, *ACS Nano* 2014, 8, 591; L. K. Ono, S. Wang, Y. Kato, S. R. Raga, Y. Qi, *Energy and Environmental Science* 2014, 7, 3989; C. D. Bailie, M. G. Christoforo, J. P. Mailoa, A. R. Bowering, E. L. Unger, W. H. Nguyen, J. Burschka, N. Pellet, J. Z. Lee, M. Grätzel, R. Noufi, T. Buonassisi, A. Salleo, M. D. McGehee, *Energy and Environmental Science* 2015, 8, 956.

- 1
2
3
4 [21] I. Grinberg, D. V. West, M. Torres, G. Gou, D. M. Stein, L. Wu, G. Chen, E. M. Gallo, A. R.
5 Akbashev, P. K. Davies, J. E. Spanier, A. M. Rappe, *Nature* 2013, 503, 509; Q. Wang, Y. Xie, F. Soltani-
6 Kordshuli, M. Eslamian, *Renewable and Sustainable Energy Reviews* 2016, 56, 347.
- 7 [22] A. Fakharuddin, R. Jose, T. M. Brown, F. Fabregat-Santiago, J. Bisquert, *Energy and*
8 *Environmental Science* 2014, 7, 3952.
- 9 [23] W. S. Yang, J. H. Noh, N. J. Jeon, Y. C. Kim, S. Ryu, J. Seo, S. I. Seok, *Science* 2015, 348, 1234.
- 10 [24] M. Saliba, S. Orlandi, T. Matsui, S. Aghazada, M. Cavazzini, J.-P. Correa-Baena, P. Gao, R.
11 Scopelliti, E. Mosconi, K.-H. Dahmen, F. De Angelis, A. Abate, A. Hagfeldt, G. Pozzi, M. Graetzel, M.
12 K. Nazeeruddin, *Nature Energy* 2016, 15017.
- 13 [25] D. Bi, W. Tress, M. I. Dar, P. Gao, J. Luo, C. Renevier, K. Schenk, A. Abate, F. Giordano, J.-P.
14 Correa Baena, J.-D. Decoppet, S. M. Zakeeruddin, M. K. Nazeeruddin, M. Grätzel, A. Hagfeldt, *Science*
15 *Adv.* 2016, 2.
- 16 [26] K. Wojciechowski, M. Saliba, T. Leijtens, A. Abate, H. J. Snaith, *Energy and Environmental*
17 *Science* 2014, 7, 1142.
- 18 [27] J. M. Ball, M. M. Lee, A. Hey, H. J. Snaith, *Energy and Environmental Science* 2013, 6, 1739.
- 19 [28] D. Liu, J. Yang, T. L. Kelly, *Journal of the American Chemical Society* 2014, 136, 17116.
- 20 [29] E. Edri, S. Kirmayer, A. Henning, S. Mukhopadhyay, K. Gartsman, Y. Rosenwaks, G. Hodes, D.
21 Cahen, *Nano Letters* 2014, 14, 1000.
- 22 [30] W. Chen, Y. Wu, J. Liu, C. Qin, X. Yang, A. Islam, Y. B. Cheng, L. Han, *Energy and*
23 *Environmental Science* 2015, 8, 629; C. G. Wu, C. H. Chiang, Z. L. Tseng, M. K. Nazeeruddin, A.
24 Hagfeldt, M. Grätzel, *Energy and Environmental Science* 2015, 8, 2725.
- 25 [31] J. H. Heo, H. J. Han, D. Kim, T. K. Ahn, S. H. Im, *Energy and Environmental Science* 2015, 8,
26 1602.
- 27 [32] S. Ye, W. Sun, Y. Li, W. Yan, H. Peng, Z. Bian, Z. Liu, C. Huang, *Nano Letters* 2015, 15, 3723.
- 28 [33] C. Tao, S. Neutzner, L. Colella, S. Marras, A. R. Srimath Kandada, M. Gandini, M. D. Bastiani,
29 G. Pace, L. Manna, M. Caironi, C. Bertarelli, A. Petrozza, *Energy and Environmental Science* 2015, 8,
30 2365.
- 31 [34] T. Salim, S. Sun, Y. Abe, A. Krishna, A. C. Grimsdale, Y. M. Lam, *Journal of Materials*
32 *Chemistry A* 2015, 3, 8943; Y. Wu, W. Chen, Y. Yue, J. Liu, E. Bi, X. Yang, A. Islam, L. Han, *ACS*
33 *Applied Materials and Interfaces* 2015, 7, 20707.
- 34 [35] A. Fakharuddin, F. Di Giacomo, I. Ahmed, Q. Wali, T. M. Brown, R. Jose, *Journal of Power*
35 *Sources* 2015, 283, 61.
- 36 [36] A. Fakharuddin, F. Di Giacomo, A. L. Palma, F. Matteocci, I. Ahmed, S. Razza, A. D'Epifanio,
37 S. Licocchia, J. Ismail, A. Di Carlo, T. M. Brown, R. Jose, *ACS Nano* 2015, 9, 8420.
- 38 [37] T. Leijtens, G. E. Eperon, S. Pathak, A. Abate, M. M. Lee, H. J. Snaith, *Nature Communications*
39 2013, 4.
- 40 [38] J. Xu, A. Buin, A. H. Ip, W. Li, O. Voznyy, R. Comin, M. Yuan, S. Jeon, Z. Ning, J. J.
41 McDowell, P. Kanjanaboos, J.-P. Sun, X. Lan, L. N. Quan, D. H. Kim, I. G. Hill, P. Maksymovych, E. H.
42 Sargent, *Nat Commun* 2015, 6.
- 43 [39] T. Leijtens, G. E. Eperon, N. K. Noel, S. N. Habisreutinger, A. Petrozza, H. J. Snaith, *Advanced*
44 *Energy Materials* 2015, 5.
- 45 [40] Y. Rong, L. Liu, A. Mei, X. Li, H. Han, *Advanced Energy Materials* 2015, 5.
- 46 [41] Q. Wali, A. Fakharuddin, I. Ahmed, M. H. Ab Rahim, J. Ismail, R. Jose, *Journal of Materials*
47 *Chemistry A* 2014, 2, 17427.
- 48 [42] Q. Wali, A. Fakharuddin, R. Jose, *Journal of Power Sources* 2015, 293, 1039.
- 49 [43] W. Ke, G. Fang, Q. Liu, L. Xiong, P. Qin, H. Tao, J. Wang, H. Lei, B. Li, J. Wan, G. Yang, Y.
50 Yan, *Journal of the American Chemical Society* 2015, 137, 6730.
- 51 [44] M. A. Peña, J. L. G. Fierro, *Chemical Reviews* 2001, 101, 1981.
- 52 [45] A. Fakharuddin, F. De Rossi, T. M. Watson, L. Schmidt-Mende, R. Jose, *APL Materials* 2016, 4,
53 091505.
- 54
55
56
57
58
59
60
61
62
63
64
65

- 1
2
3
4 [46] T. Yagi, H. K. Mao, P. M. Bell, *Physics and Chemistry of Minerals* 1978, 3, 97; H. D. Megaw,
5 *Proceedings of the Physical Society* 1946, 58, 133.
6 [47] B. Saporov, D. B. Mitzi, *Chemical Reviews* 2016, 116, 4558.
7 [48] F. Di Giacomo, A. Fakharuddin, R. Jose, T. M. Brown, *Energy & Environmental Science* 2016,
8 9, 3007.
9 [49] Y. Rakita, E. Meirzadeh, T. Bendikov, V. Kalchenko, I. Lubomirsky, G. Hodes, D. Ehre, D.
10 Cahen, *APL Materials* 2016, 4, 051101; Y. Kutes, L. Ye, Y. Zhou, S. Pang, B. D. Huey, N. P. Padture,
11 *Journal of Physical Chemistry Letters* 2014, 5, 3335; Z. Fan, J. Xiao, K. Sun, L. Chen, Y. Hu, J. Ouyang,
12 K. P. Ong, K. Zeng, J. Wang, *The Journal of Physical Chemistry Letters* 2015, 6, 1155.
13 [50] M. O. K. Matyjasek, *Condensed Matter Physics* 2013, 16, 31704:1.
14 [51] J. Bisquert, D. Cahen, G. Hodes, S. Rühle, A. Zaban, *Journal of Physical Chemistry B* 2004, 108,
15 8106.
16 [52] C. Wehrenfennig, G. E. Eperon, M. B. Johnston, H. J. Snaith, L. M. Herz, *Advanced Materials*
17 2014, 26, 1584; N. Marinova, S. Valero, J. L. Delgado, *Journal of Colloid and Interface Science* 2017,
18 488, 373.
19 [53] E. Guillén, F. J. Ramos, J. A. Anta, S. Ahmad, *Journal of Physical Chemistry C* 2014, 118,
20 22913.
21 [54] D. Bi, C. Yi, J. Luo, J.-D. Décoppet, F. Zhang, Shaik M. Zakeeruddin, X. Li, A. Hagfeldt, M.
22 Grätzel, *Nature Energy* 2016, 1, 16142.
23 [55] T. Zhao, C.-C. Chueh, Q. Chen, A. Rajagopal, A. K. Y. Jen, *ACS Energy Letters* 2016, 1, 757.
24 [56] C. S. Ponseca, T. J. Savenije, M. Abdellah, K. Zheng, A. Yartsev, T. Pascher, T. Harlang, P.
25 Chabera, T. Pullerits, A. Stepanov, J. P. Wolf, V. Sundström, *Journal of the American Chemical Society*
26 2014, 136, 5189; K. Wang, C. Liu, P. Du, J. Zheng, X. Gong, *Energy and Environmental Science* 2015, 8,
27 1245.
28 [57] Y. Liu, M. Bag, L. A. Renna, Z. A. Page, P. Kim, T. Emrick, D. Venkataraman, T. P. Russell,
29 *Advanced Energy Materials* 2016, 6.
30 [58] W. Li, J. Li, L. Wang, G. Niu, R. Gao, Y. Qiu, *Journal of Materials Chemistry A* 2013, 1, 11735;
31 F. Wang, Y. Chen, G. Han, Q. Zhang, Q. Ma, *Current Applied Physics* 2016, 16, 1353.
32 [59] K. Wojciechowski, S. D. Stranks, A. Abate, G. Sadoughi, A. Sadhanala, N. Kopidakis, G.
33 Rumbles, C. Z. Li, R. H. Friend, A. K. Y. Jen, H. J. Snaith, *ACS Nano* 2014, 8, 12701.
34 [60] Y. Bai, H. Chen, S. Xiao, Q. Xue, T. Zhang, Z. Zhu, Q. Li, C. Hu, Y. Yang, Z. Hu, F. Huang, K.
35 S. Wong, H. L. Yip, S. Yang, *Advanced Functional Materials* 2016, 26, 2950.
36 [61] L. L. Jiang, S. Cong, Y. H. Lou, Q. H. Yi, J. T. Zhu, H. Ma, G. F. Zou, *Journal of Materials*
37 *Chemistry A* 2015, 4, 217.
38 [62] A. Dualeh, T. Moehl, N. Tétreault, J. Teuscher, P. Gao, M. K. Nazeeruddin, M. Grätzel, *ACS*
39 *Nano* 2014, 8, 362; A. Pockett, G. E. Eperon, T. Peltola, H. J. Snaith, A. Walker, L. M. Peter, P. J.
40 Cameron, *Journal of Physical Chemistry C* 2015, 119, 3456; J. Z. Shao, W. W. Dong, Z. H. Deng, R. H.
41 Tao, X. D. Fang, *Gongneng Cailiao/Journal of Functional Materials* 2014, 45, 24008; A. R. Pascoe, N. W.
42 Duffy, A. D. Scully, F. Huang, Y. B. Cheng, *Journal of Physical Chemistry C* 2015, 119, 4444; V.
43 Gonzalez-pedro, E. J. Juarez-perez, W.-s. Arsyad, E. M. Barea, F. Fabregat-santiago, I. Mora-sero, J.
44 Bisquert, 2013; H. S. Kim, I. Mora-Sero, V. Gonzalez-Pedro, F. Fabregat-Santiago, E. J. Juarez-Perez, N.
45 G. Park, J. Bisquert, *Nature Communications* 2013, 4.
46 [63] E. J. Juarez-Perez, M. Wußler, F. Fabregat-Santiago, K. Lakus-Wollny, E. Mankel, T. Mayer, W.
47 Jaegermann, I. Mora-Sero, *Journal of Physical Chemistry Letters* 2014, 5, 680.
48 [64] A. Guerrero, G. Garcia-Belmonte, I. Mora-Sero, J. Bisquert, Y. S. Kang, T. J. Jacobsson, J.-P.
49 Correa-Baena, A. Hagfeldt, *The Journal of Physical Chemistry C* 2016.
50 [65] F. Fabregat-Santiago, G. Garcia-Belmonte, I. Mora-Seró, J. Bisquert, *Physical Chemistry*
51 *Chemical Physics* 2011, 13, 9083.
52 [66] M. Anaya, W. Zhang, B. C. Hames, Y. Li, F. Fabregat-Santiago, M. E. Calvo, H. J. Snaith, H.
53 Míguez, I. Mora-Sero, *Journal of Materials Chemistry C* 2017, 5, 634.
54
55
56
57
58
59
60
61
62
63
64
65

- 1
2
3
4 [67] J. Bisquert, G. Garcia-Belmonte, Á. Pitarch, H. J. Bolink, Chemical Physics Letters 2006, 422,
5 184.
6 [68] I. Zarazua, J. Bisquert, G. Garcia-Belmonte, The Journal of Physical Chemistry Letters 2016, 7,
7 525.
8 [69] I. Zarazua, G. Han, P. P. Boix, S. Mhaisalkar, F. Fabregat-Santiago, I. Mora-Seró, J. Bisquert, G.
9 Garcia-Belmonte, The Journal of Physical Chemistry Letters 2016, 7, 5105.
10 [70] L. Contreras, J. Idigoras, A. Todinova, M. Salado, S. Kazim, S. Ahmad, J. A. Anta, Physical
11 Chemistry Chemical Physics 2016, 18, 31033.
12 [71] V. W. Bergmann, Y. Guo, H. Tanaka, I. M. Hermes, D. Li, A. Klasen, S. A. Bretschneider, E.
13 Nakamura, R. Berger, S. A. L. Weber, ACS Applied Materials & Interfaces 2016, 8, 19402.
14 [72] Y. F. Chen, Y. T. Tsai, D. M. Bassani, R. Clerc, D. Forgacs, H. J. Bolink, M. Wussler, W.
15 Jaegermann, G. Wantz, L. Hirsch, Journal of Materials Chemistry A 2016, 4, 17529.
16 [73] E. J. Juarez-Perez, R. S. Sanchez, L. Badia, G. Garcia-Belmonte, Y. S. Kang, I. Mora-Sero, J.
17 Bisquert, Journal of Physical Chemistry Letters 2014, 5, 2390.
18 [74] R. Gottesman, P. Lopez-Varo, L. Gouda, Juan A. Jimenez-Tejada, J. Hu, S. Tirosh, A. Zaban, J.
19 Bisquert, Chem, 1, 776.
20 [75] D. W. deQuilettes, W. Zhang, V. M. Burlakov, D. J. Graham, T. Leijtens, A. Osherov, V.
21 Bulović, H. J. Snaith, D. S. Ginger, S. D. Stranks, Nature Communications 2016, 7.
22 [76] A. Marchioro, J. Teuscher, D. Friedrich, M. Kunst, R. van de Krol, T. Moehl, M. Gratzel, J.-E.
23 Moser, Nat Photon 2014, 8, 250.
24 [77] W. Tress, N. Marinova, O. Inganäs, M. K. Nazeeruddin, S. M. Zakeeruddin, M. Graetzel,
25 Advanced Energy Materials 2015, 5, n/a.
26 [78] D. W. DeQuilettes, S. M. Vorpahl, S. D. Stranks, H. Nagaoka, G. E. Eperon, M. E. Ziffer, H. J.
27 Snaith, D. S. Ginger, Science 2015, 348, 683.
28 [79] E. Climent-Pascual, B. C. Hames, J. S. Moreno-Ramirez, A. L. Alvarez, E. J. Juarez-Perez, E.
29 Mas-Marza, I. Mora-Sero, A. de Andres, C. Coya, Journal of Materials Chemistry A 2016, 4, 18153.
30 [80] M. A. Green, K. Emery, Y. Hishikawa, W. Warta, E. D. Dunlop, Progress in Photovoltaics:
31 Research and Applications 2016, 24, 3.
32 [81] J. H. Heo, D. H. Song, S. H. Im, Advanced Materials 2014, 26, 8179.
33 [82] E. H. Anaraki, A. Kermanpur, L. Steier, K. Domanski, T. Matsui, W. Tress, M. Saliba, A. Abate,
34 M. Gratzel, A. Hagfeldt, J.-P. Correa-Baena, Energy & Environmental Science 2016, 9, 3128.
35 [83] Y. Shao, Y. Yuan, J. Huang, Nature Energy 2016, 1, 15001.
36 [84] W. Tress, in *Organic-Inorganic Halide Perovskite Photovoltaics: From Fundamentals to Device*
37 *Architectures*, (Eds: N.-G. Park, M. Grätzel, T. Miyasaka), Springer International Publishing, Cham
38 2016, 53.
39 [85] B. Cai, Y. Xing, Z. Yang, W.-H. Zhang, J. Qiu, Energy Environ. Sci. 2013, 6, 1480.
40 [86] Y. Zou, D. Gendron, R. Badrou-Aïch, A. Najari, Y. Tao, M. Leclerc, Macromolecules 2009, 42,
41 2891.
42 [87] E. Edri, S. Kirmayer, M. Kulbak, G. Hodes, D. Cahen, Journal of Physical Chemistry Letters
43 2014, 5, 429.
44 [88] S. Chen, Y. Hou, H. Chen, M. Richter, F. Guo, S. Kahmann, X. Tang, T. Stubhan, H. Zhang, N.
45 Li, N. Gasparini, C. O. R. Quiroz, L. S. Khanzada, G. J. Matt, A. Osvet, C. J. Brabec, Advanced Energy
46 Materials 2016, 6, n/a.
47 [89] P. Tiwana, P. Docampo, M. B. Johnston, H. J. Snaith, L. M. Herz, ACS Nano 2011, 5, 5158.
48 [90] W. H. Nguyen, C. D. Bailie, E. L. Unger, M. D. McGehee, Journal of the American Chemical
49 Society 2014, 136, 10996.
50 [91] E. Edri, S. Kirmayer, D. Cahen, G. Hodes, Journal of Physical Chemistry Letters 2013, 4, 897.
51 [92] S. Ryu, J. H. Noh, N. J. Jeon, Y. Chan Kim, W. S. Yang, J. Seo, S. I. Seok, Energy and
52 Environmental Science 2014, 7, 2614.
53 [93] M. Kröger, S. Hamwi, J. Meyer, T. Riedl, W. Kowalsky, A. Kahn, Organic Electronics 2009, 10,
54 932.
55
56
57
58
59
60
61
62
63
64
65

- 1
2
3
4 [94] C. G. Wu, C. H. Chiang, S. H. Chang, *Nanoscale* 2016, 8, 4077.
- 5 [95] J. Burschka, N. Pellet, S.-J. Moon, R. Humphry-Baker, P. Gao, M. K. Nazeeruddin, M. Grätzel,
6 *Nature* 2013, 499, 316; M. Liu, M. B. Johnston, H. J. Snaith, *Nature* 2013, 501, 395; W. S. Yang, J. H.
7 Noh, N. J. Jeon, Y. C. Kim, S. Ryu, J. Seo, S. I. Seok, *Science* 2015, 348, 1234; G. Xing, N. Mathews, S.
8 S. Lim, N. Yantara, X. Liu, D. Sabba, M. Grätzel, S. Mhaisalkar, T. C. Sum, *Nat Mater* 2014, 13, 476; I.
9 Suárez, E. J. Juárez-Pérez, J. Bisquert, I. Mora-Seró, J. P. Martínez-Pastor, *Adv. Mater.* 2015, 27, 6157.
- 10 [96] Z. Xiao, Y. Yuan, Y. Shao, Q. Wang, Q. Dong, C. Bi, P. Sharma, A. Gruverman, J. Huang, *Nat*
11 *Mater* 2015, 14, 193.
- 12 [97] H. J. Snaith, A. Abate, J. M. Ball, G. E. Eperon, T. Leijtens, N. Kimberly, S. D. Stranks, J. T.-W.
13 Wang, K. Wojciechowski, W. Zhang, N. K. Noel, *The Journal of Physical Chemistry Letters* 2014, 5,
14 1511; R. S. Sanchez, V. Gonzalez-Pedro, J.-W. Lee, N.-G. Park, Y. S. Kang, I. Mora-Sero, J. Bisquert,
15 *Journal of Physical Chemistry Letters* 2014, 5, 2357–2363.
- 16 [98] E. L. Unger, E. T. Hoke, C. D. Bailie, W. H. Nguyen, A. R. Bowring, T. Heumüller, M. G.
17 Christoforod, M. D. McGehee, *Energy & Environmental Science* 2014, 7, 3690.
- 18 [99] N. J. Jeon, J. H. Noh, Y. C. Kim, W. S. Yang, S. Ryu, S. I. Seok, *Nature Materials* 2014, 13,
19 897–903.
- 20 [100] J. M. Frost, K. T. Butler, A. Walsh, *APL Mater.* 2014, 2, 081506; J. Wei, Y. Zhao, H. Li, G. Li, J.
21 Pan, D. Xu, Q. Zhao, D. Yu, *Journal of Physical Chemistry Letters* 2014, 5, 3937–3945; H.-W. Chen, N.
22 Sakai, M. Ikegami, T. Miyasaka, *Journal of Physical Chemistry Letters* 2015, 6, 164–169.
- 23 [101] Y. Shao, Z. Xiao, C. Bi, Y. Yuan, J. Huang, *Nat. Commun.* 2014, 5, 5784.
- 24 [102] A. Dualeh, T. Moehl, N. Tétreault, J. Teuscher, P. Gao, M. K. Nazeeruddin, M. Grätzel, *ACS*
25 *Nano* 2014, 8, 362; Y. Yang, J. Xiao, H. Wei, L. Zhu, D. Li, Y. Luo, H. Wu, Q. Meng, *RSC Adv.* 2014,
26 4, 52825.
- 27 [103] O. Almora, I. Zarazua, E. Mas-Marza, I. Mora-Sero, J. Bisquert, G. Garcia-Belmonte, *J. Phys.*
28 *Chem. Lett.* 2015, 6, 1645–1652; B. Chen, M. Yang, X. Zheng, C. Wu, W. Li, Y. Yan, J. Bisquert, G.
29 Garcia-Belmonte, K. Zhu, S. Priya, *J. Phys. Chem. Lett.* 2015, 6, 4693–4700.
- 30 [104] T.-Y. Yang, G. Gregori, N. Pellet, M. Grätzel, J. Maier, *Angew. Chem.* 2015, 127, 8016 ; R.
31 Gottesman, E. Haltzi, L. Gouda, S. Tirosh, Y. Bouhadana, A. Zaban, E. Mosconi, F. De Angelis, *J. Phys.*
32 *Chem. Lett.* 2014, 5, 2662–2669; E. J. Juárez-Pérez, R. S. Sánchez, L. Badia, G. Garcia-Belmonte, Y. S.
33 Kang, I. Mora-Sero, J. Bisquert, *J. Phys. Chem. Lett.* 2014, 5, 2390.
- 34 [105] J. A. Christians, J. S. Manser, P. V. Kamat, *J. Phys. Chem. Lett.* 2015, 6, 852–857.
- 35 [106] W. Tress, N. Marinova, T. Moehl, S. M. Zakeeruddin, M. K. Nazeeruddin, M. Grätzel, *Energy*
36 *Environ. Sci.* 2015, 8, 995.
- 37 [107] Hui-Seon Kim, N.-G. Park, *J. Phys. Chem. Lett.* 2014, 5, 2927–2934.
- 38 [108] K. Wojciechowski, S. D. Stranks, A. Abate, G. Sadoughi, A. Sadhanala, N. Kopidakis, G.
39 Rumbles, C.-Z. Li, R. H. Friend, A. K.-Y. Jen, H. J. Snaith, *ACS Nano* 2014, 8, 12701.
- 40 [109] Jian Xiong, Bingchu Yang, Runsheng Wua, Chenghao Cao, Yulan Huang , Chengbin Liu, Zhikun
41 Hu, H. Huang, Yongli Gao, J. Yang, *Organic Electronics* 2015, 24, 106; A. H. Ip, L. N. Quan , M. M.
42 Adachi, J. J. McDowell, J. Xu, D. H. Kim, E. H. Sargent, *Appl. Phys. Lett.* 2015, 106, 143902.
- 43 [110] J. H. Heo, M. S. You, M. H. Chang, W. Yin, T. K. Ahn, S.-J. Leec, S.-J. Sung, D. H. Kim, S.
44 HyukIm, *Nano Energy* 2015, 15, 530.
- 45 [111] H. Nagaoka, F. Ma, D. W. Dequillettes, S. M. Vorpahl, M. S. Glaz, A. E. Colbert, M. E. Ziffer, D.
46 S. Ginger, *Journal of Physical Chemistry Letters* 2015, 6, 669.
- 47 [112] J. W. Seo, S. Park, Y. C. Kim, N. J. Jeon, J. H. Noh, S. C. Yoon, S. I. Seok, *Energy &*
48 *Environmental Science* 2014, 7, 2642–2646.
- 49 [113] Jixian Xu, Andrei Buin, Alexander H. Ip, Wei Li, Oleksandr Voznyy, Riccardo Comin, Mingjian
50 Yuan, Seokmin Jeon, Zhijun Ning, Jeffrey J. McDowell, Pongsakorn Kanjanaboos, Jon-Paul Sun,
51 Xinzheng Lan, Li Na Quan, Dong Ha Kim, Ian G. Hill, Peter Maksymovych, E. H. Sargent, *Nat.*
52 *Commun.* 2015, 6, 7081.
- 53 [114] D. Bryant, S. Wheeler, B. C. O'Regan, T. Watson, P. R. F. Barnes, D. Worsley, J. Durrant, J.
54 *Phys. Chem. Lett.* 2015, 6, 3190–3194.
- 55
56
57
58
59
60
61
62
63
64
65

- 1
2
3
4 [115] I. Jeong, H. Jin Kim, B. S. Lee, H. Jung Son, J. Young Kim, D. K. Lee, D. E. Kim, J. Lee, M. J.
5 Ko, *Nano Energy* 2015, 17, 131.
6 [116] O. Almora, C. Aranda, I. Zarazua, A. Guerrero, G. Garcia-Belmonte, *ACS Energy Letters* 2016,
7 209.
8 [117] G. Garcia-Belmonte, J. Bisquert, *ACS Energy Letters* 2016, 1, 683.
9 [118] J. Carrillo, A. Guerrero, S. Rahimnejad, O. Almora, I. Zarazua, E. Mas-Marza, J. Bisquert, G.
10 Garcia-Belmonte, *Advanced Energy Materials* 2016, 6, n/a.
11 [119] W. Tress, J. P. Correa Baena, M. Saliba, A. Abate, M. Graetzel, *Advanced Energy Materials*
12 2016, 6, n/a.
13 [120] M. Valles-Pelarda, B. C. Hames, I. García-Benito, O. Almora, A. Molina-Ontoria, R. S. Sánchez,
14 G. Garcia-Belmonte, N. Martín, I. Mora-Sero, *The Journal of Physical Chemistry Letters* 2016, 7, 4622.
15 [121] J. B. Patel, J. Wong-Leung, S. Van Reenen, N. Sakai, J. T. W. Wang, E. S. Parrott, M. Liu, H. J.
16 Snaith, L. M. Herz, M. B. Johnston, *Advanced Electronic Materials* 2017, 3, n/a.
17 [122] J. You, L. Meng, T. B. Song, T. F. Guo, W. H. Chang, Z. Hong, H. Chen, H. Zhou, Q. Chen, Y.
18 Liu, N. De Marco, Y. Yang, *Nature Nanotechnology* 2016, 11, 75.
19 [123] T. Leijtens, G. E. Eperon, S. Pathak, A. Abate, M. M. Lee, H. J. Snaith, *Nature Communications*
20 2013, 4, 2885.
21 [124] W. Li, W. Zhang, S. Van Reenen, R. J. Sutton, J. Fan, A. A. Haghighirad, M. B. Johnston, L.
22 Wang, H. J. Snaith, *Energy & Environmental Science* 2016, 9, 490.
23 [125] C. Momblona, L. Gil-Escrig, E. Bandiello, E. M. Hutter, M. Sessolo, K. Lederer, J. Blochwitz-
24 Nimoth, H. J. Bolink, *Energy & Environmental Science* 2016, 9, 3456.
25 [126] F. Hao, C. C. Stoumpos, D. H. Cao, R. P. H. Chang, M. G. Kanatzidis, *Nat Photon* 2014, 8, 489;
26 M. H. Kumar, S. Dharani, W. L. Leong, P. P. Boix, R. R. Prabhakar, T. Baikie, C. Shi, H. Ding, R.
27 Ramesh, M. Asta, M. Graetzel, S. G. Mhaisalkar, N. Mathews, *Advanced Materials* 2014, 26, 7122; N. K.
28 Noel, S. D. Stranks, A. Abate, C. Wehrenfennig, S. Guarnera, A.-A. Haghighirad, A. Sadhanala, G. E.
29 Eperon, S. K. Pathak, M. B. Johnston, A. Petrozza, L. M. Herz, H. J. Snaith, *Energy & Environmental*
30 *Science* 2014, 7, 3061.
31 [127] T. Dittrich, E. A. Lebedev, J. Weidmann, *physica status solidi (a)* 1998, 165, R5.
32 [128] T. M. Brown, F. De Rossi, F. Di Giacomo, G. Mincuzzi, V. Zardetto, A. Reale, A. Di Carlo,
33 *Journal of Materials Chemistry A* 2014, 2, 10788.
34 [129] L. Schmidt-Mende, J. L. MacManus-Driscoll, *Materials Today* 2007, 10, 40.
35 [130] K. Mahmood, B. S. Swain, A. Amassian, *Advanced Energy Materials* 2015, 5, n/a.
36 [131] Z. Liang, Q. Zhang, L. Jiang, G. Cao, *Energy and Environmental Science* 2015, 8, 3442.
37 [132] K. Mahmood, B. S. Swain, A. Amassian, *Nanoscale* 2014, 6, 14674.
38 [133] S. Zhang, X. Li, X. Gao, L. Lei, X. Ding, Q. Gao, *Chemistry Letters* 2015, 44, 1022.
39 [134] Y. Cheng, Q. D. Yang, J. Xiao, Q. Xue, H. W. Li, Z. Guan, H. L. Yip, S. W. Tsang, *ACS Applied*
40 *Materials and Interfaces* 2015, 7, 19986.
41 [135] A. Nicolaev, T. L. Mitran, S. Iftimie, G. A. Nemnes, *Solar Energy Materials and Solar Cells*
42 2015.
43 [136] J. Xiao, Y. Yang, X. Xu, J. Shi, L. Zhu, S. Lv, H. Wu, Y. Luo, D. Li, Q. Meng, *Journal of*
44 *Materials Chemistry A* 2015, 3, 5289.
45 [137] S. Bai, Z. Wu, X. Wu, Y. Jin, N. Zhao, Z. Chen, Q. Mei, X. Wang, Z. Ye, T. Song, R. Liu, S. T.
46 Lee, B. Sun, *Nano Research* 2014.
47 [138] D. Y. Son, J. H. Im, H. S. Kim, N. G. Park, *Journal of Physical Chemistry C* 2014, 118, 16567; J.
48 Zhang, P. Barboux, T. Pauporté, *Advanced Energy Materials* 2014, 4.
49 [139] D. Y. Son, K. H. Bae, H. S. Kim, N. G. Park, *Journal of Physical Chemistry C* 2015, 119, 10321.
50 [140] O. Malinkiewicz, A. Yella, Y. H. Lee, G. M. Espallargas, M. Graetzel, M. K. Nazeeruddin, H. J.
51 Bolink, *Nature Photonics* 2014, 8, 128.
52 [141] W. Ke, G. Fang, Q. Liu, L. Xiong, P. Qin, H. Tao, J. Wang, H. Lei, B. Li, J. Wan, G. Yang, Y.
53 Yan, *Journal of the American Chemical Society* 2015, 137, 6730.
54 [142] Z. G. Zhu, Y. Bai, X. Liu, C.-C. Chueh, S. Yang, A. K. Y. Jen, *Adv. Mater.* 2016, n/a.
55
56
57
58
59
60
61
62
63
64
65

- 1
2
3
4 [143] J. Liu, C. Gao, L. Luo, Q. Ye, X. He, L. Ouyang, X. Guo, D. Zhuang, C. Liao, J. Mei, W. Lau,
5 Journal of Materials Chemistry A 2015, 3, 11750.
6 [144] Y. N. Atsushi Kogo, Masashi Ikegami, and Tsutomu Miyasaka, Chemistry Letters 2015, 44, 829.
7 [145] A. Bera, K. Wu, A. Sheikh, E. Alarousu, O. F. Mohammed, T. Wu, The Journal of Physical
8 Chemistry C 2014, 118, 28494.
9 [146] W. Li, J. Fan, J. Li, Y. Mai, L. Wang, Journal of the American Chemical Society 2015, 137,
10 10399.
11 [147] L. Zhu, Z. Shao, J. Ye, X. Zhang, X. Pan, S. Dai, Chemical Communications 2016, 52, 970.
12 [148] T. J. Coutts, D. L. Young, X. Li, W. P. Mulligan, X. Wu, Journal of Vacuum Science &
13 Technology A 2000, 18, 2646.
14 [149] S. S. Shin, W. S. Yang, J. H. Noh, J. H. Suk, N. J. Jeon, J. H. Park, J. S. Kim, W. M. Seong, S. I.
15 Seok, Nature Communications 2015, 6.
16 [150] B. Roose, S. Pathak, U. Steiner, Chemical Society Reviews 2015, 44, 8326.
17 [151] R. Jose, V. Thavasi, S. Ramakrishna, Journal of the American Ceramic Society 2009, 92, 289; Q.
18 Zhang, G. Cao, Nano Today 2011, 6, 91.
19 [152] K. Manseki, T. Ikeya, A. Tamura, T. Ban, T. Sugiura, T. Yoshida, RSC Advances 2014, 4, 9652.
20 [153] M. Yang, R. Guo, K. Kadel, Y. Liu, K. O'Shea, R. Bone, X. Wang, J. He, W. Li, Journal of
21 Materials Chemistry A 2014, 2, 19616.
22 [154] X. Zhang, Z. Bao, X. Tao, H. Sun, W. Chen, X. Zhou, RSC Advances 2014, 4, 64001.
23 [155] D. H. Kim, G. S. Han, W. M. Seong, J. W. Lee, B. J. Kim, N. G. Park, K. S. Hong, S. Lee, H. S.
24 Jung, ChemSusChem 2015, 8, 2392.
25 [156] R. Long, O. V. Prezhdo, ACS Nano 2015, 9, 11143; X. Yin, Y. Guo, Z. Xue, P. Xu, M. He, B.
26 Liu, Nano Research 2015, 8, 1997.
27 [157] G. Westin, M. Leideborg, K. Lashgari, V. A. Coleman, K. Jansson, A. Pohl, International Journal
28 of Nanotechnology 2009, 6, 828; K. Mahmood, B. S. Swain, H. S. Jung, Nanoscale 2014, 6, 9127; J.
29 Wang, M. Qin, H. Tao, W. Ke, Z. Chen, J. Wan, P. Qin, L. Xiong, H. Lei, H. Yu, G. Fang, Applied
30 Physics Letters 2015, 106.
31 [158] J. Dong, Y. Zhao, J. Shi, H. Wei, J. Xiao, X. Xu, J. Luo, J. Xu, D. Li, Y. Luo, Q. Meng, Chemical
32 Communications 2014, 50, 13381.
33 [159] P. Qin, A. L. Domanski, A. K. Chandiran, R. Berger, H. J. Butt, M. I. Dar, T. Moehl, N.
34 Tetreault, P. Gao, S. Ahmad, M. K. Nazeeruddin, M. Grätzel, Nanoscale 2014, 6, 1508.
35 [160] A. K. Chandiran, F. Sauvage, L. Etgar, M. Graetzel, The Journal of Physical Chemistry C 2011,
36 115, 9232; A. K. Chandiran, F. Sauvage, M. Casas-Cabanas, P. Comte, S. M. Zakeeruddin, M. Graetzel,
37 The Journal of Physical Chemistry C 2010, 114, 15849; A. Kay, M. Grätzel, Chemistry of Materials
38 2002, 14, 2930; Z. S. Wang, M. Yanagida, K. Sayama, H. Sugihara, Chemistry of Materials 2006, 18,
39 2912.
40 [161] Y. Diamant, S. Chappel, S. G. Chen, O. Melamed, A. Zaban, Coordination Chemistry Reviews
41 2004, 248, 1271; F. Fabregat-Santiago, J. García-Cañadas, E. Palomares, J. N. Clifford, S. A. Haque, J. R.
42 Durrant, G. Garcia-Belmonte, J. Bisquert, Journal of Applied Physics 2004, 96, 6903; L. Schmidt-Mende,
43 S. M. Zakeeruddin, M. Grätzel, Applied Physics Letters 2005, 86, 013504.
44 [162] G. S. Han, H. S. Chung, B. J. Kim, D. H. Kim, J. W. Lee, B. S. Swain, K. Mahmood, J. S. Yoo,
45 N. G. Park, J. H. Lee, H. S. Jung, Journal of Materials Chemistry A 2015, 3, 9160.
46 [163] C. Liu, Z. Qiu, W. Meng, J. Chen, J. Qi, C. Dong, M. Wang, Nano Energy 2015, 12, 59.
47 [164] K. Mahmood, B. S. Swain, A. Amassian, Nanoscale 2015, 7, 12812.
48 [165] K. Mahmood, B. S. Swain, A. R. Kirmani, A. Amassian, Journal of Materials Chemistry A 2015,
49 3, 9051.
50 [166] V. Gonzalez-Pedro, E. J. Juarez-Perez, W. S. Arsyad, E. M. Barea, F. Fabregat-Santiago, I. Mora-
51 Sero, J. Bisquert, Nano Letters 2014, 14, 888.
52 [167] S. D. Stranks, G. E. Eperon, G. Grancini, C. Menelaou, M. J. P. Alcocer, T. Leijtens, L. M. Herz,
53 A. Petrozza, H. J. Snaith, Science 2013, 342, 341.
54
55
56
57
58
59
60
61
62
63
64
65

- 1
2
3
4 [168] N. K. Noel, S. D. Stranks, A. Abate, C. Wehrenfennig, S. Guarnera, A. A. Haghighirad, A.
5 Sadhanala, G. E. Eperon, S. K. Pathak, M. B. Johnston, A. Petrozza, L. M. Herz, H. J. Snaith, *Energy and*
6 *Environmental Science* 2014, 7, 3061.
7 [169] W. Tian, C. Zhao, J. Leng, R. Cui, S. Jin, *Journal of the American Chemical Society* 2015, 137,
8 12458.
9 [170] J. D. Park, B. H. Son, J. K. Park, S. Y. Kim, J.-Y. Park, S. Lee, Y. H. Ahn, *AIP Advances* 2014,
10 4, 067106; W. H. Leng, P. R. F. Barnes, M. Juozapavicius, B. C. O'Regan, J. R. Durrant, *The Journal of*
11 *Physical Chemistry Letters* 2010, 1, 967.
12 [171] E. Hendry, M. Koeberg, B. O'Regan, M. Bonn, *Nano Letters* 2006, 6, 755.
13 [172] A. Fakharuddin, I. Ahmed, Z. Khalidin, M. M. Yusoff, R. Jose, *J. Appl. Phys.* 2014, 115.
14 [173] F. Zhang, X. Yang, M. Cheng, J. Li, W. Wang, H. Wang, L. Sun, *Journal of Materials Chemistry*
15 *A* 2015, 3, 24272.
16 [174] C. Tanase, E. J. Meijer, P. W. M. Blom, D. M. de Leeuw, *Phys. Rev. Lett.* 2003, 91, 216601.
17 [175] H. S. Kim, J. W. Lee, N. Yantara, P. P. Boix, S. A. Kulkarni, S. Mhaisalkar, M. Grätzel, N. G.
18 Park, *Nano Letters* 2013, 13, 2412.
19 [176] S. S. Mali, C. S. Shim, H. K. Park, J. Heo, P. S. Patil, C. K. Hong, *Chemistry of Materials* 2015,
20 27, 1541.
21 [177] L. Liang, Z. Huang, L. Cai, W. Chen, B. Wang, K. Chen, H. Bai, Q. Tian, B. Fan, *ACS Applied*
22 *Materials and Interfaces* 2014, 6, 20585.
23 [178] K. Mahmood, B. S. Swain, A. Amassian, *Advanced Energy Materials* 2015, 5.
24 [179] B. Cai, D. Zhong, Z. Yang, B. Huang, S. Miao, W. H. Zhang, J. Qiu, C. Li, *Journal of Materials*
25 *Chemistry C* 2015, 3, 729.
26 [180] D. Zhong, B. Cai, X. Wang, Z. Yang, Y. Xing, S. Miao, W. H. Zhang, C. Li, *Nano Energy* 2015,
27 11, 409.
28 [181] G. Peng, J. Wu, S. Wu, X. Xu, J. E. Ellis, G. Xu, A. Star, D. Gao, *Journal of Materials Chemistry*
29 *A* 2016, 4, 1520.
30 [182] S. H. Lee, X.-G. Zhang, B. Smith, S. S. A. Seo, Z. W. Bell, J. Xu, *Applied Physics Letters* 2010,
31 96, 193116.
32 [183] W. Q. Wu, F. Huang, D. Chen, Y. B. Cheng, R. A. Caruso, *Advanced Functional Materials* 2015,
33 25, 3264.
34 [184] J. Qiu, Y. Qiu, K. Yan, M. Zhong, C. Mu, H. Yan, S. Yang, *Nanoscale* 2013, 5, 3245.
35 [185] H. Tao, W. Ke, J. Wang, Q. Liu, J. Wan, G. Yang, G. Fang, *Journal of Power Sources* 2015, 290,
36 144.
37 [186] X. Gao, J. Li, J. Baker, Y. Hou, D. Guan, J. Chen, C. Yuan, *Chemical Communications* 2014, 50,
38 6368; R. Salazar, M. Altomare, K. Lee, J. Tripathy, R. Kirchgeorg, N. T. Nguyen, M. Mokhtar, A.
39 Alshehri, S. A. Al-Thabaiti, P. Schmuki, *ChemElectroChem* 2015, 2, 824; X. G. Bai, Y. T. Shi, K. Wang,
40 Q. S. Dong, Y. J. Xing, H. Zhang, L. Wang, T. L. Ma, *Wuli Huaxue Xuebao/ Acta Physico - Chimica*
41 *Sinica* 2015, 31, 285; J. Zhang, T. Pauporté, *ChemPhysChem* 2015, 16, 2836.
42 [187] P. Qin, M. Paulose, M. I. Dar, T. Moehl, N. Arora, P. Gao, O. K. Varghese, M. Grätzel, M. K.
43 Nazeeruddin, *Small* 2015, 11, 5533.
44 [188] G. S. Han, H. S. Chung, D. H. Kim, B. J. Kim, J. W. Lee, N. G. Park, I. S. Cho, J. K. Lee, S. Lee,
45 H. S. Jung, *Nanoscale* 2015, 7, 15284.
46 [189] S. H. Lin, Y. H. Su, H. W. Cho, P. Y. Kung, W. P. Liao, J. J. Wu, *Journal of Materials Chemistry*
47 *A* 2016, 4, 1119.
48 [190] W. Huang, F. Huang, E. Gann, Y. B. Cheng, C. R. McNeill, *Advanced Functional Materials*
49 2015, 25, 5529.
50 [191] Y. Yu, J. Li, D. Geng, J. Wang, L. Zhang, T. L. Andrew, M. S. Arnold, X. Wang, *ACS Nano*
51 2015, 9, 564.
52 [192] X. Chen, S. Yang, Y. C. Zheng, Y. Chen, Y. Hou, X. H. Yang, H. G. Yang, *Advanced Science*
53 2015, 2, n/a.
54
55
56
57
58
59
60
61
62
63
64
65

- 1
2
3
4 [193] X. Xu, H. Zhang, J. Shi, J. Dong, Y. Luo, D. Li, Q. Meng, *Journal of Materials Chemistry A* 2015, 3, 19288.
5
6 [194] W. Qiu, M. Buffière, G. Brammertz, U. W. Paetzold, L. Froyen, P. Heremans, D. Cheyns, *Organic Electronics: physics, materials, applications* 2015, 26, 30.
7
8 [195] L. Etgar, *MRS Bulletin* 2015, 40, 674; Y. Liu, S. Ji, S. Li, W. He, K. Wang, H. Hu, C. Ye, *Journal of Materials Chemistry A* 2015, 3, 14902.
9
10 [196] S. K. Pathak, A. Abate, P. Ruckdeschel, B. Roose, K. C. Gödel, Y. Vaynzof, A. Santhala, S.-I. Watanabe, D. J. Hollman, N. Noel, A. Sepe, U. Wiesner, R. Friend, H. J. Snaith, U. Steiner, *Advanced Functional Materials* 2014, 24, 6046.
11
12 [197] H. J. Snaith, N. C. Greenham, R. H. Friend, *Advanced Materials* 2004, 16, 1640.
13
14 [198] S. Hong, A. Han, E. C. Lee, K.-W. Ko, J.-H. Park, H.-J. Song, M.-H. Han, C.-H. Han, *Current Applied Physics* 2015, 15, 574.
15
16 [199] X. Wang, Y. Fang, L. He, Q. Wang, T. Wu, *Materials Science in Semiconductor Processing* 2014, 27, 569.
17
18 [200] G. E. Eperon, V. M. Burlakov, P. Docampo, A. Goriely, H. J. Snaith, *Advanced Functional Materials* 2014, 24, 151.
19
20 [201] S. Shi, Y. Li, X. Li, H. Wang, *Materials Horizons* 2015, 2, 378.
21
22 [202] H. J. Snaith, A. Abate, J. M. Ball, G. E. Eperon, T. Leijtens, N. K. Noel, S. D. Stranks, J. T. W. Wang, K. Wojciechowski, W. Zhang, *Journal of Physical Chemistry Letters* 2014, 5, 1511.
23
24 [203] L. K. Ono, S. R. Raga, S. Wang, Y. Kato, Y. Qi, *Journal of Materials Chemistry A* 2015, 3, 9074; B. Wu, K. Fu, N. Yantara, G. Xing, S. Sun, T. C. Sum, N. Mathews, *Advanced Energy Materials* 2015, 5; C. Li, Y. Li, Y. Xing, Z. Zhang, X. Zhang, Z. Li, Y. Shi, T. Ma, R. Ma, K. Wang, J. Wei, *ACS Applied Materials and Interfaces* 2015, 7, 15117.
25
26 [204] W. J. Yin, T. Shi, Y. Yan, *Advanced Materials* 2014, 26, 4653.
27
28 [205] J. P. Correa Baena, L. Steier, W. Tress, M. Saliba, S. Neutzner, T. Matsui, F. Giordano, T. J. Jacobsson, A. R. Srimath Kandada, S. M. Zakeeruddin, A. Petrozza, A. Abate, M. K. Nazeeruddin, M. Grätzel, A. Hagfeldt, *Energy and Environmental Science* 2015, 8, 2928.
29
30 [206] J. Song, E. Zheng, X.-F. Wang, W. Tian, T. Miyasaka, *Solar Energy Materials and Solar Cells* 2016, 144, 623.
31
32 [207] Z.-L. Tseng, C.-H. Chiang, C.-G. Wu, *Scientific Reports* 2015, 5, 13211.
33
34 [208] W. Qiu, U. W. Paetzold, R. Gehlhaar, V. Smirnov, H.-G. Boyen, J. G. Tait, B. Conings, W. Zhang, C. B. Nielsen, I. McCulloch, L. Froyen, P. Heremans, D. Cheyns, *Journal of Materials Chemistry A* 2015, 3, 22824.
35
36 [209] J. H. Heo, M. H. Lee, H. J. Han, B. R. Patil, J. S. Yu, S. H. Im, *Journal of Materials Chemistry A* 2016, 4, 1572.
37
38 [210] L. Meng, J. You, T. F. Guo, Y. Yang, *Accounts of Chemical Research* 2016, 49, 155.
39
40 [211] S. Sun, T. Salim, N. Mathews, M. Duchamp, C. Boothroyd, G. Xing, T. C. Sum, Y. M. Lam, *Energy & Environmental Science* 2014, 7, 399.
41
42 [212] G. Xing, N. Mathews, S. Sun, S. S. Lim, Y. M. Lam, M. Grätzel, S. Mhaisalkar, T. C. Sum, *Science* 2013, 342, 344.
43
44 [213] W. A. Laban, L. Etgar, *Energy and Environmental Science* 2013, 6, 3249.
45
46 [214] M. Hu, L. Liu, A. Mei, Y. Yang, T. Liu, H. Han, *Journal of Materials Chemistry A* 2014, 2, 17115.
47
48 [215] J. Shi, J. Dong, S. Lv, Y. Xu, L. Zhu, J. Xiao, X. Xu, H. Wu, D. Li, Y. Luo, Q. Meng, *Applied Physics Letters* 2014, 104.
49
50 [216] J. Y. Jeng, Y. F. Chiang, M. H. Lee, S. R. Peng, T. F. Guo, P. Chen, T. C. Wen, *Advanced Materials* 2013, 25, 3727.
51
52 [217] W. Nie, H. Tsai, R. Asadpour, J. C. Blancon, A. J. Neukirch, G. Gupta, J. J. Crochet, M. Chhowalla, S. Tretiak, M. A. Alam, H. L. Wang, A. D. Mohite, *Science* 2015, 347, 522.
53
54 [218] C. Bi, Q. Wang, Y. Shao, Y. Yuan, Z. Xiao, J. Huang, *Nature Communications* 2015, 6.
55
56
57
58
59
60
61
62
63
64
65

- 1
2
3
4 [219] H. Zhang, J. Cheng, F. Lin, H. He, J. Mao, K. S. Wong, A. K. Y. Jen, W. C. H. Choy, ACS Nano
5 2016, 10, 1503.
6 [220] J. H. Park, J. Seo, S. Park, S. S. Shin, Y. C. Kim, N. J. Jeon, H.-W. Shin, T. K. Ahn, J. H. Noh, S.
7 C. Yoon, C. S. Hwang, S. I. Seok, Advanced Materials 2015, n/a.
8 [221] J. Seo, S. Park, Y. Chan Kim, N. J. Jeon, J. H. Noh, S. C. Yoon, S. I. Seok, Energy and
9 Environmental Science 2014, 7, 2642.
10 [222] J. You, Z. Hong, T. B. Song, L. Meng, Y. Liu, C. Jiang, H. Zhou, W. H. Chang, G. Li, Y. Yang,
11 Applied Physics Letters 2014, 105.
12 [223] F. Hou, Z. Su, F. Jin, X. Yan, L. Wang, H. Zhao, J. Zhu, B. Chu, W. Li, Nanoscale 2015, 7, 9427.
13 [224] P. W. Liang, C. C. Chueh, S. T. Williams, A. K. Y. Jen, Advanced Energy Materials 2015, 5.
14 [225] L. Q. Zhang, X. W. Zhang, Z. G. Yin, Q. Jiang, X. Liu, J. H. Meng, Y. J. Zhao, H. L. Wang,
15 Journal of Materials Chemistry A 2015, 3, 12133.
16 [226] P. Docampo, J. M. Ball, M. Darwich, G. E. Eperon, H. J. Snaith, Nature Communications 2013,
17 4.
18 [227] X. Li, D. Bi, C. Yi, J.-D. Décoppet, J. Luo, S. M. Zakeeruddin, A. Hagfeldt, M. Grätzel, Science
19 2016.
20 [228] N. Ahn, D.-Y. Son, I.-H. Jang, S. M. Kang, M. Choi, N.-G. Park, Journal of the American
21 Chemical Society 2015, 137, 8696.
22 [229] K. Aitola, K. Sveinbjornsson, J.-P. Correa-Baena, A. Kaskela, A. Abate, Y. Tian, E. M. J.
23 Johansson, M. Gratzel, E. I. Kauppinen, A. Hagfeldt, G. Boschloo, Energ. Environ.Sci. 2016, 9, 461.
24 [230] W.-Q. Wu, F. Huang, D. Chen, Y.-B. Cheng, R. A. Caruso, Advanced Energy Materials 2016,
25 n/a.
26 [231] J. F. Li, Z. L. Zhang, H. P. Gao, Y. Zhang, Y. L. Mao, Journal of Materials Chemistry A 2015, 3,
27 19476.
28 [232] L. S. Oh, D. H. Kim, J. A. Lee, S. S. Shin, J. W. Lee, I. J. Park, M. J. Ko, N. G. Park, S. G. Pyo,
29 K. S. Hong, J. Y. Kim, Journal of Physical Chemistry C 2014, 118, 22991.
30 [233] S. S. Mali, C. S. Shim, C. K. Hong, Scientific Reports 2015, 5.
31 [234] J. Song, E. Zheng, J. Bian, X.-F. Wang, W. Tian, Y. Sanehira, T. Miyasaka, Journal of Materials
32 Chemistry A 2015, 3, 10837.
33 [235] Y. Dkhissi, F. Huang, S. Rubanov, M. Xiao, U. Bach, L. Spiccia, R. A. Caruso, Y.-B. Cheng,
34 Journal of Power Sources 2015, 278, 325.
35 [236] M. M. Tavakoli, K.-H. Tsui, Q. Zhang, J. He, Y. Yao, D. Li, Z. Fan, ACS Nano 2015, 9, 10287.
36 [237] J. Troughton, D. Bryant, K. Wojciechowski, M. J. Carnie, H. Snaith, D. A. Worsley, T. M.
37 Watson, Journal of Materials Chemistry A 2015, 3, 9141.
38 [238] Q. Hu, J. Wu, C. Jiang, T. Liu, X. Que, R. Zhu, Q. Gong, ACS Nano 2014, 8, 10161.
39 [239] J. T. W. Wang, J. M. Ball, E. M. Barea, A. Abate, J. A. Alexander-Webber, J. Huang, M. Saliba,
40 I. Mora-Sero, J. Bisquert, H. J. Snaith, R. J. Nicholas, Nano Letters 2014, 14, 724.
41 [240] D. Bi, S. J. Moon, L. Häggman, G. Boschloo, L. Yang, E. M. J. Johansson, M. K. Nazeeruddin,
42 M. Grätzel, A. Hagfeldt, RSC Advances 2013, 3, 18762.
43 [241] H. Zhou, Y. Shi, K. Wang, Q. Dong, X. Bai, Y. Xing, Y. Du, T. Ma, The Journal of Physical
44 Chemistry C 2015, 150216032236005.
45 [242] Z. Wei, H. Chen, K. Yan, X. Zheng, S. Yang, Journal of Materials Chemistry A 2015, 3, 24226.
46 [243] K. Yan, Z. Wei, J. Li, H. Chen, Y. Yi, X. Zheng, X. Long, Z. Wang, J. Wang, J. Xu, S. Yang,
47 Small 2015, 11, 2269.
48 [244] Y. Yang, K. Ri, A. Mei, L. Liu, M. Hu, T. Liu, X. Li, H. Han, Journal of Materials Chemistry A
49 2015, 3, 9103.
50 [245] C. Y. Chang, K. T. Lee, W. K. Huang, H. Y. Siao, Y. C. Chang, Chemistry of Materials 2015, 27,
51 5122.
52 [246] L. Zheng, D. Zhang, Y. Ma, Z. Lu, Z. Chen, S. Wang, L. Xiao, Q. Gong, Dalton Transactions
53 2015, 44, 10582.
54
55
56
57
58
59
60
61
62
63
64
65

- 1
2
3
4 [247] L. Qiu, J. Deng, X. Lu, Z. Yang, H. Peng, *Angewandte Chemie International Edition* 2014, 53,
5 10425.
6 [248] M. Lee, Y. Ko, Y. Jun, *Journal of Materials Chemistry A* 2015, 3, 19310.
7 [249] Y. Zhong, P. Chen, B. Yang, X. Zuo, L. Zhou, X. Yang, G. Li, *Applied Physics Letters* 2015,
8 106.
9 [250] E. M. Hutter, G. E. Eperon, S. D. Stranks, T. J. Savenije, *The Journal of Physical Chemistry*
10 *Letters* 2015, 6, 3082.
11 [251] T. Leijtens, S. D. Stranks, G. E. Eperon, R. Lindblad, E. M. J. Johansson, I. J. McPherson, H.
12 Rensmo, J. M. Ball, M. M. Lee, H. J. Snaith, *ACS Nano* 2014, 8, 7147; Y. Zhang, M. Liu, G. E. Eperon,
13 T. Leijtens, D. P. McMeekin, M. Saliba, W. Zhang, M. De Bastiani, a. petrozza, L. Herz, M. B. Johnston,
14 H. Lin, H. Snaith, *Mater. Horiz.* 2015, 2, 315.
15 [252] a. Mei, X. Li, L. Liu, Z. Ku, T. Liu, Y. Rong, M. Xu, M. Hu, J. Chen, Y. Yang, M. Gratzel, H.
16 Han, *Science* 2014, 345, 295.
17 [253] C. S. Ponseca, T. J. Savenije, M. Abdellah, K. Zheng, A. Yartsev, T. Pascher, T. Harlang, P.
18 Chabera, T. Pullerits, A. Stepanov, J.-P. Wolf, V. Sundström, *Journal of the American Chemical Society*
19 2014, 136, 5189.
20 [254] Q. Lin, A. Armin, R. C. R. Nagiri, P. L. Burn, P. Meredith, *Nature Photonics* 2015, 9, 106.
21 [255] E. Edri, S. Kirmayer, S. Mukhopadhyay, K. Gartsman, G. Hodes, D. Cahen, *Nature*
22 *Communications* 2014, 5.
23 [256] S. Ryu, J. Seo, S. S. Shin, Y. C. Kim, N. J. Jeon, J. H. Noh, S. I. Seok, *Journal of Materials*
24 *Chemistry A* 2015, 3, 3271.
25 [257] Y. Zhou, C. Fuentes-Hernandez, J. Shim, J. Meyer, A. J. Giordano, H. Li, P. Winget, T.
26 Papadopoulos, H. Cheun, J. Kim, M. Fenoll, A. Dindar, W. Haske, E. Najafabadi, T. M. Khan, H.
27 Sojoudi, S. Barlow, S. Graham, J.-L. Brédas, S. R. Marder, A. Kahn, B. Kippelen, *Science* 2012, 336,
28 327; H. Kang, S. Hong, J. Lee, K. Lee, *Advanced Materials* 2012, 24, 3005.
29 [258] M. Spiro, Vol. 2017, 2017.
30 [259] Z. M. Beiley, M. D. McGehee, *Energy & Environmental Science* 2012, 5, 9173.
31 [260] A. Kay, M. Grätzel, *Solar Energy Materials and Solar Cells* 1996, 44, 99.
32 [261] Z. Ku, Y. Rong, M. Xu, T. Liu, H. Han, *Scientific Reports* 2013, 3.
33 [262] Z. Li, S. A. Kulkarni, P. P. Boix, E. Shi, A. Cao, K. Fu, S. K. Batabyal, J. Zhang, Q. Xiong, L. H.
34 Wong, N. Mathews, S. G. Mhaisalkar, *ACS Nano* 2014, 8, 6797.
35 [263] H. Wei, J. Xiao, Y. Yang, S. Lv, J. Shi, X. Xu, J. Dong, Y. Luo, D. Li, Q. Meng, *Carbon* 2015,
36 93, 861.
37 [264] Y. Chen, J. Peng, D. Su, X. Chen, Z. Liang, *ACS Applied Materials and Interfaces* 2015, 7, 4471.
38 [265] F. Zhang, X. Yang, H. Wang, M. Cheng, J. Zhao, L. Sun, *ACS Applied Materials and Interfaces*
39 2014, 6, 16140.
40 [266] S. Gamliel, A. Dymshits, S. Aharon, E. Terkieltaub, L. Etgar, *Journal of Physical Chemistry C*
41 2015, 119, 19722.
42 [267] F. Zhang, X. Yang, M. Cheng, W. Wang, L. Sun, *Nano Energy* 2016, 20, 108.
43 [268] S. N. Habisreutinger, T. Leijtens, G. E. Eperon, S. D. Stranks, R. J. Nicholas, H. J. Snaith, *Nano*
44 *Letters* 2014, 14, 5561.
45 [269] K. Cao, Z. Zuo, J. Cui, Y. Shen, T. Moehl, S. M. Zakeeruddin, M. Grätzel, M. Wang, *Nano*
46 *Energy* 2015, 17, 171.
47 [270] C.-Y. Chen, J.-H. Chang, K.-M. Chiang, H.-L. Lin, S.-Y. Hsiao, H.-W. Lin, *Advanced Functional*
48 *Materials* 2015, n/a.
49 [271] Y. Li, L. Meng, Y. Yang, G. Xu, Z. Hong, Q. Chen, J. You, G. Li, Y. Yang, Y. Li, *Nat Commun*
50 2016, 7.
51 [272] D. Yang, R. Yang, J. Zhang, Z. Yang, S. Liu, C. Li, *Energy and Environmental Science* 2015, 8,
52 3208.
53 [273] H. C. Weerasinghe, Y. Dkhissi, A. D. Scully, R. A. Caruso, Y.-B. Cheng, *Nano Energy* 2015, 18,
54 118.
55
56
57
58
59
60
61
62
63
64
65

- 1
2
3
4 [274] M. Kaltenbrunner, G. Adam, E. D. Glowacki, M. Drack, R. Schwodiauer, L. Leonat, D. H.
5 Apaydin, H. Groiss, M. C. Scharber, M. S. White, N. S. Sariciftci, S. Bauer, *Nat Mater* 2015, 14, 1032.
6 [275] NREL, (Ed: NREL), 2015.
7 [276] G. Hashmi, K. Miettunen, T. Peltola, J. Halme, I. Asghar, K. Aitola, M. Toivola, P. Lund,
8 *Renewable and Sustainable Energy Reviews* 2011, 15, 3717.
9 [277] V. Zardetto, T. M. Brown, A. Reale, A. Di Carlo, *Journal of Polymer Science Part B: Polymer*
10 *Physics* 2011, 49, 638; B. Susrutha, L. Giribabu, S. P. Singh, *Chemical Communications* 2015, 51, 14696.
11 [278] S. S. Shin, W. S. Yang, J. H. Noh, J. H. Suk, N. J. Jeon, J. H. Park, J. S. Kim, W. M. Seong, S. I.
12 Seok, *Nature Communications* 2015, 6, 7410.
13 [279] J. Yang, B. D. Siempelkamp, E. Mosconi, F. De Angelis, T. L. Kelly, *Chemistry of Materials*
14 2015, 27, 150529083734008.
15 [280] M. Lee, Y. Jo, D. S. Kim, H. Y. Jeong, Y. Jun, *Journal of Materials Chemistry A* 2015, 3, 14592.
16 [281] J. Deng, L. Qiu, X. Lu, Z. Yang, G. Guan, Z. Zhang, H. Peng, *J. Mater. Chem. A* 2015.
17 [282] S. He, L. Qiu, X. Fang, G. Guan, P. Chen, Z. Zhang, H. Peng, *Journal of Materials Chemistry A*
18 2015, 3, 9406; R. Li, X. Xiang, X. Tong, J. Zou, Q. Li, *Advanced Materials* 2015, 27, 3831.
19 [283] M. Peng, D. Zou, *Journal of Materials Chemistry A* 2015, 3, 20435.
20 [284] H. Sun, H. Li, X. You, Z. Yang, J. Deng, L. Qiu, H. Peng, *Journal of Materials Chemistry A*
21 2014, 2, 345.
22 [285] D. Liu, M. Zhao, Y. Li, Z. Bian, L. Zhang, Y. Shang, X. Xia, S. Zhang, D. Yun, Z. Liu, A. Cao,
23 C. Huang, *ACS Nano* 2012, 6, 11027.
24 [286] X. Liang, W. Li, J. Li, G. Niu, L. Wang, *Journal of Materials Chemistry A* 2016, 4, 16913.
25 [287] Y. Li, Y. Zhao, Q. Chen, Y. Yang, Y. Liu, Z. Hong, Z. Liu, Y. T. Hsieh, L. Meng, Y. Li, Y.
26 Yang, *Journal of the American Chemical Society* 2015, 137, 15540.
27 [288] Y. Xu, Y. Wang, J. Yu, B. Feng, H. Zhou, J. Zhang, J. Duan, X. Fan, P. A. Van Aken, P. D.
28 Lund, H. Wang, *IEEE Journal of Photovoltaics* 2016, PP.
29 [289] Y. Dong, W. Li, X. Zhang, Q. Xu, Q. Liu, C. Li, Z. Bo, *Small* 2016, 12, 1098.
30 [290] G. Yang, H. Tao, P. Qin, W. Ke, G. Fang, *Journal of Materials Chemistry A* 2016, 4, 3970; H.-S.
31 Kim, I.-H. Jang, N. Ahn, M. Choi, A. Guerrero, J. Bisquert, N.-G. Park, *The Journal of Physical*
32 *Chemistry Letters* 2015, 6, 4633.
33 [291] J. M. Azpiroz, E. Mosconi, J. Bisquert, F. De Angelis, *Energy and Environmental Science* 2015,
34 8, 2118.
35 [292] Q. Fu, X. Tang, L. Tan, Y. Zhang, Y. Liu, L. Chen, Y. Chen, *Journal of Physical Chemistry C*
36 2016, 120, 15089.
37 [293] W. Li, W. Zhang, S. Van Reenen, R. J. Sutton, J. Fan, A. A. Haghighirad, M. B. Johnston, L.
38 Wang, H. J. Snaith, *Energy and Environmental Science* 2016, 9, 490.
39 [294] J. Cao, J. Yin, S. Yuan, Y. Zhao, J. Li, N. Zheng, *Nanoscale* 2015, 7, 9443.
40 [295] H. P. Dong, Y. Li, S. F. Wang, W. Z. Li, N. Li, X. D. Guo, L. D. Wang, *Journal of Materials*
41 *Chemistry A* 2015, 3, 9999.
42 [296] L. F. Zhu, Y. Z. Xu, J. J. Shi, H. Y. Zhang, X. Xu, Y. H. Zhao, Y. H. Luo, Q. B. Meng, D. M. Li,
43 *RSC Advances* 2016, 6, 82282.
44 [297] S. F. Shaikh, H. C. Kwon, W. Yang, H. Hwang, H. Lee, E. Lee, S. Ma, J. Moon, *Journal of*
45 *Materials Chemistry A* 2016, 4, 15478.
46 [298] Z. K. Wang, M. Li, D. X. Yuan, X. B. Shi, H. Ma, L. S. Liao, *ACS Applied Materials and*
47 *Interfaces* 2015, 7, 9645.
48 [299] Y. Xu, J. Shi, S. Lv, L. Zhu, J. Dong, H. Wu, Y. Xiao, Y. Luo, S. Wang, D. Li, X. Li, Q. Meng,
49 *ACS Applied Materials and Interfaces* 2014, 6, 5651.
50 [300] R. Roesch, T. Faber, E. Von Hauff, T. M. Brown, M. Lira-Cantu, H. Hoppe, *Advanced Energy*
51 *Materials* 2015, 5.
52 [301] X. Guo, G. Niu, L. Wang, *Acta Chimica Sinica* 2015, 73, 211; T. A. Berhe, W. N. Su, C. H.
53 Chen, C. J. Pan, J. H. Cheng, H. M. Chen, M. C. Tsai, L. Y. Chen, A. A. Dubale, B. J. Hwang, *Energy*
54 *and Environmental Science* 2016, 9, 323.
55
56
57
58
59
60
61
62
63
64
65

- 1
2
3
4 [302] M. Shahbazi, H. Wang, *Solar Energy* 2016, 123, 74; D. Wang, M. Wright, N. K. Elumalai, A.
5 Uddin, *Solar Energy Materials and Solar Cells* 2016, 147, 255.
6 [303] Y. H. Lee, J. Luo, R. Humphry-Baker, P. Gao, M. Grätzel, M. K. Nazeeruddin, *Advanced*
7 *Functional Materials* 2015, 25, 3925.
8 [304] E. L. Unger, E. T. Hoke, C. D. Bailie, W. H. Nguyen, A. R. Bowring, T. Heumüller, M. G.
9 Christoforo, M. D. McGehee, *Energy and Environmental Science* 2014, 7, 3690; W. Tress, N. Marinova,
10 T. Moehl, S. M. Zakeeruddin, M. K. Nazeeruddin, M. Grätzel, *Energy and Environmental Science* 2015,
11 8, 995.
12 [305] M. K. Gangishetty, R. W. J. Scott, T. L. Kelly, *Nanoscale* 2016.
13 [306] G. E. Eperon, S. N. Habisreutinger, T. Leijtens, B. J. Bruijnaers, J. J. Van Franeker, D. W.
14 Dequillettes, S. Pathak, R. J. Sutton, G. Grancini, D. S. Ginger, R. A. J. Janssen, A. Petrozza, H. J. Snaith,
15 *ACS Nano* 2015, 9, 9380.
16 [307] J. Yang, B. D. Siempelkamp, D. Liu, T. L. Kelly, *ACS Nano* 2015, 9, 1955; J. M. Frost, K. T.
17 Butler, F. Brivio, C. H. Hendon, M. Van Schilfhaarde, A. Walsh, *Nano Letters* 2014, 14, 2584.
18 [308] L. Zheng, Y. H. Chung, Y. Ma, L. Zhang, L. Xiao, Z. Chen, S. Wang, B. Qu, Q. Gong, *Chemical*
19 *Communications* 2014, 50, 11196.
20 [309] T. A. Berhe, W.-n. Su, C.-H. Chen, C.-J. Pan, J. Cheng, H.-M. Chen, M.-c. Tsai, L.-Y. Chen, A.
21 A. Dubale, B. J. Hwang, *Energy & Environmental Science* 2015; B. Conings, J. Drijkoningen, N.
22 Gauquelin, A. Babayigit, J. D'Haen, L. D'Olieslaeger, A. Ethirajan, J. Verbeeck, J. Manca, E. Mosconi, F.
23 D. Angelis, H. G. Boyen, *Advanced Energy Materials* 2015; K. Leo, *Nature Nanotechnology* 2015, 10,
24 574; L. Peedikakkandy, P. Bhargava, *Materials Science in Semiconductor Processing* 2015, 33, 103; D. F.
25 Zhang, L. L. Zheng, Y. Z. Ma, S. F. Wang, Z. Q. Bian, C. H. Huang, Q. H. Gong, L. X. Xiao, *Wuli*
26 *Xuebao/Acta Physica Sinica* 2015, 64.
27 [310] N. A. Manshor, Q. Wali, K. K. Wong, S. K. Muzakir, A. Fakharuddin, L. Schmidt-Mende, R.
28 Jose, *PCCP* 2016, 18, 21629; Y. Zhao, J. Wei, H. Li, Y. Yan, W. Zhou, D. Yu, Q. Zhao, *Nature*
29 *Communications* 2016, 7, 10228.
30 [311] X. Xu, Z. Liu, Z. Zuo, M. Zhang, Z. Zhao, Y. Shen, H. Zhou, Q. Chen, Y. Yang, M. Wang, *Nano*
31 *Letters* 2015, 15, 2402.
32 [312] S. K. Pathak, A. Abate, P. Ruckdeschel, B. Roose, K. C. Gödel, Y. Vaynzof, A. Santhala, S. I.
33 Watanabe, D. J. Hollman, N. Noel, A. Sepe, U. Wiesner, R. Friend, H. J. Snaith, U. Steiner, *Advanced*
34 *Functional Materials* 2014, 24, 6046.
35 [313] J. Yin, J. Cao, X. He, S. Yuan, S. Sun, J. Li, N. Zheng, L. Lin, *Journal of Materials Chemistry A*
36 2015, 3, 16860.
37 [314] J. Xiong, B. Yang, C. Cao, R. Wu, Y. Huang, J. Sun, J. Zhang, C. Liu, S. Tao, Y. Gao, J. Yang,
38 *Organic Electronics* 2016, 30, 30.
39 [315] J. Hyuck Heo, M. Sang You, M. Hyuk Chang, W. Yin, T. K. Ahn, S.-J. Lee, S.-J. Sung, D. Hwan
40 Kim, S. Hyuk Im, *Nano Energy* 2015.
41 [316] F. Matsumoto, S. M. Vorpahl, J. Q. Banks, E. Sengupta, D. S. Ginger, *Journal of Physical*
42 *Chemistry C* 2015, 119, 20810.
43 [317] K. Schwanitz, E. Mankel, R. Hunger, T. Mayer, W. Jaegermann, *CHIMIA International Journal*
44 *for Chemistry* 2007, 61, 796; K. Schwanitz, U. Weiler, R. Hunger, T. Mayer, W. Jaegermann, *The Journal*
45 *of Physical Chemistry C* 2007, 111, 849.
46 [318] S. Ito, S. Tanaka, K. Manabe, H. Nishino, *Journal of Physical Chemistry C* 2014, 118, 16995.
47 [319] I. Hwang, M. Baek, K. Yong, *ACS Applied Materials & Interfaces* 2015, 7, 27863.
48 [320] D. Bi, G. Boschloo, S. Schwarzmüller, L. Yang, E. M. J. Johansson, A. Hagfeldt, *Nanoscale*
49 2013, 5, 11686.
50 [321] A. Bera, A. D. Sheikh, M. A. Haque, R. Bose, E. Alarousu, O. F. Mohammed, T. Wu, *ACS*
51 *Applied Materials and Interfaces* 2015, 7, 12404.
52 [322] J. S. Yun, A. Ho-Baillie, S. Huang, S. H. Woo, Y. Heo, J. Seidel, F. Huang, Y. B. Cheng, M. A.
53 Green, *Journal of Physical Chemistry Letters* 2015, 6, 875.
54
55
56
57
58
59
60
61
62
63
64
65

- 1
2
3
4 [323] C. Law, L. Miseikis, S. Dimitrov, P. Shakya-Tuladhar, X. Li, P. R. F. Barnes, J. Durrant, B. C.
5 O'Regan, *Advanced Materials* 2014, 26, 6268.
- 6 [324] T. M. Schmidt, T. T. Larsen-Olsen, J. E. Carlé, D. Angmo, F. C. Krebs, *Advanced Energy*
7 *Materials* 2015, 5.
- 8 [325] Y. Zhang, X. Hu, L. Chen, Z. Huang, Q. Fu, Y. Liu, L. Zhang, Y. Chen, *Organic Electronics*
9 2016, 30, 281.
- 10 [326] H. Choi, C. K. Mai, H. B. Kim, J. Jeong, S. Song, G. C. Bazan, J. Y. Kim, A. J. Heeger, *Nature*
11 *Communications* 2015, 6.
- 12 [327] J. H. Kim, P. W. Liang, S. T. Williams, N. Cho, C. C. Chueh, M. S. Glaz, D. S. Ginger, A. K. Y.
13 Jen, *Advanced Materials* 2015, 27, 695.
- 14 [328] Z. Yu, L. Sun, *Advanced Energy Materials* 2015, 5.
- 15 [329] B. Cai, Y. Xing, Z. Yang, W.-H. H. Zhang, J. Qiu, *Energy and Environmental Science* 2013, 6,
16 1480; A. Emly, E. Kioupakis, A. Van Der Ven, *Chemistry of Materials* 2013, 25, 4663; G. Niu, W. Li, F.
17 Meng, L. Wang, H. Dong, Y. Qiu, *Journal of Materials Chemistry A* 2014, 2, 705; I. C. Smith, E. T.
18 Hoke, D. Solis-Ibarra, M. D. McGehee, H. I. Karunadasa, *Angewandte Chemie - International Edition*
19 2014, 53, 11232; I. Hwang, I. Jeong, J. Lee, M. J. Ko, K. Yong, *ACS Applied Materials and Interfaces*
20 2015, 7, 17330.
- 21 [330] L. Badia, E. Mas-Marzá, R. S. Sánchez, E. M. Barea, J. Bisquert, I. Mora-Seró, *APL Materials*
22 2014, 2.
- 23 [331] X. Dong, X. Fang, M. Lv, B. Lin, S. Zhang, J. Ding, N. Yuan, *Journal of Materials Chemistry A*
24 2015, 3, 5360; S. Guarnera, A. Abate, W. Zhang, J. M. Foster, G. Richardson, A. Petrozza, H. J. Snaith,
25 *Journal of Physical Chemistry Letters* 2015, 6, 432.
- 26 [332] S. S. Reddy, K. Gunasekar, J. H. Heo, S. H. Im, C. S. Kim, D. H. Kim, J. H. Moon, J. Y. Lee, M.
27 Song, S. H. Jin, *Advanced Materials* 2016, 28, 686.
- 28 [333] J. Liu, Y. Wu, C. Qin, X. Yang, T. Yasuda, A. Islam, K. Zhang, W. Peng, W. Chen, L. Han,
29 *Energy and Environmental Science* 2014, 7, 2963; M. Franckevičius, A. Mishra, F. Kreuzer, J. Luo, S. M.
30 Zakeeruddin, M. Grätzel, *Materials Horizons* 2015, 2, 613; Y. Liu, Q. Chen, H. S. Duan, H. Zhou, Y.
31 Yang, H. Chen, S. Luo, T. B. Song, L. Dou, Z. Hong, Y. Yang, *Journal of Materials Chemistry A* 2015, 3,
32 11940; Q. Luo, Y. Zhang, C. Liu, J. Li, N. Wang, H. Lin, *Journal of Materials Chemistry A* 2015, 3,
33 15996; C. Steck, M. Franckevičius, S. M. Zakeeruddin, A. Mishra, P. Bäuerle, M. Grätzel, *Journal of*
34 *Materials Chemistry A* 2015, 3, 17738.
- 35 [334] W. Chen, X. Bao, Q. Zhu, D. Zhu, M. Qiu, M. Sun, R. Yang, *Journal of Materials Chemistry C*
36 2015, 3, 10070; S. Kazim, F. J. Ramos, P. Gao, M. K. Nazeeruddin, M. Grätzel, S. Ahmad, *Energy and*
37 *Environmental Science* 2015, 8, 1816.
- 38 [335] N. J. Jeon, J. Lee, J. H. Noh, M. K. Nazeeruddin, M. Grätzel, S. I. Seok, *Journal of the American*
39 *Chemical Society* 2013, 135, 19087; B. Abdollahi Nejad, V. Ahmadi, H. R. Shahverdi, *ACS Applied*
40 *Materials and Interfaces* 2015, 7, 21807; M. I. Hossain, F. H. Alharbi, N. Tabet, *Solar Energy* 2015, 120,
41 370; M. Lv, J. Zhu, Y. Huang, Y. Li, Z. Shao, Y. Xu, S. Dai, *ACS Applied Materials and Interfaces* 2015,
42 7, 17482.
- 43 [336] K. Zhao, R. Munir, B. Yan, Y. Yang, T. Kim, A. Amassian, *Journal of Materials Chemistry A*
44 2015, 3, 20554.
- 45 [337] J. H. Yun, I. Lee, T. S. Kim, M. J. Ko, J. Y. Kim, H. J. Son, *Journal of Materials Chemistry A*
46 2015, 3, 22176.
- 47 [338] A. Abate, T. Leijtens, S. Pathak, J. Teuscher, R. Avolio, M. E. Errico, J. Kirkpatrick, J. M. Ball, P.
48 Docampo, I. McPherson, H. J. Snaith, *Physical chemistry chemical physics : PCCP* 2013, 15, 2572; H.
49 Zhang, Y. Shi, F. Yan, L. Wang, K. Wang, Y. Xing, Q. Dong, T. Ma, *Chemical Communications* 2014,
50 50, 5020; H. Bi, Y. Zhang, *Materials Letters* 2015, 161, 767.
- 51 [339] L. Badia, E. Mas-Marzá, R. S. Sánchez, E. M. Barea, J. Bisquert, I. Mora-Seró, *APL Materials*
52 2014, 2, 081507.
- 53
54
55
56
57
58
59
60
61
62
63
64
65

- 1
2
3
4 [340] X. Bao, Y. Wang, Q. Zhu, N. Wang, D. Zhu, J. Wang, A. Yang, R. Yang, *Journal of Power*
5 *Sources* 2015, 297, 53; A. Guerrero, J. You, C. Aranda, Y. S. Kang, G. Garcia-Belmonte, H. Zhou, J.
6 Bisquert, Y. Yang, *ACS Nano* 2016, 10, 218.
7 [341] J. Y. Jeng, K. C. Chen, T. Y. Chiang, P. Y. Lin, T. D. Tsai, Y. C. Chang, T. F. Guo, P. Chen, T.
8 C. Wen, Y. J. Hsu, *Advanced Materials* 2014, 26, 4107.
9 [342] M. P. d. Jong, L. J. v. IJzendoorn, M. J. A. d. Voigt, *Applied Physics Letters* 2000, 77, 2255.
10 [343] L. Hu, J. Peng, W. Wang, Z. Xia, J. Yuan, J. Lu, X. Huang, W. Ma, H. Song, W. Chen, Y. B.
11 Cheng, J. Tang, *ACS Photonics* 2014, 1, 547; H. Wang, X. Zeng, Z. Huang, W. Zhang, X. Qiao, B. Hu,
12 X. Zou, M. Wang, Y. B. Cheng, W. Chen, *ACS Applied Materials and Interfaces* 2014, 6, 12609; Z. Liu,
13 M. Zhang, X. Xu, L. Bu, W. Zhang, W. Li, Z. Zhao, M. Wang, Y. B. Cheng, H. He, *Dalton Transactions*
14 2015, 44, 3967; Z. Liu, M. Zhang, X. Xu, F. Cai, H. Yuan, L. Bu, W. Li, A. Zhu, Z. Zhao, M. Wang, Y.
15 B. Cheng, H. He, *Journal of Materials Chemistry A* 2015, 3, 24121; V. Trifiletti, V. Roiati, S. Colella, R.
16 Giannuzzi, L. De Marco, A. Rizzo, M. Manca, A. Listorti, G. Gigli, *ACS Applied Materials and*
17 *Interfaces* 2015, 7, 4283.
18 [344] S. Chavhan, O. Miguel, H. J. Grande, V. Gonzalez-Pedro, R. S. Sánchez, E. M. Barea, I. Mora-
19 Seró, R. Tena-Zaera, *Journal of Materials Chemistry A* 2014, 2, 12754.
20 [345] W. E. I. Sha, X. Ren, L. Chen, W. C. H. Choy, *Applied Physics Letters* 2015, 106, 221104.
21 [346] M. O. Reese, S. A. Gevorgyan, M. Jørgensen, E. Bundgaard, S. R. Kurtz, D. S. Ginley, D. C.
22 Olson, M. T. Lloyd, P. Morvillo, E. A. Katz, A. Elschner, O. Haillant, T. R. Currier, V. Shrotriya, M.
23 Hermenau, M. Riede, K. R. Kirov, G. Trimmel, T. Rath, O. Inganäs, F. Zhang, M. Andersson, K.
24 Tvingstedt, M. Lira-Cantu, D. Laird, C. McGuinness, S. Gowrisanker, M. Pannone, M. Xiao, J. Hauch, R.
25 Stein, D. M. DeLongchamp, R. Rösch, H. Hoppe, N. Espinosa, A. Urbina, G. Yaman-Uzunoglu, J.-B.
26 Bonekamp, A. J. J. M. van Breemen, C. Girotto, E. Voroshazi, F. C. Krebs, *Solar Energy Materials and*
27 *Solar Cells* 2011, 95, 1253.
28 [347] M. Jørgensen, K. Norrman, S. A. Gevorgyan, T. Tromholt, B. Andreasen, F. C. Krebs, *Advanced*
29 *Materials* 2012, 24, 580.
30 [348] E. Zimmermann, P. Ehrenreich, T. Pfadler, J. A. Dorman, J. Weickert, L. Schmidt-Mende, *Nat*
31 *Photon* 2014, 8, 669.
32 [349] W. K. K. Zimmermann E., Müller M., Hu H., Ehrenreich P., Kohlstädt M., Würfel U.,
33 Mastroianni S., Mathiazhagan G., Hinsch A, Gujar T.P., Thelakkat M, Pfadler T., Schmidt-Mende, L.,
34 *APL Materials* 2016, Under review, xx.
35 [350] *Nat Mater* 2015, 14, 1073.
36 [351] Z. H. Bakr, Q. Wali, A. Fakharuddin, L. Schmidt-Mende, T. M. Brown, R. Jose, *Nano Energy*
37 2017.
38
39
40
41
42
43
44
45
46
47
48
49
50
51
52
53
54
55
56
57
58
59
60
61
62
63
64
65